Politecnico di Torino
Collegio di Ingegneria Civile ed Edile
Corso di Laurea Magistrale in Ingegneria Civile

Analysis of Rockfall Phenomena Based on Detailed Release-Area Characterization

Case Study Application in Venaus (TO)

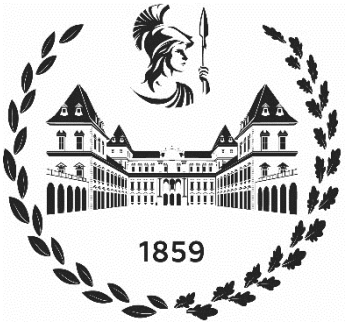

Supervisors:
Prof. Monica Barbero
Eng. Maria Lia Napoli

External Supervisor:
Eng. Luisella Vai (GEODES S.r.l.)

Candidate:
Agustin Ezequiel Silvestre Szkarlatiuk
(s335223)

March 2026

Abstract

This thesis presents a comprehensive analysis of rockfall phenomena, focusing on the detailed characterization of release areas to enhance hazard assessment and the design of mitigation measures. The research is centred on a case study in Venaus (Turin, Italy), where a rockfall event in April 2025 involved blocks impacting the local hydroelectric power plant facilities, highlighting the site's vulnerability.

The methodology integrates traditional geomechanical field surveys with aerial photogrammetry to identify unstable rock sectors. The Susceptibility Index to Failure (SIF) was applied to eight identified rock walls to objectively quantify the likelihood of block detachment. Subsequently, advanced numerical modelling was employed to simulate rockfall propagation. The QPROTO plugin, based on the Cone Method, was used for initial 3D runout analysis and to compute the Source Affecting Index (SAI) via the RADAR plugin, identifying specific source areas that pose the greatest risk to infrastructure. Detailed 3D simulations were conducted using Rockyfor3D, accounting for forest cover and slope macro-roughness. Finally, 2D analyses were performed in Rocfall2 to determine the kinematic parameters required for the design of protection barriers in compliance with the Italian UNI 11211 standard.

The study concludes that integrating detailed source-area characterization with multi-dimensional modelling significantly optimizes the design and positioning of defence structures, ensuring more efficient and site-specific risk mitigation for critical infrastructure.

Acknowledgements

First and foremost, I would like to express my deepest gratitude to my family. Especially my parents for their unconditional support, encouragement, and sacrifices, which have been the foundation of everything I have achieved. Being able to pursue my studies abroad as an international student has been a privilege that would not have been possible without their constant effort and belief in me. Even from afar, their love and trust have given me the strength and motivation to overcome the challenges along the way.

I would also like to sincerely thank my professor and thesis supervisor, Monica Barbero, and her colleague, Maria Lia Napoli, for their guidance, insightful feedback, and continuous support throughout the development of this research.

I would like to express my sincere gratitude to the company Geodes S.r.l., and in particular to Eng. Luisella Vai and Eng. Antonella Chiappone, for giving me the opportunity to carry out this internship and thesis within the company. I am also grateful to Geol. Fabrizzio Elettri for his valuable support and guidance during the development of this thesis, as well as to all my colleagues at the company for their assistance, collaboration, and the positive working environment they provided. I would like to thank also Eng. A. Poggi, Head of Hydroelectric Plants for the NW Italy Area, and Eng. G. Vallese, Head of Maintenance Activities for the Hydroelectric Plants in the NW Italy Area, for their availability and for allowing the event occurred at the hydroelectric power plant to be used as a case study for this research.

My gratitude extends to the professors and academic staff of both Politecnico di Torino in Italy and my home institution, the Universidad Nacional de Córdoba in Argentina, for their dedication to teaching and for the knowledge they have shared throughout this journey. Their guidance, commitment, and academic support have played a fundamental role in my professional and personal development.

Furthermore, I would like to thank my friends and colleagues who have accompanied me during this journey. Sharing this experience with people from different backgrounds has made these years abroad both memorable and meaningful. Their friendship, support, and encouragement have played an important role during the most challenging and rewarding moments of this experience.

Finally, I would like to acknowledge everyone who, directly or indirectly, contributed to the completion of this thesis and to my academic journey as a whole.

To all of you, thank you.

Table of Contents

List of Appendix

List of Figures

List of Tables

Introduction

The geodynamic processes that affect most of the terrestrial surface give rise to movements of various characteristics, magnitude and velocity. Driven by the action of gravity and the progressive weakening of geomaterials, these movements are relatively common within the geological environment. However, they constitute potential geological hazards because they can cause significant economic and social damage, directly affecting human safety, economic activities and civil infrastructure. Preventing these harmful effects is the ultimate goal of studying ground movements, their characteristics, types, instability mechanisms, and triggering factors. Through accurate modelling of these phenomena, it is possible to gather the necessary information to design effective mitigation structures and redefine land use in affected areas.

Among these geological hazards, rockfall phenomena represent one of the most rapid and unpredictable types of slope movement. Although individual events may involve relatively small volumes, their high dynamic characteristics pose a severe risk to infrastructures and lives, especially in mountainous regions.

The objective of this thesis is to present a comprehensive analysis of rockfall phenomena, focusing on the detailed characterization of release areas to optimize the design of protection measures. The proposed methodology integrates traditional geomechanical field surveys with aerial photogrammetry to identify unstable sectors. A central element of this study is the application of the Susceptibility Index to Failure (SIF), which quantifies the probability of block detachment across source areas.

This research focuses on a case study in Venaus (Turin, Italy), where a rockfall event in April 2025 involved blocks of approximately 4 m^3 impacting a local hydroelectric power plant. This event highlighted the site's vulnerability and highlighted the necessity for an advanced characterization of release areas to improve hazard assessment. Following the characterization of source areas, advanced numerical modelling was employed to simulate propagation. The first rockfall analysis was carried out using the QPROTO plugin, based on the Cone Method and implemented on the GIS environment. Following, the RADAR plugin was applied to compute the Source Affecting Index (SAI), identifying the specific source points that pose the greatest risk to the exposed elements. Furthermore, detailed 3D simulations were conducted using Rockyfor3D, accounting for forest cover and slope macro-roughness to provide more precise kinematic data. Finally, 2D analyses were performed in Rocfall2 to determine the parameters required for the design of protection barriers in compliance with the Italian standards.

Chapter 1

The Blocky Nature of Rock Masses

The rock formations that make up the Earth's crust vary widely in their characteristics, like type, composition, mechanical properties, and other features. Despite this variability, all rock masses are composed of two fundamental components: the intact rock and the discontinuities. The interaction between these components forms blocks and controls the behaviour of the rock mass. An accurate characterization of these components is crucial for defining the initial conditions of the site and for developing safe and efficient structural solutions.

1.1 Intact Rock

Intact rock is defined in engineering terms as rock containing no significant fractures and it might be considered as a continuum material. However, at the microscopic scale it is composed of mineral grains, with the form of the microstructure being governed by the basic rock forming processes. Subsequent geological events may affect the rock mechanical properties, behaviour and susceptibility to water permeation and weathering effects.

The properties of the intact rock are governed by the physical properties of the constituent minerals and the way in which they are bonded to each other. Intact rocks may be classified from a geological or a geomechanical point of view; in the first case the mineral content of the rock, its texture and any changes that the rock has undergone since its formation are fundamental for its sub-classification. Geomechanical classifications of intact rock are more related to the engineering properties of the rock, such as strength and deformability. Rock types with the same genetic basis may show a wide dispersion in their mechanical properties (Zhang, 2017).

Therefore, it is recommended to begin the material characterization with a mineralogical-petrographic analysis. This analysis allows the definition of microscopic parameters such as mineral composition, grain size distribution, and rock texture.

1.1.1 Geological Classification

Rocks are composed of minerals, each of which possesses a characteristic chemical composition and crystalline structure. Although hundreds of minerals have been identified, only a limited number are common, like quartz, feldspar, mica and calcite. The common rock forming minerals can often be identified in a hand specimen with magnifying lens, this task is typically performed by experienced geologists. For more detailed or definitive mineral characterization,

X-ray diffraction and scanning electron microscopic analysis provide higher precision and facilitate an accurate mineral identification.

Hardness and specific gravity are the most used physical properties for mineral identification. Hardness refers to the relative ability of a mineral to scratch, or be scratched by, another. A standard methodology for classifying minerals according to their hardness is the Mohs scale (Table 1.1), which consists of a standard of 10 minerals arranged in order of increasing hardness. The scale goes from one for talc, the softest mineral, to ten for diamond, the hardest. Specific gravity, another key diagnostic property, is defined as the ratio of the weight of a mineral to the weight of an equal volume of water at a standard temperature. Most common rock-forming minerals exhibit specific gravity values of about 2,65.

Table 1.1 - Mohs hardness scale.

Mineral	Hardness
Talc	1
Gypsum	2
Calcite	3
Fluorite	4
Apatite	5
Orthoclase	6
Quartz	7
Topaz	8
Corundum	9
Diamond	10

Intact rocks are generally classified into three main groups according to their forming processes: igneous, metamorphic and sedimentary. Table 1.2 shows an extended rock classification.

Igneous rocks are formed by crystallization of molten magma. The mode of crystallization of the magma, at depth in the Earth's crust or by extrusion, together with the cooling rate, influences the rock texture and crystal structure. The igneous rocks are subdivided into plutonic, hypabyssal, and extrusive, according to their texture. They are further subdivided into acid, intermediate, basic, and ultrabasic, according to the silica content.

Metamorphic rocks are the result pre-existing rocks that have been subjected to solid state conversion by temperature, pressure and/or chemical changes. The great varieties of metamorphic rocks are characterized, classified and named according to their mineral assemblages and textures.

Sedimentary rocks are the result of the consolidation of sediments. This type of rock covers three-quarters of the continental areas and most of the oceanic floor. In the process of erosion, rocks weather and they broke down into small particles or are totally dissolved, these detrital particles may be transported by water, wind or glaciers, and deposited far from their original position. When these sediments start to form thick deposits, they consolidate under their own weight and eventually turn into solid rock through chemical or biochemical precipitation, or organic process. As a result of this processes, sedimentary rocks almost invariably possess a distinct stratified, or bedded, structure.

Table 1.2 - Rock Classification (based on Sivakugan *et al.,* 2013).

Main Rock Type	Classifications	Sub classification	Examples	Key Characteristics
Igneous Rocks	By Origin	Extrusive	Basalt, Rhyolite, Andesite	Rapid cooling; fine-grained; volcanic
		Intrusive	Granite, Dolerite, Gabbro, Syenite	Slow cooling; coarse-grained; crystalline
	By Silica Content	Acidic (>66%)	Granite, Rhyolite, Pegmatite	Light coloured; high silica
		Intermediate (55–66%)	Andesite, Diorite	Moderate silica
		Basic (44–55%)	Basalt, Dolerite, Gabbro	Dark; dense; low silica
		Ultrabasic (<44%)	Peridotite	Very low silica; very dense
Metamorphic Rocks	Foliated	-	Slate, Schist, Gneiss	Layered/banded due to pressure
	Non-Foliated	-	Marble, Quartzite, Anthracite	Massive; recrystallized minerals
Sedimentary Rocks	Clastic	-	Sandstone, Shale, Conglomerate, Breccia	Deposited fragments; bedded or massive
	Chemical/ Evaporites	-	Limestone, Gypsum, Halite	Precipitated minerals; fine-grained
	Organic	-	Coal	Carbon-rich; biological origin

In nature, a dynamic process called rock cycle occurs constantly, where one type of rock is slowly transformed into another. This cycle begins when the igneous rocks are exposed at the Earth's surface and subjected to weathering, which generates sediments. These sediments can then consolidate through hardening or cementation to form sedimentary rocks. Sedimentary or even existing metamorphic rocks are subjected at great depths to high temperatures and pressure leading to the creation of metamorphic rocks. Finally, if metamorphic or sedimentary rocks are exposed to intense heat at great depths, they melt to produce magma. This magma may eventually cool and solidify, either deep underground or upon reaching the surface, thus completing the cycle by forming new igneous rocks. The rock cycle is schematized in Figure 1.1.

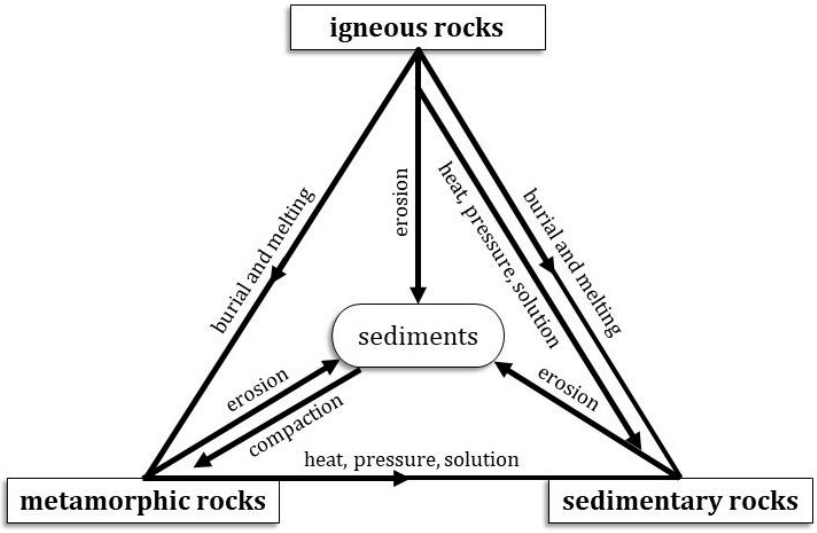

Figure 1.1 - Rock cycle (Sivakugan, *et al.*, 2013).

1.1.2 Geomechanical Classification

The geomechanical classification of intact rocks relies primarily on mechanical parameters such as strength and deformability. A commonly used representation of the mechanical behaviour of a rock is the complete stress-strain curve under uniaxial compression. It reveals the effects of the rock microstructure and stress history on the mechanical behaviour.

The stress-strain curve is obtained from the uniaxial compressive strength (UCS) test. During this test, a cylindrical rock specimen is subjected to an axial load without any lateral confinement. The axial load is increased gradually until the specimen fails. The vertical normal stress at failure is defined as the unconfined, or uniaxial, compressive strength (σ_c) of the rock. By monitoring the axial deformation throughout the test, the corresponding axial strain can be computed and, by plotting the stress-strain curve, the elastic modulus (E) can be determined. In addition, by monitoring the radial, or circumferential, deformation, the Poisson's ratio (ν) can be determined. Figure 1.2 shows a generic complete stress-strain curve for a sample of rock loaded in uniaxial compression and illustrates how the elastic modulus and Poisson's ratio can be obtained.

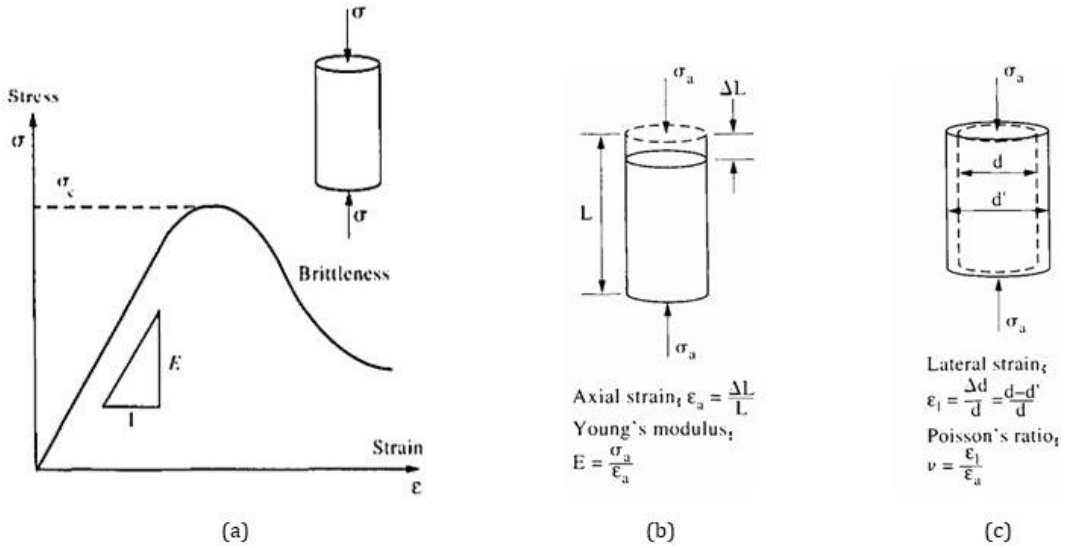

Figure 1.2 - (a) Stress-strain curve of a rock specimen in uniaxial compression, (b) elastic modulus, and (c) Poisson's ratio determination (Hudson, *et al.*, 1997).

It is important to consider that the uniaxial compressive strength is not an intrinsic property of the material. Intrinsic material properties do not depend on the specimen geometry or the loading conditions used on the test, while the compressive strength is influenced by both.

In the post peak region, the trend of the stress-strain curve indicates whether the material is ductile or brittle. If strain continues to increase while the stress remains approximately constant, the material is considered ductile. In contrast, if the stress rapidly drops to zero with little additional strain, the material is classified as brittle. The steepness of the post-peak descent reflects the degree of brittleness between these two extremes, as illustrated on Figure 1.3.

In practice, the situation can be more complex. Some materials exhibit strain-hardening behaviour, with a trend above the ductile limit, while others may show exceptionally rapid stress reduction, placing the trend to the left of the brittle limit and characterizing them as super brittle materials.

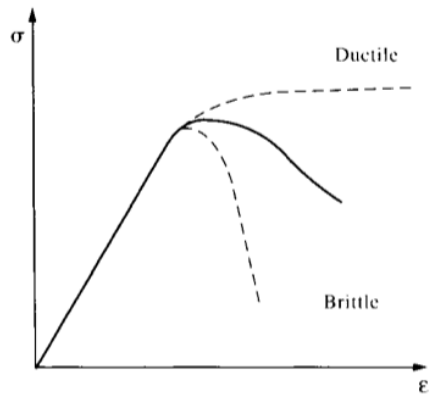

Figure 1.3 - Characteristic limits between ductile and brittle material (Hudson, *et al.*, 1997).

1.1.3 Intact Rock Intrinsic Properties

The intrinsic physical properties of rock material have a significant influence on its mechanical behaviour, determining these properties is essential for a complete material characterization. Some of the principal properties of the intact rock that control how the rock interacts with stresses, fluids and temperature, influencing its mechanical behaviour and engineering performance are listed in Table 1.3. The International society for Rock Mechanics (ISRM) on its guideline "*The complete ISRM Suggested Methods for Rock Characterization, Testing and Monitoring*" (1978-2006), outlines standardized laboratory and field tests methods to determine the key physical properties of rock materials.

Table 1.3 - Intrinsic properties of intact rocks (ISRM, 1978).

Properties	Description	Units
Density/ Unit weight	mass per unit volume	kg/m^3
Specific gravity	ratio of rock density to water density	-
Porosity	ratio of the void volume to total volume	%
Water content	amount of water in pores	%
Saturation degree	ratio of the volume of water to the volume of voids	%
Permeability	ease with which fluids pass through pores	m^2
Abrasiveness	ease to cause wear or erode	-
P waves velocity	wave propagation speed	m/s

As Hudson and Harrison (1997) emphasized, *"The subject of rock characterization is far more complex and intractable than might appear at first sight. The subject does not merely concern the optimal length-to-diameter ratio for a compression test specimen and other similar tactical aspects of testing procedures; it concerns the whole strategic concept of how to characterize naturally occurring rock masses, which have been in existence for millions of years, have been operating as natural process-response systems for all that time and are about to be perturbed by engineers in order to achieve particular objectives."*

1.2 Discontinuities

The term discontinuity defines any separation in the rock mass that possesses zero or low tensile strength. It is a collective designation for joints, bedding planes, schistosity planes, weakness zones, and faults. Given that traditional mechanics and stress analysis assume that materials act as a continuous media, these geological features can represent mechanically significant discontinuities within the continuum.

Throughout the rock geological history there have certainly been orogenic periods and other less severe loading processes applied. Consequently, the intact rock might have already failed and formed discontinuities, where there is little or no strength present. It is, in fact, very helpful to understand the way in which the discontinuities were formed to have an initial idea of their likely mechanical characteristics (Hudson, *et al.*, 1997).

The main types of discontinuities present in rock masses can be grouped into the following categories, each with distinct origins and mechanical implications:

(a) Faults: discontinuities on which identifiable shear displacement has taken place. They may be recognized by the relative displacement of the rock on the opposite sides of the fault plane. Fault thickness may vary from meters in case of major, regional formations to millimetres in the case of local faults. Inside the opening, the fault might contain weak material filling. The zone adjacent to the fault may be disturbed and weakened by associated discontinuities such as drag folds or secondary faults. These factors result in faults being zones of low shear strength on which slipping failure may occur.
(b) Bedding planes: bedding planes divide sedimentary rocks into layers or strata. They represent interruptions during deposition of material and are generally persistent features. They might contain parting material of different grainsize from the sediments forming the rock mass, or they may have been partially healed by low-grade metamorphism. In either of these two cases, there would be some apparent cohesion between layers; otherwise, the shear resistance between planes would be purely frictional.
(c) Joints: they are the most common and generally the most geotechnically significant discontinuities in rocks. They are breaks of geological origin where there has been no significant relative displacement. A group of joints in the same orientation and having similar characteristics is defined as joint set, and joint sets intersect each other to form a joint system.
(d) Foliation planes: are planar features formed during metamorphism, where minerals form aligned parallel arrangements. They create mechanical anisotropy in the rock mass, typically having lower shear strength than the surrounding material.
(e) Lithological contacts: contacts are boundaries between different rock units or intrusive bodies. When there is a strong contrast in material properties across the boundary, they can behave as mechanical discontinuities.

1.2.1 Discontinuity properties

Discontinuities exhibit a range of geometrical and mechanical characteristics that frequently control the overall response of the rock mass. Each discontinuity set has a particular shape, a specific size, and a distinct orientation, and these attributes strongly influence how the rock mass behaves under loading. The ISRM defines ten parameters to describe the characteristics of discontinuities:

(1) Orientation: the position of a discontinuity in space is described by the dip direction (azimuth) and dip of the line of steepest declination in the plane of the discontinuity.
(2) Spacing: the perpendicular distance between adjacent discontinuities. It normally refers to the mean or modal spacing of a set of discontinuities. Associated, the frequency is defined as the number of discontinuities per meter.
(3) Persistence: the discontinuity trace length as observed in an exposed area or volume. It may give a rough measure of the areal extent or penetration length of a discontinuity. Termination in solid rock or against other discontinuities reduces the persistence.
(4) Roughness: the natural surface roughness and waviness relative to the mean plane of a discontinuity. Both roughness and waviness contribute to the shear strength. Large-scale

waviness may also alter the dip locally. It is typically determined by comparison with the Joint Roughness Coefficient (JRC) scale.

(5) Wall strength: the equivalent compressive strength of the adjacent walls of a discontinuity. It is usually lower than rock block strength due to weathering or alteration of the walls. It is an important component of shear strength if rock walls are in contact. It is obtained with correlation charts with data from the Schmidt hammer test.

(6) Aperture: the perpendicular distance between adjacent rock walls of a discontinuity, in which the intervening space might be filled with air, water or solid material.

(7) Filling: the material that exist between the adjacent rock walls of a discontinuity, usually it is weaker than the intact rock. Typical filling materials are sand, silt, clay, breccia, gouge, and mylonite. It also includes thin mineral coatings and healed discontinuities such as quartz and calcite veins.

(8) Seepage: the water flow and free moisture visible in individual discontinuities or in the rock mass as a whole.

(9) Number of sets: the number of discontinuity sets part of the intersecting discontinuity system.

(10) Block size: the rock block dimensions resulting from the mutual orientation of intersecting discontinuity sets and from the spacing of the individual sets. Individual discontinuity sets may further influence the block size and shape.

In Figure 1.4 a schematic representation of two planes within a rock mass is presented, highlighting the mentioned geometrical and mechanical properties of discontinuities.

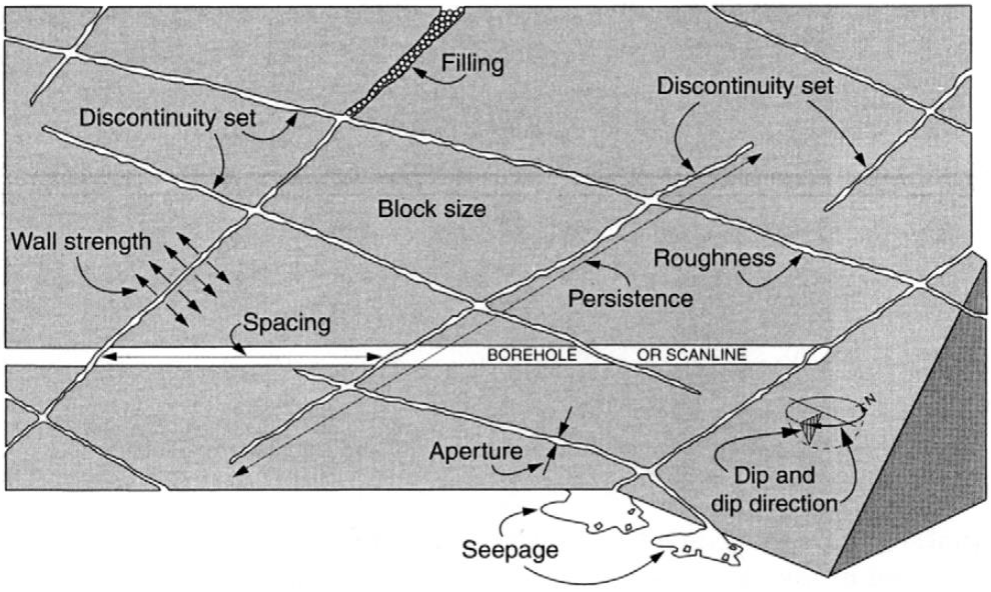

Figure 1.4 - Schematic of the primary properties of discontinuities in rock (Hudson, *et al.*, 1997).

Stereographic Representation

Assuming a discontinuity to be a planar feature, then its orientation can be uniquely defined by two parameters, dip direction (α) and dip angle (ψ). The dip angle is defined as the steepest line in a plane, *i.e.* the line through which a ball would roll down; the dip direction is the compass bearing of this line, measured clockwise from the true North. In the field during a geomechanical survey procedure, a geological compass is used to provide direct readings of these parameters.

In general, a large number of (α, ψ) data pairs are obtained from a survey. Therefore, it is useful to present these data in a graphical form, like on Figure 1.5, to facilitate an easier assimilation and understanding. In rock mechanics and rock engineering, the stereographical equal-angle lower-hemisphere projection has always been the most accepted form of representation.

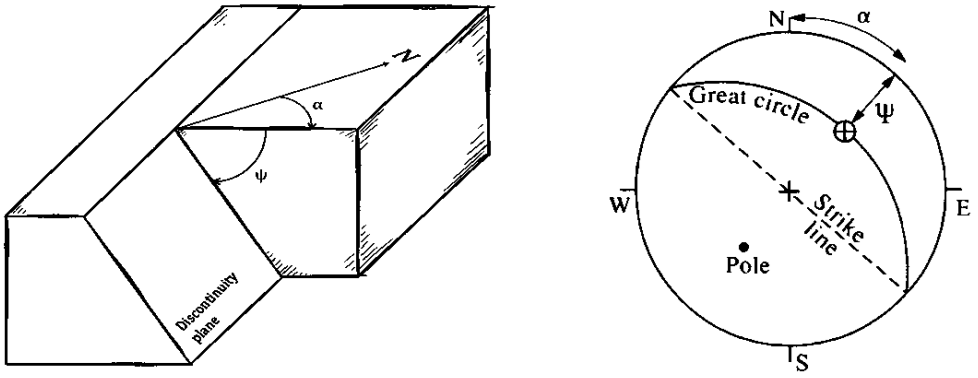

Figure 1.5 - Discontinuity plane and the associated hemispherical projection.

The dip direction is plotted as the compass bearing and the dip angle is plotted inwards from the perimeter of the projection plane. This defines a point on the projection representing the line of maximum dip of the plane. Another line in the plane is the strike line, *i.e.* the line with zero dip, this auxiliary line is plotted as two diametrically opposed points on the perimeter of the projection. In the same way, all lines in the plane can be plotted using their particular (α, ψ) values, resulting in the great circle shown in the figure. Thus, a line in the plane is plotted as a point, and the plane itself is plotted as a curve.

An alternative method of uniquely specifying the plane is to plot the position of a line perpendicular to the plane, this line is known as the normal and the associated point plotted on the projection is known as the pole, also plotted in Figure 1.5. As mentioned, generally, it is necessary to plot a large number of discontinuity planes, which makes poles preferable to great circles, as they are easier to interpret when dealing with large datasets. Once many poles have been plotted on the stereographic projection, the generalized rock structure can be analysed by clustering these normals, *i.e.* identifying groups of similar oriented planes. This clustering is conventionally studied by contouring the projection to identify the densest regions. More advanced approaches use clustering algorithms, which may be based on statistical methods or fuzzy-set theory. In Figure 1.6, an example of plotted data, the resulting contoured plot, and the principal sets are shown.

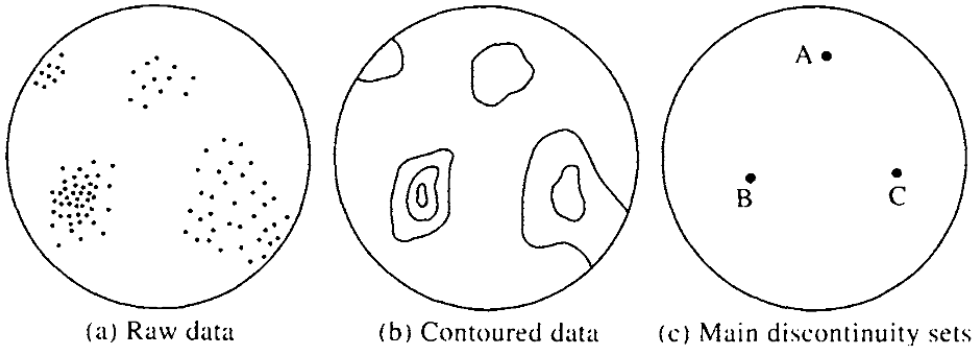

Figure 1.6 - Poles clustering procedure (Hudson, *et al.,* 1997).

It is common to idealize a set of discontinuities as a group of parallel, persistent and planar elements. In practice, not only a set might consist of sub-parallel discontinuities, but also it can be difficult to determine to which set a particular discontinuity belongs. For this reason, each discontinuity is characterized, not only by its geometrical parameters but also by the properties described above, allowing for a more comprehensive analysis of the clustering (Hudson, *et al.*, 1997).

1.2.2 Block Formation

One subject where the concept of discontinuity sets, and their mutual interaction, is important is the formation of rock blocks, in determining the distribution of their sizes and shapes. The way different sets of discontinuities intersect, their persistence, orientation, spacing, and degree of randomness, play a critical role in defining the geometry of the resulting blocks. Figure 1.7 shows different rock shapes and volumes that can be formed according to interaction of the mentioned factors.

Block dimensions are determined by discontinuity spacing, by the number of discontinuity sets and by their persistence. Block shapes are determined by the number of sets and orientations of the discontinuities defining potential blocks.

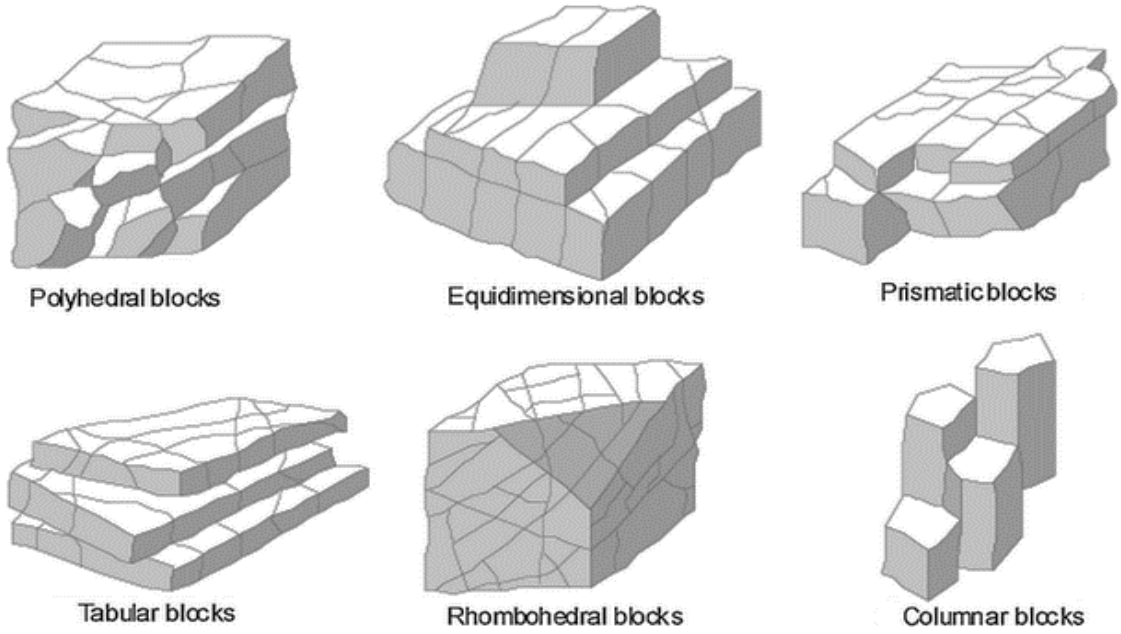

Figure 1.7 - Examples of block shapes (Dearman, 1991).

On particular formations where individual blocks can be identified on the surface, their volumes can be estimated by measuring the dimensions of several representative blocks and averaging the results. In most cases, the block shapes are irregular and can only be roughly described. Where three persistent discontinuity sets occur, the block volume can be calculated as:

$$V_b = \frac{s_1 s_2 s_3}{sin\gamma_1 sin\gamma_2 sin\gamma_3} \qquad \textit{(Eq. 1.1)}$$

where s_1, s_2, s_3 are the normal set spacing of the three discontinuity sets, respectively; and γ_1, γ_2, γ_3 are the angles between the discontinuity sets.

If non-persistent discontinuities are present, the equivalent block volume can be determined by (Kim, *et al*., 2004, 2007):

$$V_b = \frac{s_1 s_2 s_3}{sin\gamma_1 sin\gamma_2 sin\gamma_3 \sqrt{p_1 p_2 p_3}} \qquad \textit{(Eq. 1.2)}$$

where p_1, p_2,

p_3 are the persistence of the three discontinuity sets, respectively.

1.3 Rock Masses

A rock mass is considered to be the complete structure of a rock in its natural position, integrating both the intact rock and the discontinuities that divide the rock into interlocking blocks of varying shapes and sizes.

Even with the most generous available resources for site investigation, challenges remain present when applying theoretical models to real engineering conditions, as not everything can be fully generalized or quantified across the entire rock mass. As a consequence, many engineers have developed rock mass classification systems that consider a few or key rock mass parameters and assign numerical values to the classes in which these parameters lie for a given rock type (Hudson, *et al.*, 1997). The classification systems ensure that engineer, geologists and any involved professionals use consistent terminology when referring to a specific rock mass. The three major and commonly applied rock mass classification systems are:

(a) Rock Mass Rating (RMR)
(b) Q-System (Q)
(c) Geological Strength Index (GSI)

The last classification systems is presented in detail in the following section, selected because it provides a reliable assessment of rock structure and surface conditions, which is useful for evaluating rock quality from reachable outcrops.

1.3.1 Geological Strength Index

GSI is a relatively recent rock mass classification system that was introduced by Dr. Evert Hoek in 1994. Focusing primarily on geological observations, and less on numerical values, the two major parameters for this classification are: (i) surface condition of the discontinuity; and (ii) interlocking among the rock blocks. The surface condition ranges from very good for fresh unweathered surfaces to very poor for highly weathered or slickensided surfaces with clay infill. The interlocking blocks can be literally massive at the upper end of the scale to crushed or laminated at the lower end. Analysing these two qualitative parameters, a GSI value is assigned using the chart shown in Figure 1.8.

The GSI classification system is based on visual inspection and it has been extensively used by the rock mechanics professionals since its publication. However, due to the lack of measurable parameters for describing the rock mass conditions, it is possible for different persons to estimate different GSI values from the chart to the same rock mass (Zhang, 2017).

The subjectivity associated with visual GSI estimation has motivated several attempts to improve the reproducibility of rock mass characterization using this parameter. In particular, correlations between GSI and measurable parameters such as joint frequency, spacing, and mechanical indices have been proposed to reduce observer-dependent variability. Nevertheless, the GSI system remains primarily a field-based engineering judgement tool, widely used due to its simplicity and practical applicability.

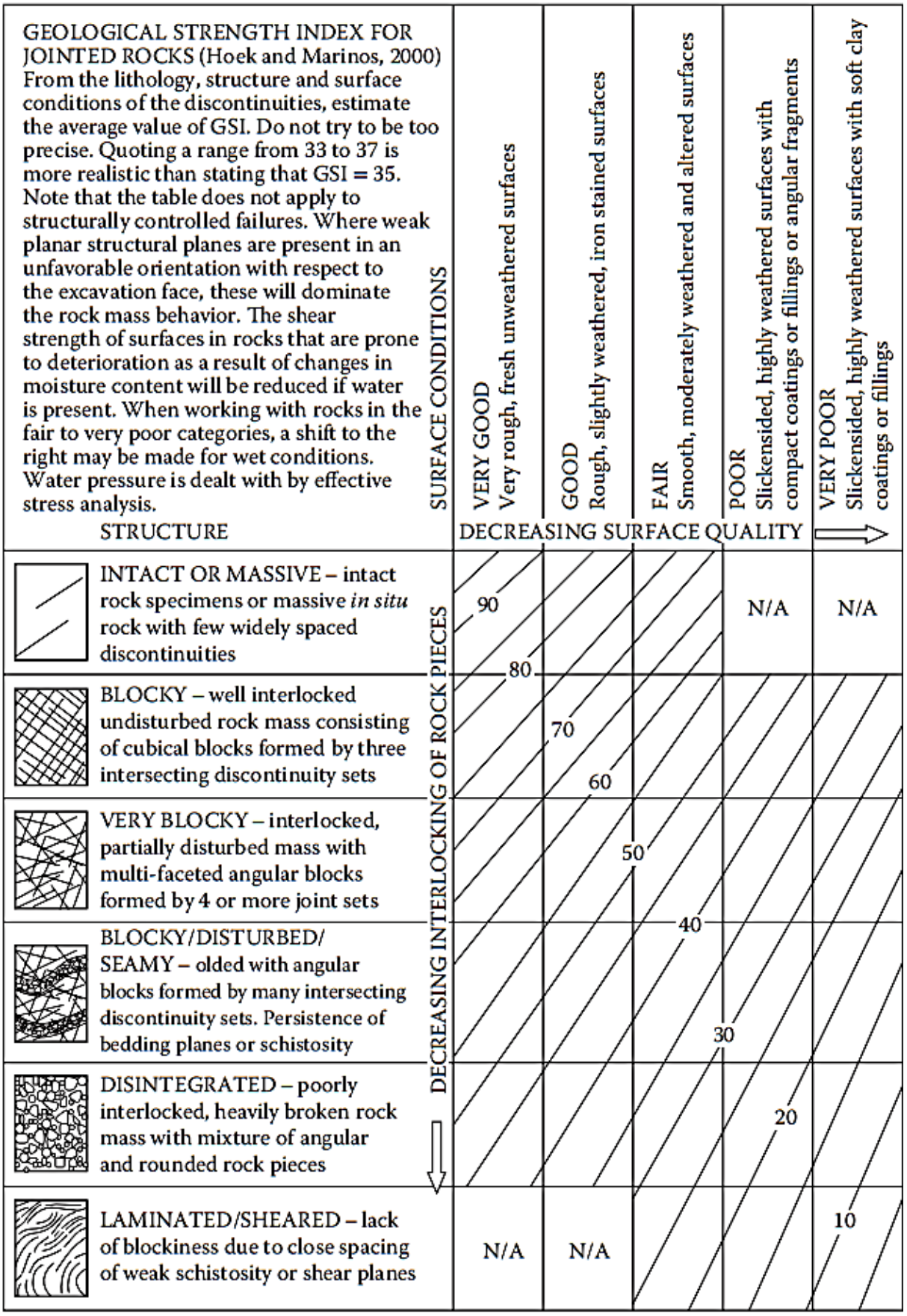

Figure 1.8 - Geological Strength Index for jointed rocks (Hoek, *et al.*, 1997).

Chapter 2

Rock Slopes

Rock slopes are features that occur naturally or are engineered by people as a product of excavations for civil engineering purposes. The stability of rock slopes is strongly influenced by the structural geology of the rock, especially by the natural occurring discontinuities. The significance of discontinuities on the stability of slopes is that they are planes of weakness integrated in a much stronger material, so failure tends to occur preferentially along these features.

All rock slope stability studies should evaluate the structural geology conditions of the site, such studies involve two steps. First, determine the properties of the discontinuities, described in Section 1.2.1, which involve mapping outcrops and existing cuts; and second, determine the influence of discontinuities on stability. For a reliable analysis, it is important to recognise the modes and mechanisms in which rock slopes might fail.

2.1 Failure Mechanisms of Rock Slopes

There are two general slope-failure mechanisms, according to the level of fracturing and degradation of the rock mass, one in which the rock mass behaves as an equivalent continuum, and another in which it behaves as a discontinuum. The main difference between these behaviours is the definition of the formed slip surface. Figure 2.1 (a) shows that the failure surface is developed through the rock mass and has a curvilinear shape that cannot be defined in advance with certainty, whereas in Figure 2.1 (b) the failure surfaces is dictated by the presence of specific pre-existing discontinuities that can sometimes be identified *a priori*. However, cases may occur where the failure occurs partly along the discontinuities and partly through bridges of intact rock, which is a case in between these two modes.

The majority of rock slope instabilities are caused by blocks formed by the intersection of individual discontinuities; this is because, as already mentioned, the strength of the intact rock in the formed blocks is much higher than shear strength of the discontinuities.

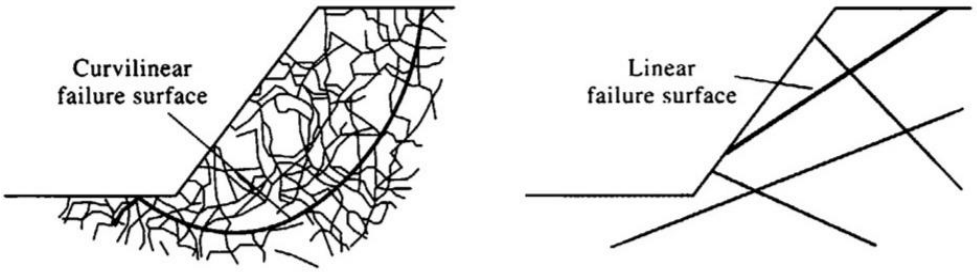

(a) Many discontinuities, weak rock mass, equivalent continuum.

(b) Few discontinuities, strong rock mass, discontinuum.

Figure 2.1 - Rock slope failure mechanisms (Hudson, *et al.*, 1997).

Figure 2.2 presents idealized and simplified illustrations of the most common failure modes. The geometry of the curvilinear slip surface in (a) is a function of the geometry of the slope, the shear strength and the degree of fracturing of the involved material. Figure 2.2 (b), (c) and (d) show how the boundaries of the instability are governed by the discontinuities, giving essentially one or more faces to the sliding or block detachment, which occurs when the driving force exceeds the resisting forces, disrupting the limit equilibrium along these discontinuities.

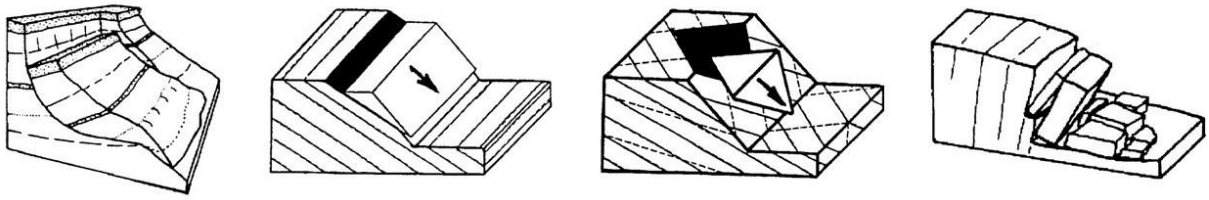

(a) Curvilinear failure (b) Plane failure (c) Wedge failure (d) Toppling failure

Figure 2.2 - Most common rock slope failure modes (Simons, *et al.*, 2001).

In the curvilinear failure mode, a heavily jointed and weathered rock mass exhibiting a soil-like mechanical behaviour slides along a curvilinear surface towards the free face of the slope. The shape and depth of the slip surface depends on the strength characteristics of the rock mass.

In plane failure mode, the rock block slides along a single face determined by pre-existing weaker planes striking parallel to the slope face and dipping towards the slope face at an angle greater than the angle of internal friction along the sliding plane. Similarly, in wedge failure mode, the block slides simultaneously along two intersecting discontinuity planes that strike obliquely to the slope face, sliding occurs along their line of intersection into the slope face if the inclination of this line exceeds the frictional resistance of the discontinuity surfaces.

In toppling failure, multiple rock columns or layers formed by steeply dipping joint sets rotate around their bases towards the slope face, potentially leading to detachment or overturning of the rock blocks when the limit equilibrium state is exceeded.

It is worth noting that in large rock slopes composed of a variety of rock types and structural features, more than one of the basic failure modes mentioned above may occur in combination. At the same time, it is not uncommon for multiple basic failure modes to occur within a single sliding mass at a given site.

A more extended and well known classification system is the one proposed by Varnes (1978), presented in Table 2.1. This classification considers that different types of landslides can be differentiated by the kind of material involved and the mode of movement.

Table 2.1 - Slope movement classification (Varnes, 1978).

TYPE OF MOVEMENT	TYPE OF MATERIAL		
	BEDROCK	SOILS	
		Coarse-predominant	Fine-predominant
FALL	Rock fall	Debris fall	Earth fall
TOPPLE	Rock topple	Debris topple	Earth topple
SLIDE – ROTATIONAL / TRANSLATIONAL	Rock slide	Debris slide	Earth slide
SPREAD	Rock spread	Debris spread	Earth spread
FLOW	Rock flow (deep creep)	Debris flow (soil creep)	Earth flow
COMPLEX	Combination of two or more principal types of movement and/or materials.		

2.2 Stability Analysis of Rock Slopes

The stability of rock slopes is greatly controlled by the shear strength along the discontinuities and interfaces between the unstable rock block or mass and the intact rock or stable mass, as well as by the geometric interaction of joint sets in the rock mass forming the slope. The determination of the magnitude of the available shear strength along the joints and interfaces is a difficult task due to the inherent variability of the material and the difficulties and limitations associated with sampling and laboratory testing. According to Bromhead (1992) and Abramson *et al.* (2002), some of the factors that directly or indirectly influence the strength include:

(a) The planarity and smoothness of the joint's surfaces; a smooth planar surface will have a lower strength than an irregular and rough surface.
(b) The inclination of the discontinuity plane with respect to the slope.
(c) The width of the opening of the discontinuity, which can range from a slight opening to a noticeable joint.
(d) The extent of the weathering along the surfaces and the possible infill of the joints with soft material.

In practice, the shear resistance is often estimated through parameters such as cohesion and friction angle within the framework of the Mohr–Coulomb representation, which can be derived from laboratory shear tests or field back-analysis. For rock engineering applications, the formulation proposed by Hoek (2002) is widely used to link discontinuity shear strength to surface condition, roughness, and infill characteristics, allowing the estimation of shear strength parameters when direct testing is not possible.

Once the failure mode has been recognized and the joint strength determined, the factor of safety can be estimated using the principle of statics and free body diagrams created based on geological maps and surveys. All the relevant forces acting on the slope are evaluated and applied to the system.

Limit equilibrium methods have been fundamental in developing a basic understanding of rock slope stability. These methods are based on simplifying the slope into discrete slices and evaluating the balance of forces and moments acting on them. The factor of safety can be estimated by assuming a potential failure surface and analysing the resisting and driving forces along it. Limit equilibrium approaches are particularly useful for identifying critical failure surfaces, understanding how different geometrical and material properties influence stability, and providing an initial assessment prior to conducting more detailed analyses.

Numerical methods complement limit equilibrium approaches by allowing more detailed and flexible analysis of rock slopes. Without the requirement of a predefined sliding surface, they

can simulate more complex geometries, heterogeneous materials, and combined failure mechanisms that are difficult to capture with traditional approaches. These methods are particularly valuable when slopes fail due to the combination of different processes or additional mechanisms such as erosion, material failing or sliding. Numerical models can also incorporate time-dependent effects, dynamic loading, and interactions between multiple forces, providing a more realistic prediction of slope behaviour under various conditions.

2.2.1 Stability Analysis Workflow

Given the wide variability in geological conditions, material properties, and loading scenarios, it is essential to adopt a systematic and flexible workflow that can be extended to different types of slope stability problems. A typical slope stability analysis workflow is presented by Lambert, *et al.* (2011); it can be applied for both soil and rock slopes, providing a structured framework that integrates site characterization, selection of appropriate material parameters and analysis methods, stability evaluation, and finally the design of mitigation structures. This workflow example is divided into six phases:

(1) Preparation and data collection phase.
(2) Definition of potential failure scenarios.
(3) Stability and/or runout analysis.
(4) Validity check and validation of analysis results.
(5) Interpretation of the model results.
(6) Results processing and presentation.

Whether all six phases are carried out depends on the level of detail of the analysis. In general, three different levels of detail can be defined. The first level (L1) provides an overview, which is mostly, but not necessarily, used at a regional scale with the objective to obtain a rapid first indication of potentially unstable ones for large areas. The second level (L2) is a local view, mostly but not necessarily applied at the scale of a community, this often accounts for hazard maps. The third level (L3) zooms in on a part of a single slope affected by potential instability. This last is a highly detailed level required for the design of structural measures. In a cartography terminology, L1 would roughly represent map scales of 1:50.000 to 1:10.000, L2 would correspond to 1:10.000 to 1:5.000, and L3 to 1:5.000 to 1:1.000 (Bundesamt für Umwelt (BAFU), 2011).

Chapter 3

The Rockfall Phenomena

Rockfall is a natural geological hazard that occurs when rock fragments detach from a steep slope or cliff, driven by gravity and other contributing environmental factors. Rockfalls represent one of the most rapid and unpredictable types of slope movement, often occurring with little or no warning. Although individual events may involve relatively small volumes of material, their high velocities and impact energies make them particularly dangerous for infrastructure, transportation corridors, human activities, and lives on their path.

3.1 Triggering Factors of Rockfall

Rockfall occurrence is controlled by a combination of long-term predisposing conditions and short-term initiating events. The long-term conditioning factors are intrinsic and slowly evolving characteristics of a slope that determine its susceptibility to rockfall. Key conditioning factors include lithology, rock mass strength, degree of jointing and fracturing, orientation of discontinuities, and presence of weathered areas, among many others. The short-term initiating events act as the trigger of the phenomenon; they represent the final cause that disrupt the balance between driving and resisting forces, consequently, setting the mass in motion. Depending on their origin, triggering factors can be classified into natural and anthropic.

Natural triggering factors include intense or prolonged rainfall, snowmelt, freeze-thaw cycles, seismic and volcanic activity, and strong temperature fluctuations. These processes can increase pore water pressure, induce crack propagation, or generate dynamic loading that leads to failure. In many mountainous and cold regions with rockfall predisposing conditions, seasonal climatic variations are a controlling factor in the temporal distribution of rockfall events.

Anthropic triggering factors, associated with human activities, also can disturb the natural equilibrium of slopes. These include vibrations induced by blasting operations in mining and quarrying, road and tunnel construction activities including slope cutting, and deforestation, among others. Such activities may act as direct triggers or may accelerate the ongoing degradation process, shortening the time to failure.

3.2 Rockfall Analysis

When characterizing an active rockfall area, a complete rockfall analysis is needed to fully comprehend the level of hazard affecting the zone. A rockfall analysis consists of two key components: the delimitation of the invasion area and the intensity of the rockfall event. This analysis aims at evaluating the trajectories and intensity of the potentially falling blocks; and it is essential for identifying vulnerable areas, the elements within them, and implementing effective stabilization or protection measures.

It is common to define three important zones on each slope affected by active rockfalls. Figure 3.1 represents these three zones, the uppermost is the release zone, also called source, which is the area where the rock blocks detach and the rockfall process is initiated. In most cases it corresponds to a bedrock outcrop forming a steep rock wall. The second zone is the transit zone, which is the area through which the falling rock traverses by means of different movement mechanisms. The last one is the deposit zone, the area where the rock blocks stop moving because its energy has been completely absorbed by the downslope movement process from its source.

There is an inevitable overlap between the transit and deposit zones because different blocks have varying shapes, sizes, and trajectories, dissipate energy differently along their path and stop at different spots along the slope.

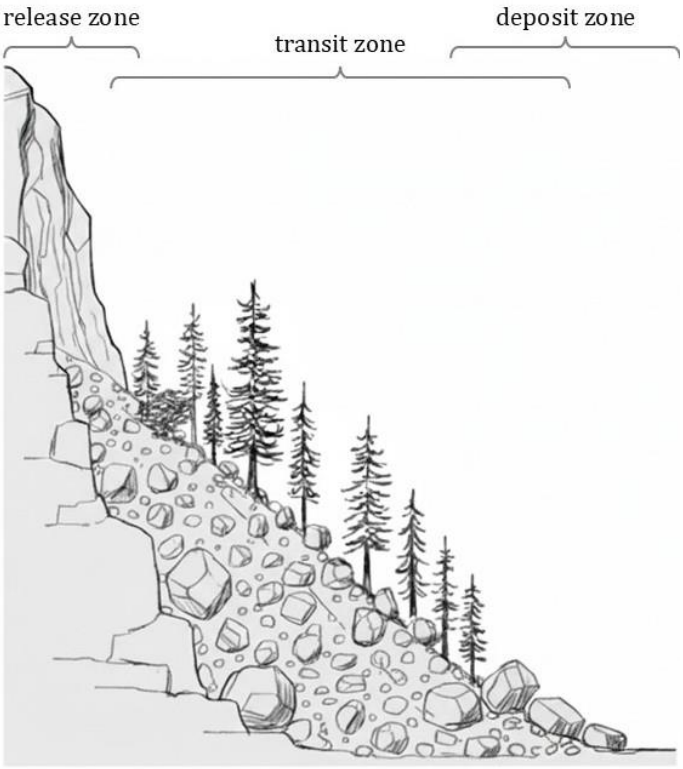

Figure 3.1 - Typical zones on a rockfall active slope (Lambert, *et al.*, 2011).

Applying the procedure introduced in Section 2.2.1, a workflow specifically for a rockfall affected area can be derived. Lambert, *et al.* (2011), in the book *Rockfall Engineering,* present an example of a workflow diagram applied to a rockfall trajectory study, which is reported in Table 3.1.

Table 3.1 - Workflow chart for a rockfall trajectory study (Lambert, *et al.*, 2011).

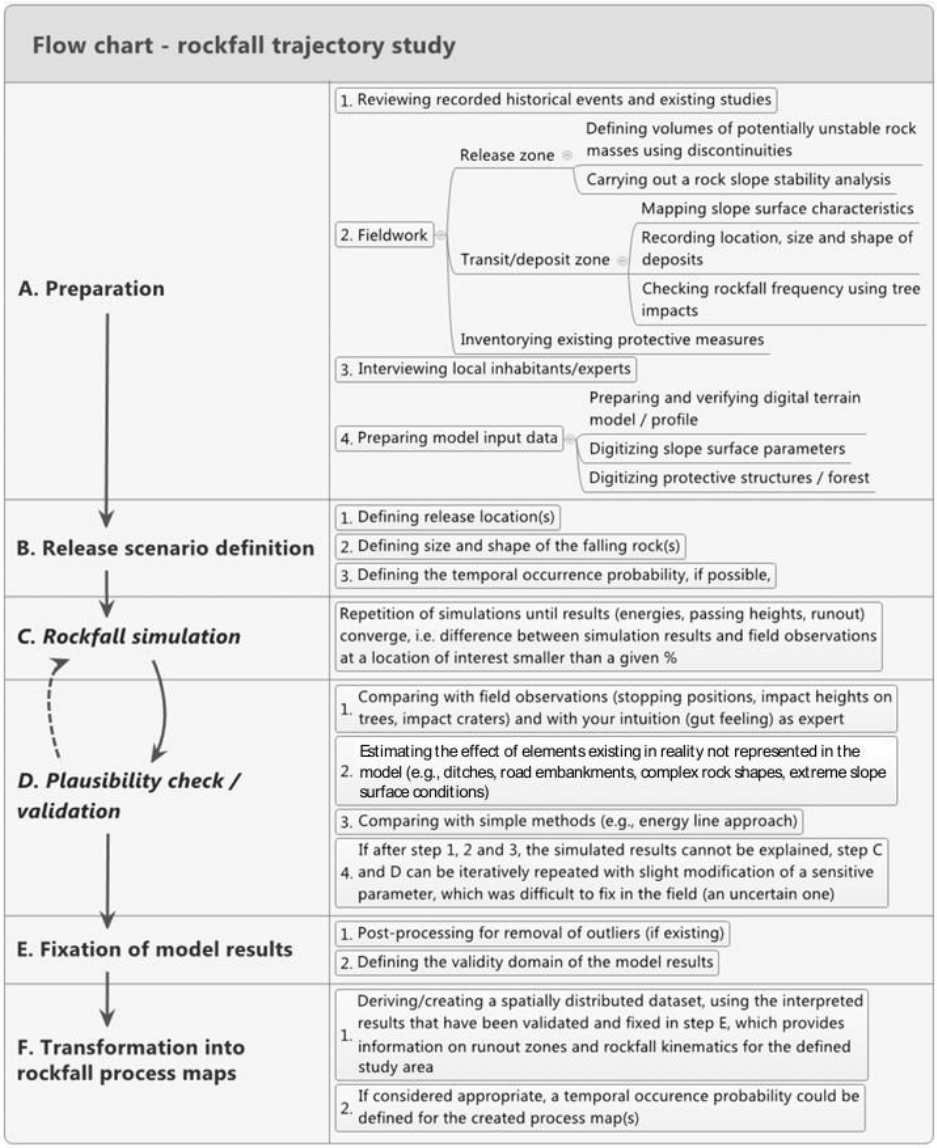

3.3 Characterization of Rockfall Release Areas

To assess the rockfall level of hazard or risk, the location of the potentially unstable rock areas must be identified, the block volume estimated, and their susceptibility to failure and event return time evaluated. The estimation of the temporal occurrence requires a detailed historical inventory of the rockfall events that have occurred in the area under investigation. In many cases, historical inventories are either non-existent or insufficient for an accurate analysis. Therefore, researchers often rely on susceptibility analysis to assess relative hazard, as these methods function independently of the temporal frequency of the events.

Several authors have proposed methods for assessing a relative hazard for these events. In this context, Napoli, *et al.* (2024) introduced a methodology based on a Susceptibility Index to Failure (SIF), designed to quantify the propensity of block detachment associated with rockfall events.

3.3.1 Susceptibility Index to Failure (SIF)

The SIF index can be defined based on the presence and intensity of a group of causative factors. These factors are classified according to the investigated environment, mountainous or coastal-marine, and the analysis scale, small or medium-large. In association with a suitable systematic method, the SIF index can be assigned to individual source points. This enables the implementation of a weighted frequency 3D runout analysis, leading to more reliable relative rockfall hazard, or susceptibility, and risk maps.

In order to assess the susceptibility to failure of the analysed sources, the main factors responsible for rock block detachment were selected for different scales of interest and environments according to a detailed literature review, these factors are presented in Table 3.2. The first part of the table includes the causative factors that are applicable to any territorial context, the final section contains those specific of a coastal-marine environment. Each factor (f) is ranked into classes to which a numerical score (P) is assigned, ranging from the lowest susceptibility to failure (0), to the highest (3). An exception is given by the presence of stabilization works if they are considered sufficiently efficient or effective in reducing the probability of block detachment; therefore, a negative score, up to a maximum value of -1 can be assigned.

By collecting information, conducting surveys and analysing the data, the presence and intensity of each causative factor can be determined. Subsequently, a rockfall Susceptibility Index to Failure (SIF), in the range 0 to 1, can be calculated and assigned to each rockfall source point considered, according to the following equation:

$$SIF = \frac{\sum(P_{fi}) - \sum min(P_{fi})}{\sum max(P_{fi}) - \sum min(P_{fi})} \in [0, 1] \qquad \textit{(Eq. 3.1)}$$

where *fi* is the ith factor of Table 3.2; P_{fi} is the weight assigned to the ith factor from the table; $\Sigma min(P_{fi})$ equals the summation of the minimum weights that can be assigned to all the factors; and $\Sigma max(P_{fi})$ equals the summation of the maximum weights that can be assigned to all the factors.

It is important to remark that if one or more of the factors cannot be evaluated or detected, the summations $\Sigma min(P_{fi})$ and $\Sigma max(P_{fi})$ must not take into account the contribution of these parameters. The reason to this is that since its weight cannot be defined it can only be assumed null, such consideration may underestimate its true influence, and the SIF index would be in some way affected by this assumption. On the contrary, if one or more parameters are present but they do not affect the study area, their weight is zero; however, their contribution is indeed considered in the calculation of the summations of the minimum and maximum weights, since their incidence on the stability of the rock blocks is relevant.

This consideration is particularly important for comparative analyses between sites that guide local authorities in prioritizing further investigations or implementing mitigation measures. With all other factors being equal, if a specific parameter is absent at one site but present at another, the resulting SIF index will differ. Consequently, this difference directly affects the rockfall susceptibility and hazard assessment, even if the same number of rock blocks could impact an element at risk, one site will present a higher relative hazard due to its greater SIF index.

Table 3.2 - Factors and relative weights for SIF index calculation (Napoli, *et al.*, 2024).

	Factors affecting the susceptibility to failure of potentially unstable rock blocks - SIF Index							
	WEIGHT, P / FACTOR, f	-1	-0,5	0	0,5	1	2	3
ANY TERRITORIAL CONTEXT	Slope angle			< 15°	15° - 30°	30° - 45°	45° - 70°	> 70°
	Rock mass structural conditions *			Massive rock with no or a few discontinuities. (Jn=0.1÷1)	One set of discontinuities. (Jn=2÷3)	Two set of discontinuities. (Jn=4÷6)	Three sets of discontinuities, rock mass subdivided into small cubes. (Jn=9÷12)	More than three sets of discontinuities, highly fractured rock mass. (Jn=9÷12)
	Condition of discontinuities *			Very rough surfaces; not continuous; no separation; unweathered wall rock.	Slightly rough surfaces; separation < 1 mm; slightly weathered walls.	Slightly rough surfaces; separation < 1 mm; highly weathered walls.	Slickensided surfaces or gouge < 5 mm thick or separation 1-5 mm; continuous.	Soft gouge < 5 mm thick or separation < 5 mm; continuous.
	Stability conditions (kinematic analysis and/or factor of safety)			Stable		Partially stable	Unstable	
	Fracturing degree of the rock mass **			Low		Medium	High	Very high
	Lithology (sensitivity to weathering processes such as rainfall, wind, sea spray, salt, etc.)			Good quality rock. Very low sensitivity to weathering process.		Medium quality rock. Low sensitivity to weathering process.	Soft rock. High sensitivity to weathering process.	
	Expected rockfall events			Few events (1/10 years); no rockfall scars.		Occasional events (3/years).	Many events (6/year); visible rockfall scars.	Numerous and frequent events (9/year).
	Water			Low precipitation; no water seeps.		Moderate precipitation; a few water seeps.	Intense precipitations; numerous water seeps.	
	Seismicity			Low	Moderate	High	Very high	
	Unstable blocks and/or overhanging sectors			None			Present	
	Aggravating conditions (presence of faults, low resistance interlayers, heterogeneity, karst features, etc.)			None	Present, low criticity.	Present, critical.	Present, very high criticity.	
	Lateral or foot erosion			None		Present		
	Stabilization works	Fully efficient/ effective	Partially efficient/ effective	None				
	Freeze-thaw cycles			None		Present		
MARINE ENVIRONMENT	Wave enargy			Low, or altitude of the source area sufficiently high.	Moderate, or high with favorable slope orientation (shore line subparallel to main storm wave fronts).	High, with adverse slope orientation (roughly shore-normal storm wave fronts).	Very high, with adverse slope orientation (roughly shore-normal storm wave fronts).	
	Cliff directly exposed to waves/tides/ abrasive action of sediments			Non applicable. Protective benches or engineering structures or high elevation.	Not high enough to exclude possible undirectly effects caused by waves and sea spray, with protective benches or engineering structures.	Not high enough to exclude possible undirectly effects caused by waves and sea spray, without protective benches or engineering structures.	Directly affected by waves sea spray, tides and abrasive action of sediments, without protective benches or engineering structures.	
	Coastal retreat rate *			Very limited / limited		Significant		

** detailed scale only* *** medium-large scale only*

3.4 Rockfall Risk Analysis

Risk analysis for rockfall events is based on probabilistic approaches that evaluate the potential effects of the phenomena and represents a fundamental tool for land-use planning and the design of structural mitigation works. In fact, the study of rockfall propagation is aimed at supporting risk analysis for the design of protecting measures intended to mitigate the associated hazard and risk.

The level of risk is defined as the product of three main components: (i) hazard (*H*); (ii) value of the element at risk (*E*), and (iii) vulnerability (*V*). Hazard represents the probability of occurrence of a potentially destructive event in a given area within a defined time interval. The elements at risk include all the constituents that can be exposed to the phenomenon. And vulnerability expresses the expected degree of damage suffered by the exposed elements. The interaction between hazards, exposure of the elements at risk and vulnerability allows for the definition of the expected level of risk for the area under analysis. In this context, a detailed understanding of the rockfall propagation process and the delimitation of the area of invasion is essential.

Hazard assessment is typically carried out with the aim of developing hazard maps, where each portion of the area under investigation is assigned with a specific hazard class associated to a probability of occurrence. The construction of these maps generally involves five main parts:

(1) Typological prediction, aimed at identifying the type of instability expected and selecting the appropriate modelling approach;
(2) Spatial prediction, which defines the potentially unstable areas;
(3) Temporal prediction, used to estimate the time interval in which the event may occur;
(4) Evolution prediction, concerning the expected development and spatial extent of the event;
(5) Intensity prediction, which evaluates the block volumes, velocity and the resulting kinetic energy value.

With specific reference to rockfall phenomena, risk analysis requires the implementation of models capable of reproducing the different phases of block motion, which will be explained on Chapter 4, as well as their frequency of occurrence and kinematic characteristics. As mentioned, the main objectives of rockfall modelling are the identification of the runout area and the assessment of the intensity of the event.

The runout area is identified as the envelope of all the possible block trajectories, extending from the detachment zone to the limit of the deposit area. This information is crucial if there are trajectories that may intersect the elements at risk, and the location of the stopping points helps to assess whether blocks can reach vulnerable areas downslope. The intensity of the rockfall event, generally expressed in terms of velocity or kinetic energy, is equally important as it defines the potential damage and determines the required energy absorption capacity of the protective structures.

Chapter 4

Fundamentals of Rockfall Dynamics

After the limit equilibrium conditions are reached and one of the acting agents generates the detachment of the block, downslope motion driven by gravity begins. Rockfall dynamics analysis is carried out by considering the motion of a single block that detaches from a steep rock wall and propagates along the slope, interacting with the terrain through impacts, rolling, bouncing and sliding mechanisms, with progressive energy dissipation that leads to the stopping of the rock block.

4.1 Detachment

The initiation of movement is generally determined by a shear or traction failure along a present discontinuity that divides the potentially unstable block with the stable part of the rock mass. The causes of failures have already been discussed in Section 3.1. When the block detaches, it may undergo immediate free fall with a purely vertical trajectory in cases where the rock wall is subvertical or has overhanging sectors, or it may topple, or slide on the wall itself when the stability conditions are overcome, as illustrated in Figure 4.1.

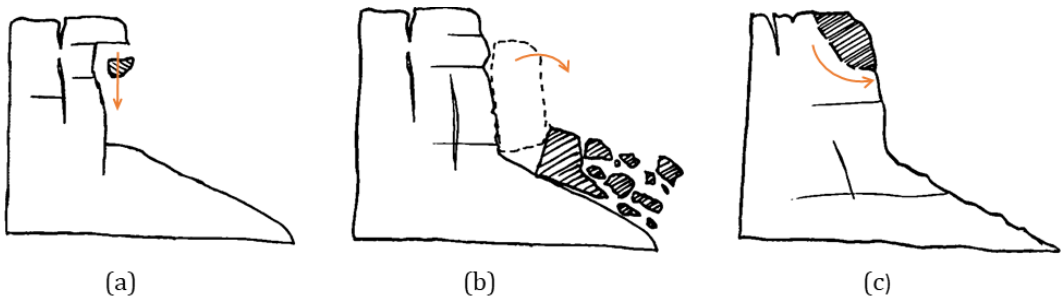

Figure 4.1 - Detachment modes; (a) free fall; (b) toppling and (c) sliding.

Following detachment, the rockfall enters its motion phase. Depending on the initial conditions, the detachment may involve a single block or a mass of blocks of varying sizes moving driven by gravity. It is worth mentioning that during movement, this block or mass can evolve into, or trigger, other instability phenomena, such as landslides or debris flow.

4.2 Motion in the Air

The free fall motion occurs when the block loses its contact with the slope. This can happen either after the detachment or along the downslope path where sudden changes in the topographic surface set off a new free fall motion. Classic free fall equations can be used to describe this phase. In any case, to understand the motion of the block, it is necessary to know the velocity immediately before and after the impact.

Under the assumptions of negligible air friction on the block, parabolic trajectory, and a two-dimensional motion problem; the impact point, determined by the intersection between the parabolic trajectory and a slope surface segment, illustrated in Figure 4.2, can be determined by solving the following system of equations:

$$\begin{cases} y = -\frac{1}{2} \cdot g \cdot \frac{(x - x_0)^2}{V_{0x}^2} + V_{0y} \cdot \frac{x - x_0}{V_{0x}} + y_0 \\ \frac{y - y_1}{y_2 - y_1} = \frac{x - x_1}{x_2 - x_1} \end{cases} \quad \textit{(Eq. 4.1)}$$

where, g is the acceleration of gravity, the starting point is $P_0(x_0, y_0)$, with the initial velocity is $v_0(v_{x0}, v_{y0})$, and $A(x_1, y_1)$ and $B(x_2, y_2)$ are points contained in the intersected slope segment. The solution of the system provides the coordinates of the impact point $P(x_P, y_P)$.

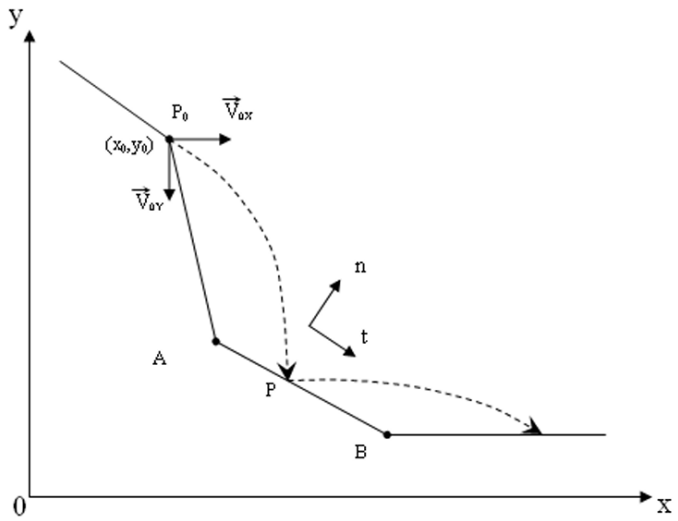

Figure 4.2 - Parabolic trajectory of the falling block (Giani, 1997).

4.3 Impact on the Slope

After motion in the air, the block once again comes into contact with the slope. The impact can be physically described as an impulsive event where the block arrives with a velocity having a given magnitude and direction relative to the slope surface. In the moment when the block collides with the slope, part of its kinetic energy is transformed into deformation of the ground and/or the block itself. If a significant amount of the energy is dissipated by the impact, the impact can be classified as inelastic. On the contrary, if the slope and the block are almost rigid elements and no appreciable deformation occurs during the impact, the energy loss is minimal and the block retains nearly the same kinetic energy after the impact; in this case, the impact can be considered elastic.

Taking into account that impact is a superficial phenomenon, it is sufficient to know the properties of the first couple of meters under the surface. In any case, the characteristics of the terrain are affected by a high level of uncertainty since they are no easy to determine, and the conduction of *in situ* tests become challenging when dealing with extensive and heterogeneous areas. For this reason, analysis are carried out in selected representative zones, and the resulting properties are then extrapolated to larger sectors. Given the large uncertainties, the problem of the impact dynamics can be simplified by introducing coefficients of restitution.

4.3.1 Restitution Coefficients

Restitution coefficients represent the ratio between the outgoing and the incoming velocity, that is, the ratio between the velocities after and before the impact. In this way, all the mechanical characteristics of the block and the slope surface are condensed into a single coefficient, representing the impact dynamics providing a measure of the energy dissipation as a consequence of the impact, without addressing the mechanical deformative process. Due to energy dissipation during impact, these coefficients are lower than the unit and it is common to express them in terms of their normal and tangential components:

$$R_n = \frac{v_n}{v_n'} \qquad R_t = \frac{v_t}{v_t'} \qquad \textit{(Eq. 4.2, Eq. 4.3)}$$

where, $v_{n,t}$ are the velocities after the impact, and $v_{n,t}'$ are the velocities before the impact. Figure 4.3 illustrates the instant of impact.

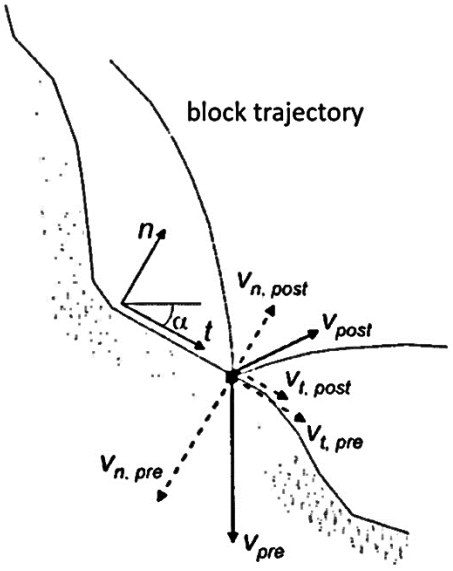

Figure 4.3 - Block's velocity components pre and post impact (Ribacchi, 2018).

Extensive data on restitution coefficients have been collected over the years by numerous authors, like the classification shown in Table 4.1, derived from *in situ* experimental tests, real cases observation or back analysis procedures. However, it is essential to highlight that these coefficients vary depending on site specific conditions. For this reason, back analysis plays an important role in case studies, where literature coefficients can be a starting point to the retrospective analysis of the event, but they might need to be adjusted in order to reproduce the event correctly.

Table 4.1 - Restitution coefficients (Pfeiffer, *et al.*, 1989).

Material	R_n	R_t
Bedrock or boulders with little soil or vegetation	0,33 – 0,37	0,83 – 0,87
Talus slope with little vegetation	0,30 – 0,33	0,83 – 0,87
Talus slope with some vegetation	0,30 – 0,33	0,80 – 0,83
Soft soil slope with little vegetation	0,28 – 0,32	0,80 – 0,83
Vegetated soil slope	0,28 – 0,32	0,78 – 0,82
Hard surface paving	0,37 – 0,42	0,87 – 0,92

4.4 Motion along the Slope

The behaviour of the block following the impact can vary. In the simplest case, all the energy that the block possesses is absorbed during the impact and the block stops its motion. More generally, however, the block undergoes bouncing, rolling, or sliding motion phases (Giani, 1997).

During a real case of downslope motion, the concepts of pure rolling or pure sliding are theoretical. When analysing these motion types with traditional dynamics approaches, the block is idealized as simple geometric shapes, such as spheres, ellipsoids or discs, and the slope is assumed to be perfectly planar. In reality, the irregularities of both the block and the slope surface invalidate these assumptions and, consequently, a redefinition of the problem is necessary.

Experimental observations (Azzoni, *et al.*, 1991) indicate that the motion more analogous to rolling is rotation in the air with multiple collisions. In order to simplify the problem, the mass is considered as a circular rigid body that rolls downslope in the presence of rolling friction. A scheme of the idealized model with all the parameters required to define the problem is shown in Figure 4.1.

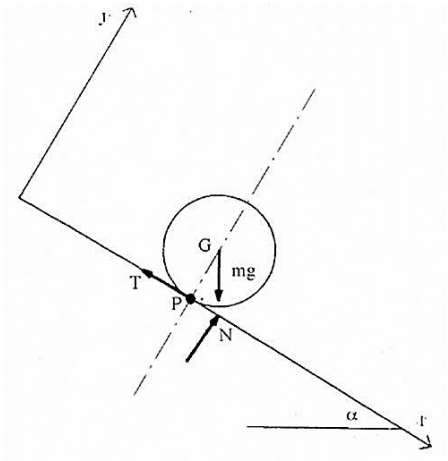

Figure 4.4 - Rolling phase motion (Giani, 1997).

The line of action of the normal force *N* does not intersect the point of contact between the block and the slope surface, instead, it has an eccentricity relative to it. This displacement of the application point of the normal force, generates a restoring moment, which is directly correlated with the rolling resistance. For a rock falling down a natural slope, this phenomenon is significantly more complex.

Resistance to motion occurs due to both the non-linearity of material behaviour and, more importantly, the irregular shapes of the rock and the rolling surface. Therefore, there is the need of consolidating this complex phenomenon into a single rolling friction coefficient, which can be calculated following the formulation proposed by Statham (1979) and Azzoni, *et al.* (1991):

$$tan\phi_{\mu d} = tan\phi_0 + K\frac{d}{D} \qquad \textit{(Eq. 4.4)}$$

where, $tan\phi_0$ is the dynamic rolling coefficient, K is a parameter obtained experimentally, d the characteristic diameter from the granulometry of the material composing the slope, and D is the diameter of the block. As for the restitution coefficients, values of the dynamic rolling coefficient are presented in the literature according to numerous authors.

4.5 Rock Block Shape and Volume Effects

Field observations of rockfall experiments allowed to highlight how blocks having different shapes and mechanical resistance follow distinct trajectories and exhibit different failure types during their motion along the slope. Blocks composed of relatively soft rock present polyhedral shape, this is because repeated impacts with the slope surface lead to progressive edge breakage. As impacts accumulate, blocks tend to evolve their motions due to the progressive forming of a more rounded shape, as shown in Figure 4.5.

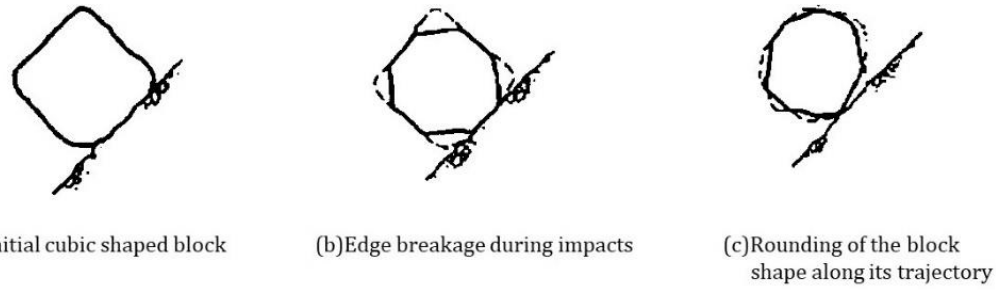

Figure 4.5 - Variation of the block shape during its trajectory (Giani, 1997).

In the case of blocks that detach from rock masses having a schistose structure, impact often induce failure along the schistosity planes, these fractures generate blocks with a tabular or laminar shape that will govern their motion mode.

Experimental investigation on *in situ* rockfall tests by Giani (1992) demonstrate that both shape and dimensions of the falling block significantly influence the post-impact behaviour. When prismatic blocks impact the slope with one of their faces, the most probable subsequent movement is the sliding, which persist until the slope surface conditions induce tipping or free fall. Alternatively, when impact occurs along the block edges, the most likely motion mode is tipping followed by rolling. These landing alternatives are schematized in Figure 4.6.

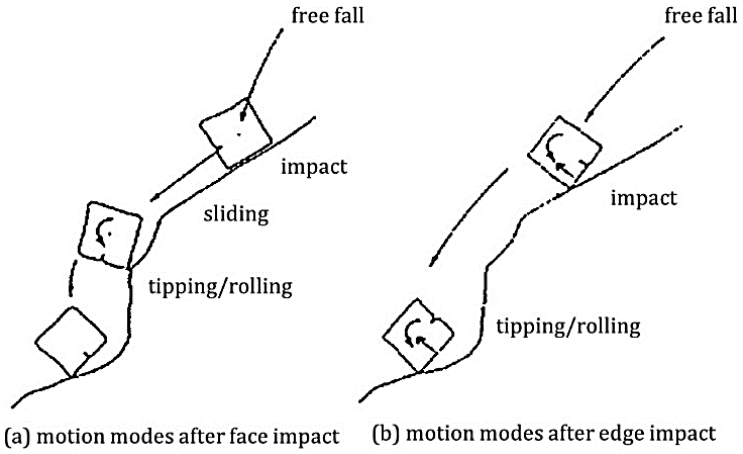

Figure 4.6 - Most probable motion modes after (a) face or (b) edge impact (Giani, 1997).

In addition, these *in situ* observations showed that if the block has a volume greater than the characteristic diameter of debris covering the slope, the impact results in a greater energy loss and the block tends to roll. If the slope surface is rough and undulated, rolling is combined with tipping. In contrast, if the block dimensions are lower than the characteristic diameter of the slope covering, the tipping mode is predominant over rolling with multiple impacts along the trajectory.

4.6 Vegetation Effects

Slope vegetation has a dual effect in the detachment phase of the rockfall phenomena. In wet climates that favour vegetation and particularly tree growth, roots can penetrate considerably into cracks on the bedrock surface, acting as a triggering agent to rockfall activity. Root growth is often strong enough to open and extend cracks and even create new fractures into the intact rock, allowing also for water infiltration and accelerate the weathering process. However, roots can also form a containing net for blocks attaching them to the slope, therefore, reducing its probability of detachment.

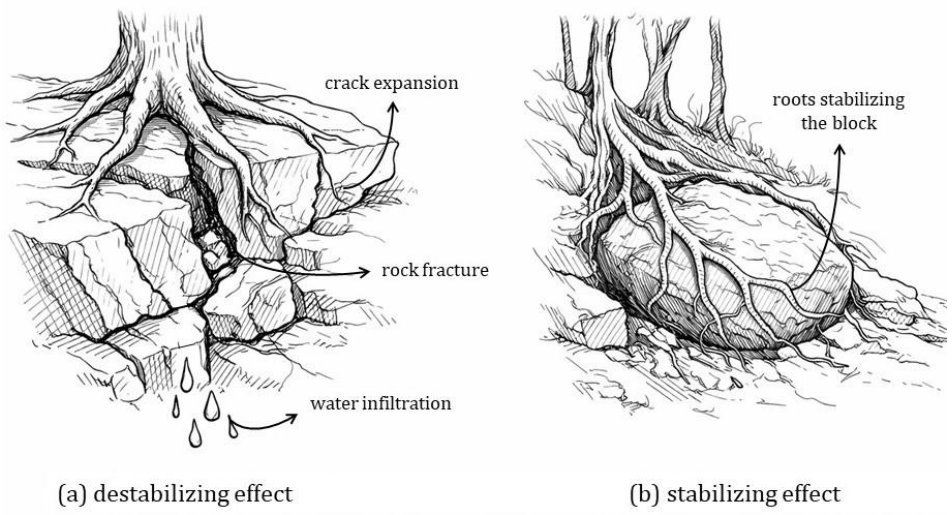

Figure 4.7 - Vegetation effects on detachment (AI generated image).

During rockfall dynamic phases, vegetation plays the role of a natural protection, deflecting, slowing and stopping falling blocks. The impacts against the trees follow the same rule as the block-slope impacts, with different magnitudes of restitution coefficients. These impacts can significantly influence the trajectory and energy dissipation of the falling block, depending on the forest density, as well as tree diameter, height, and species.

Chapter 5

Modelling Methods and Computational Tools

For the definition of the risk level, described in Section 3.4, it is necessary the implementation of an analysis model capable of describing the different phases of the block movement downslope, as well as the frequency of occurrence and the magnitude of the event in terms of kinematic variables. The objective is to identify the areas that might be impacted and to quantify the energies, passing frequency and bouncing heights of the falling blocks.

5.1 Rockfall Modelling

When modelling a dynamic process such as rockfall, one of the main challenges lies in the selection of input parameters, particularly those that strongly influence the results, such as slope roughness and restitution coefficients. For this reason, model validation, also referred to as back analysis, is always recommended; it is performed by comparing simulation outputs with observed events in terms of frequency, involved volumes, runout area, impact energy, and the resulting damage to the elements at risk. In the field of rockfall modelling, several classifications can be considered according to:

(a) Spatial representation:	Two-dimensional (2D)
	Almost three-dimensional (2.5D)
	Three dimensional (3D)
(b) Mathematical formulation:	Analytical approach
	Numerical approach
(c) Block modelling:	Lumped mass
	Rigid body
	Hybrid
(d) Simulation strategy:	Deterministic
	Probabilistic

Based on the spatial dimensions considered, 2D models simulate block motion along a singular longitudinal slope profile and assume that the block movement is confined to a vertical plane. Whereas computationally efficient, they do not capture lateral dispersion effects. Almost three-dimensional models extend the 2D approach by considering multiple slope profiles and introducing statistical variability to account for lateral dispersion, representing a compromise

between efficiency and physical realism. Finally, 3D models simulate block motion on a full spatial representation of the slope surface, allowing for free movement in all spatial directions. These models provide the most realistic description of rockfall trajectories and impact distribution but involve higher computational effort and more detailed input data.

According to the mathematical formulation used, models can be grouped into analytical and numerical models. Analytical rockfall models are based on simplified, close-form equations that describe the motion of a falling block using idealized assumptions. These models typically represent the block trajectory through basic kinematic relations and empirical rebound laws, and due to their simplicity, they are computationally efficient and suitable for a preliminary assessment; however, their limitation lies on their ability to represent complex slope geometries, block-slope interaction, and trajectory dispersion. On the other hand, numerical rockfall models simulate block motion through step-by-step integration of the governing equations of motion. This approach allows for a more detailed representation of the physical processes involved, including multiple impact phases, energy dissipation, and complex geometries interaction. Numerical analysis can be implemented in all the kinds of spatial representation. As a result, they are widely used for detailed hazard and risk assessments, despite requiring higher computational effort and detailed parameter calibration.

Considering how the falling block is represented, the models can be classified into lumped mass, rigid body or hybrid approaches. In lumped, or point, mass models, the block is idealized as a point having a defined mass, neglecting its shape and rotational motion. Energy losses during impacts are typically described using empirical restitution coefficients. Rigid body models represent the block with defined geometry and allow for both translational and rotational motion. This approach provides a more realistic description of block-slope interactions, but requires more complex contact formulations and, thereby, it has an elevated computational cost. Hybrid models combine features of lumped mass and rigid body approaches in order to balance efficiency and physical realism. In these models, the block is represented as a point mass during most phases of motion, while rotational effects or simplified geometric characteristic are introduced during impacts and rebound only. Hybrid approaches are particularly suitable for probabilistic analyses, where a large number of simulations is required while maintaining a reasonable level of physical consistency.

Finally, rockfall models can be classified according to the type of analysis adopted. Deterministic analysis use fixed input parameters and produce reproducible results for a given scenario. In contrast, probabilistic analysis accounts for the inherent variability and uncertainty of input parameters by assigning statistical distributions and performing multiple simulations. For this reason, the adoption of a probabilistic approach is recommended, as it allows the trajectory dispersion to be accounted for by considering uncertainties related to the detachment source location, block size, initial release conditions, slope characteristics, and the simplifications inherent in the model equations when compared to the real physical process.

In the following sections, a detailed description of the software tools that will be applied throughout the development of the case study will be provided. These tools were used for data processing, analysis, simulation and result validation. The following sub-sections describe the main functionalities of each software, the input and output data, and their role within the workflow.

5.2 Dips

Dips is a specialized graphical and statistical analysis software developed by Rocscience Inc. It is designed for the interactive analysis and visualization of orientation based geological data using the stereographic projection techniques described in Section 1.2.1. The program allows the user to examine structural data such as planes, poles, clustering, and intersections on stereonet projections, following the techniques used in traditional stereonet construction enhanced with computational features. In addition, many computational features are available, including statistical contouring of orientation clustering, mean orientation calculation and quantitative and qualitative feature attribute analysis.

The primary input data for Dips are discontinuity measurements expressed commonly as dip and dip direction, which may be obtained from geological structural surveys, boreholes, or digital mapping techniques; additional discontinuity properties such as the presented in Section 1.2.1 can also be included for the statistical analysis. The software process these data to produce graphical and statistical outputs.

5.3 QGIS

QGIS is an open-source Geographical Information System (GIS) software, created and supported by the Open-Source Geospatial Foundation (OSGeo), primarily used for the visualization, management, analysis, and interpretation of spatial and georeferenced data. It allows users to integrate data types, such as vector and raster layers, satellite imagery, and attribute tables, enabling visual analysis, mapping and data-driven decision making in academic, engineering and scientific applications. A key feature of QGIS are their extents through plugins that can be used to perform specialized tasks such as spatial analysis automation, terrain analysis and even rockfall runout analysis, allowing the software to be customized to meet the specific requirements of a given project or case study.

5.3.1 QPROTO plugin

The QPROTO plugin (QGIS Predictive ROckfall TOol) was created for implementing the well-known Cone Method in the QGIS environment. The Cone Method is a three-dimensional variation of the Energy Angle Method, a simplified model in which the complex dynamics of rockfall propagation are represented as an equivalent sliding motion of a rigid block along a straight line, referred to as energy line. The line connects the rockfall source to the farthest limit of the deposition area at the foot of the slope, and its inclination is defined by the energy angle (ϕ_p) (Castelli, *et al.*, 2021). This principle, illustrated in Figure 5.1, can be used to model the runout distances of moving masses. The rockfall velocity *v(x)*, and consequently the rockfall energy, at a given horizontal coordinate *x* given that the rock mass is known, can be easily calculated as it follows:

$$v(x) = f_v\sqrt{2g\Delta h(x)} \qquad \textit{(Eq. 5.1)}$$

where, f_v is a velocity correction factor, g is the acceleration of gravity and Δh is the height difference between the energy line and the topography at a given horizontal coordinate x. Assuming that the rotational energies represent around 20% of the total kinetic energy of a falling block, f_v is set to 0,9 (Lambert, *et al.*, 2011). Nowadays, the energy line principles are still commonly used in rockfall modelling, often in a 2D spatially distributed form.

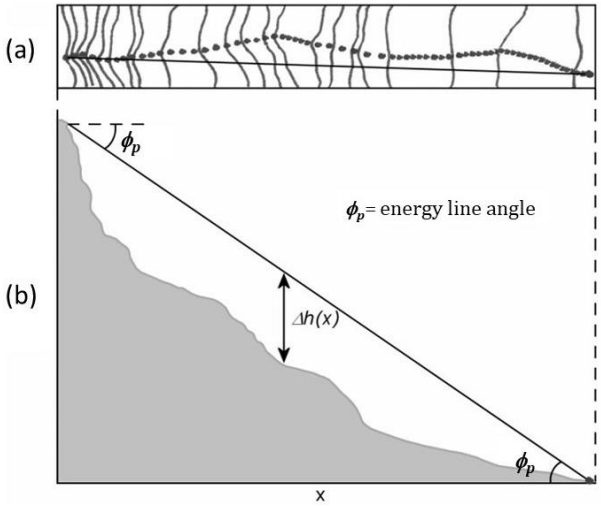

Figure 5.1 - Energy line principle, (a) aerial representation of a slope and rebound positions of a rockfall event; (b) slope cross-section with the energy line of the rockfall event (Lambert, *et al*., 2011).

As mentioned, the Cone Method is a three-dimensional variation of the Energy Line Method, where rockfall propagation is modelled by projecting a series of three-dimensional cones from the identified source points. These cones represent a potential energy dissipation envelope and are defined by an energy line angle and a lateral dispersion angle in the horizontal plane. The intersection between the cones and the digital terrain model delimitates the potential rockfall propagation area, as terrain cells located below the energy line are considered reachable by falling blocks. Through the Cone Method is also possible to evaluate the velocity *v(x,y*) of the falling block on a given point *P(x,y)* of the slope surface by using the following equation:

$$v(x,y) = \sqrt{2g\left[H(x_0,y_0) - h_p(x,y) - tan\phi_p\sqrt{(x-x_0)^2(y-y_0)^2}\right]} \qquad \textit{(Eq. 5.2)}$$

where, g is the gravity acceleration, x_0 and y_0 are the coordinates of the source point, $H(x_0,y_0)$ is the elevation of the source point, $h_p(x,y)$ the elevation of the topographic surface at $P(x,y)$ and ϕ_p the energy angle. In Figure 5.2, the heights at the location of point *P* are linked to the energy balance of the falling block. $H(x_0,y_0)$ represents the total energy content of the block, which is defined by the conservation principle as the sum of the potential $h_p(x,y)$ and kinetic $h_k(x,y)$ energy, considering also friction or dissipative contributions.

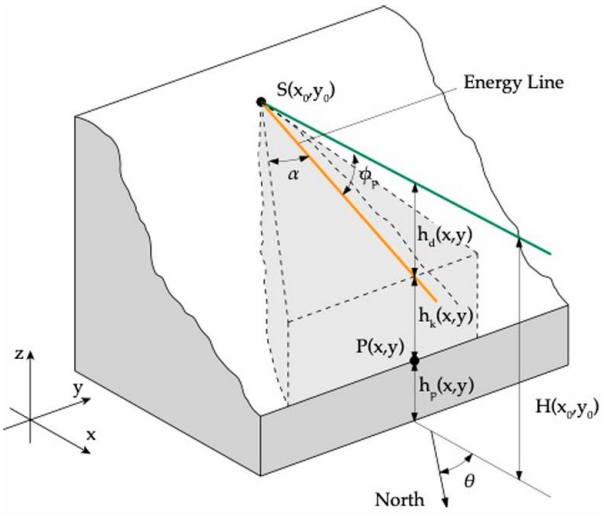

Figure 5.2 - Cone method representation (Castelli, *et al.*, 2021).

From the velocity, it is possible to obtain the kinetic energy at each point of the cone adopting the following relationship:

$$E_k(x,y) = \frac{1}{2} m[v(x,y)]^2 \qquad \textit{(Eq. 5.3)}$$

where, *m* is the mass of the block and *v(x,y)* is the velocity at point *P(x,y).*

It is important to consider that the calculated energy does not takes into account the combination of free flight, bouncing, rolling and sliding phenomena that actually occur during the propagation phase, all these movement mechanisms are simulated through an equivalent sliding motion. Energy estimation through the Cone Method can provide a preliminary assessment of the hazard, which is useful for identifying the most critical zones within a wide area in terms of both trajectory intensity and susceptibility.

The QPROTO plugin is based on GRAS GIS7 module *r.sviewshed*, which allows the evaluation of the visibility of surrounding areas from a given set of viewpoints, as illustrated in Figure 5.3. Each viewpoint represents the apex of a visibility cone covering a portion of the slope. As described previously, the geometry of the cone is defined by three angles: the dip direction, the energy angle, and the lateral dispersion angle (Figure 5.2). An additional visibility distance parameter, defined as visibility distance, delimitates the maximum extent of the analysis.

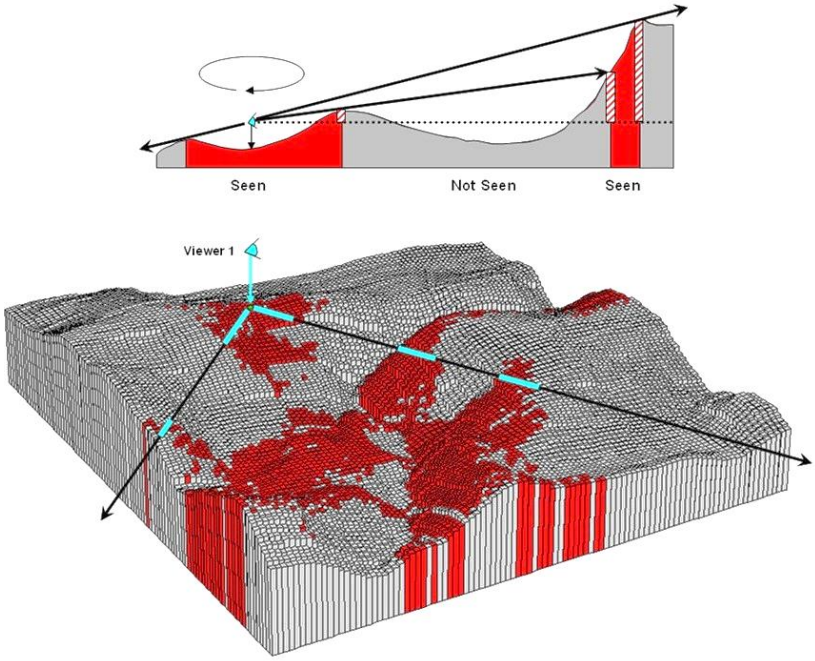

Figure 5.3 - Viewshed map creation (http://www.innovativegis.com).

Up to date, the QPROTO plugin is the only available tool that allows to assign different propensity detachment index, *i.e.* SIF index, to each source point, weighting and differentiating accordingly the most likely source areas to trigger rockfall events. The detachment propensity index allows the calculation of weighted frequency or susceptibility map and time-independent spatial hazard maps. The susceptibility map describes the spatial distribution of the rockfall event over the propagation area, highlighting the most affected areas with a simplified non-temporal probability of being reached. Time-independent hazard maps combine information of the detachment propensity of each source point with the estimated kinetic energy at each cell of the propagation area, in this way, each cell in the invasion area is associated with weighted energy values.

For a proper execution of the plugin, vector and raster files, and a set of source points, each representing a single block in the source areas, need to be created *a priori*. To each source point, the attributes listed in Table 5.1 have to be associated. Some of the mentioned attributes can be inferred with analysis tools from the DTM, such as point elevation and aspect; others have to be defined by the user on the basis of available information about slope geometry and condition, like the energy and lateral angles and the detachment propensity index. At last, boulder mass related to a specific scenario, characterized by a reference block volume.

Table 5.1 - List of attributes needed to perform a propagation analysis with the QPROTO plugin.

No.	Attribute	Description	Units
0	ID	identification number of the source point	-
1	ELEVATION	height of the source point a.s.l.	m
2	ASPECT	dip direction of the slope in the source point	°
3	ENERGY ANGLE	energy line angle of the cone with apex in the source point	°
4	LATERAL ANGLE	lateral angle of the cone with apex in the source point	°
5	VISIBILITY DISTANCE	distance to which the analysis can be extended	m
6	DETACHMENT PROPENSITY	detachment propensity index of each source point	-
7	BOULDER MASS	mass of the rock block	kg

The output of the QPROTO analysis are 10 raster files, listed in Table 5.2.

Table 5.2 - List of the QPROTO output files.

File name	Type	Description
count	Raster map	Number of source points that each cell can view
susceptibility	Raster map	Weighted view frequency
v_min	Raster map	Minimum computed block velocity
v_mean	Raster map	Mean computed block velocity
v_max	Raster map	Maximum computed block velocity
e_min	Raster map	Minimum computed block energy
e_mean	Raster map	Mean computed block energy
e_max	Raster map	Maximum computed block energy
w_en	Raster map	Maximum weighted kinetic energy
w_tot_en	Raster map	Total weighted kinetic energy
finalpoints	Shape file	Details on points located in the runout zone
log	Log text file	Report of the computed analysis

After the computation, the outputs are automatically loaded within the QGIS visualization screen. Velocity and energy raster values are expressed in m/s and Joules, respectively. The count and susceptibility files are associated with a qualitative classification on a five-level scale.

5.3.2 RADAR Plugin

Through the application of the RADAR plugin, the Source Affecting Index (SAI) can be determined. This index allows the characterization of the source areas according to their greatest affecting potential, *i.e.* source areas from which blocks impacting the selected elements at risk are most likely to detach. This approach is applied with reference to specific elements at risk located within the rockfall invasion zone and serves to the identification of critical sectors on the source area where additional surveys have to be carried out, and where monitoring systems or active mitigation structures can be most effectively installed to mitigate the overall risk (Milan, *et al.*, 2023).

The RADAR tool allows for implementing systematically this methodology for identifying the most influential rockfall sources with reference to specific elements at risk placed within the invasion area. The Ranking of Affecting Potential of Detachment Areas in Rockfall (RADAR) was introduced in the QGIS environment as a plugin.

The RADAR analysis uses the *finalpoints* vector file given as output by the QPROTO analysis; therefore, is designed to be used sequentially with QPROTO in QGIS. At the area of study, within the rockfall event invasion area, specific elements at risk can be selected. Each of these elements at risk is affected by different points belonging to the source areas with a given frequency, this means that there are sectors of the source areas that most affect the elements at risk. The inputs required for the RADAR analysis are:

(1) the *sourcepoints* vector file used in the preliminary runout susceptibility analysis conducted with QPROTO;
(2) the *finalpoints* vector file, output of the QPROTO analysis that represents the set of points visible from the source points, *i.e.*, the points that can be impacted by rockfall events originated from the source areas; and
(3) the *criticalareas* vector file, a set of polygons containing the elements at risk located in the invasion area, on which the RADAR analysis is focused.

The analysis begins by assessing the correspondence between the *sourcepoints* and the *finalpoints* within the *criticalareas*, collected in a vector file referred to as *finalpoints_crop*. Since multiple final points may overlap inside one cell affected by rockfalls from different sources, it is necessary to treat the overlapping final points as distinct entities. For this reason, for each source point, the number of points belonging to *finalpoints_crop* is determined and included in the attribute table of the *sourcepoints* vector as *Distinct_FP*.

This correspondence allows for the computation of the Geometrical Affecting Index (GAI), defined as the ratio between the corresponding *Distinct_FP* value and the total number of DTM cells contained in the *criticalareas* and containing at least one *finalpoint* cell associated, named *Total_DFP*; multiplied by 100. The index ranges between 0, for source cells that do not generate any *finalpoint* within the critical areas, and 100, with a maximum influence for source cells whose *finalpoints* intersect all the DTM cells of critical areas, and can be mathematically expressed as:

$$GAI\ (\%) = \frac{Distinct\_FP}{Total\_DFP} \cdot 100 \qquad \textit{(Eq. 5.4)}$$

Then, the GAI is combined with the SIF index associated with each source point to account for the detachment propensity of the source areas. This results in the SAI, which is added in the attribute table.

$$SAI(\%) = GAI \cdot SIF \qquad \textit{(Eq. 5.5)}$$

The resulting Source Affecting Index can therefore be interpreted as a weighted GAI that integrates the influence of slope morphology through the *viewshed* analysis, the physical characteristics of the falling blocks and the runout zone by means of the Cone Method analysis, and the stability conditions and runout susceptibility of the source zones through the SIF.

The final result of RADAR is the characterization of each source point with new attributes, specifically, *Distinct_FP*, *Total_DFP*, GAI, and SAI, described in Table 5.3, which can be used to create source influence maps.

Table 5.3 - List of attributes output of the RADAR plugin.

No.	Attribute	Description	Units
8	*Distinct_FP*	number of cells contained in the critical areas visible from a source cell.	-
9	*Total_DFP*	number of cells in the critical area containing at least one final point	-
10	GAI	Geometrical Affecting Index of the source point	%
11	SAI	Source Affecting Index of the source point	%

It is important to note that the GAI and SAI indices of a source point depend on the choice of the exposed elements, *i.e.*, the critical areas. A source point may strongly influence one exposed element, like a road, but it might less influential concerning another element, for example, a residential area. Consequently, the release relevance of the detachment points is not absolute, but rather related to the considered level of importance of the exposed elements.

This formulation can be applied to any spatial representation, including discrete grid cells, polygons, or points in a three-dimensional space. It provides a normalized measure of source influence on the elements at risk. The application of this approach allows the spatial distribution of the Source Affecting Index to be mapped, highlighting the most critical release areas. This type of analysis represents an effective tool for risk-oriented decision making, as it enables the concentration of mitigation measures on the most influential source areas, thereby improving the efficiency of both monitoring strategies and structural protection measures. This approach uniquely directs the analysis from the elements at risk toward the source area where rock blocks can detach, an inverted perspective to conventional methods that are applied from the source to the element at risk.

5.4 RockyFor3D

Rocktfor3D is a three-dimensional simulation model developed by ecorisQ that calculates trajectories of individual falling rock blocks. The model combines physically-based deterministic algorithms with stochastic approaches, thereby classifying as a probabilistic process-based rockfall trajectory model.

The model simulates the rockfall trajectories of blocks as 3D vector data, by computing sequences of basic parabolic free falls through the air and rebounds in the slope surface, as well as impacts against trees when applicable. Particularly, the rolling phase is represented as a sequence of short distance rebounds, while sliding of the block is not considered in the simulation. The model flow diagram is shown in Figure 5.4, where the coloured figures indicate modelling steps where changes in the fall direction of the simulated block may occur.

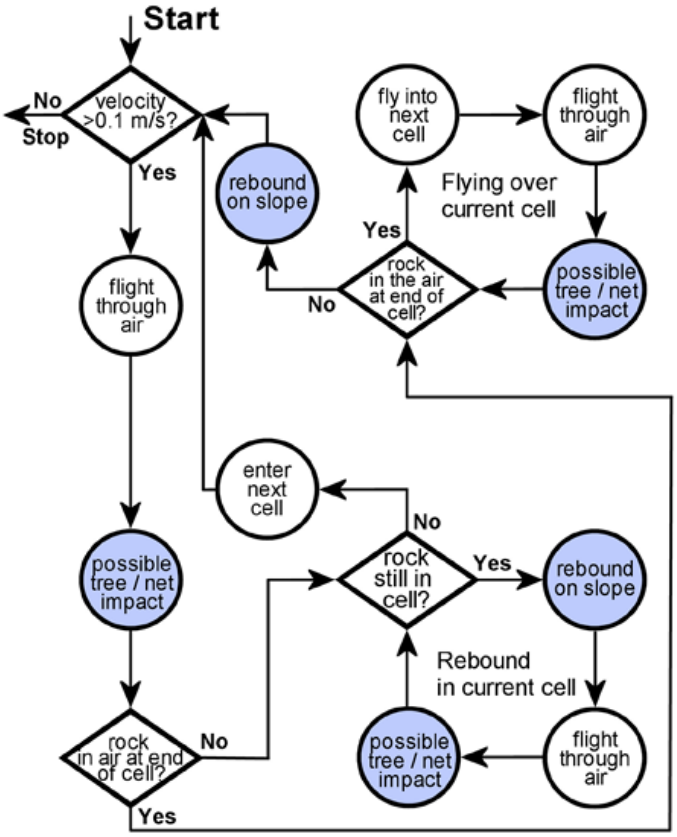

Figure 5.4 - Flow diagram of Rockyfor3D (Dorren, 2024).

5.4.1 Input Data

The minimum input data required by Rockyfor3D consists in a set of 6 raster files in ESRI ASCII grid format. All this raster maps are required to have the same map extent and the same cellsize. It is important to mention that with increasing cellsize both the spatial precision of the simulated maps and the accuracy of the simulated kinematics decrease; however, evidence demonstrated that an ideal resolution is 2 x 2 m and that smaller resolution does lead to trajectories that take excessively long to develop. In the following list, the 6 raster maps needed for the analysis will be described:

(1) *dem.asc*: a raster map of a Digital Elevation Model (DEM), which describes the topography of the area under analysis. From the DEM, the model calculates a slope map and an aspect map after the approach proposed by Zevenbergen, *et al.* (1987).

(2) *rockdensity.asc*: a raster map describing the block density on each source cell. Raster cells having a value of 0 will not be considered as source cells, while cells with a value between 2000 and 3400 kg/m^3 will simulate the fall of blocks.

(3)(4)(5) rg70.asc, rg20.asc, rg10.asc: three different raster maps defining the slope surface roughness, representing the blocks lying on the slope as the probability of a falling boulder impacting an obstacle of a given height. The *rg70* raster represents the height of a representative obstacle encountered in 70% of rebounds, *rg20* corresponds to 20% of rebounds, and *rg10 t*o 10% of rebounds within the defined area, as exemplified in Figure 5.5. Roughness values range from 0 to 100 m in all maps.

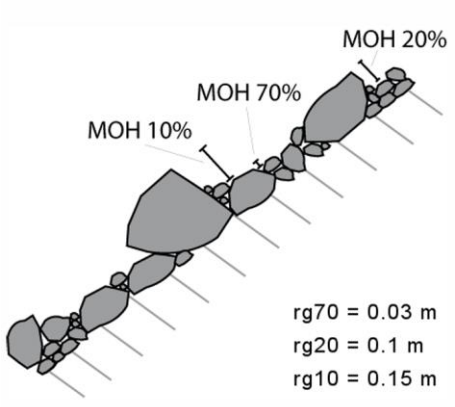

Figure 5.5 - Obstacle heights representative for the70%, 20% and 10% of the surface.

(6) *soiltype.asc*: a raster map defining, with a value ranging from 0 to 7, the type of ground present on the area and its elasticity. Rockyfor3D uses 8 soil types, listed in Table 5.4, directly linked to normal restitution values.

Table 5.4 - Soiltypes used by Rockyfor3D and the related R_n values.

Soiltype	General description of the underground	mean R_n value	R_n value range
0	river, or swamp, or material in which a rock could penetrate completely	0	0
1	fine soil material (depth >~100 cm)	0,23	0,21 – 0,25
2	fine soil material (depth <~100 cm), or sand/gravel mix in the valley	0,28	0,25 – 0,31
3	scree (Ø<~10 cm), or medium compact soil with small rock fragments, or forest road	0,33	0,30 – 0,36
4	talus slope (Ø>~10 cm), or compact soil with large rock fragments	0,38	0,34 – 0,42
5	bedrock with thin weathered material or soil cover	0,43	0,39 – 0,47
6	bedrock	0,53	0,48 – 0,58
7	asphalt road	0,35	0,32 – 0,39

The following raster maps are optional for the analysis, since these characteristics can be defined also by the user in the Graphical User Interphase (GUI).

(7) *d1.asc, d2.asc, d3.asc*: three raster files that allow for the definition of the size of the block for every start cell by providing a height, width and length value, between 0 and 20 m. The three block dimensions defined in each source cell are randomly varied according to a uniform distribution within the specified volume variation, between ±0% and ±50% in the GUI, before each simulation.

(8) *blshape.asc*: this raster map allows for a spatial definition of the shape of the falling block for each source cell. The shape figures, ranging from 0 to 4, are listed in Table 5.5.

Table 5.5 - Block shapes used by Rockyfor3D.

blshape	Block shape	Rule
0	no block defined / no source cell defined	
1	rectangular block	all three dimensions can be completely different
2	ellipsoidal block	all three dimensions can be completely different
3	spherical block	all three dimensions are identical
4	disc shaped block	smallest dimension is max. 1/3 of the other two larger dimensions

Following, the settings that can be defined directly within the graphical user interface (GUI), shown in Figure 5.6, will be described in detail.

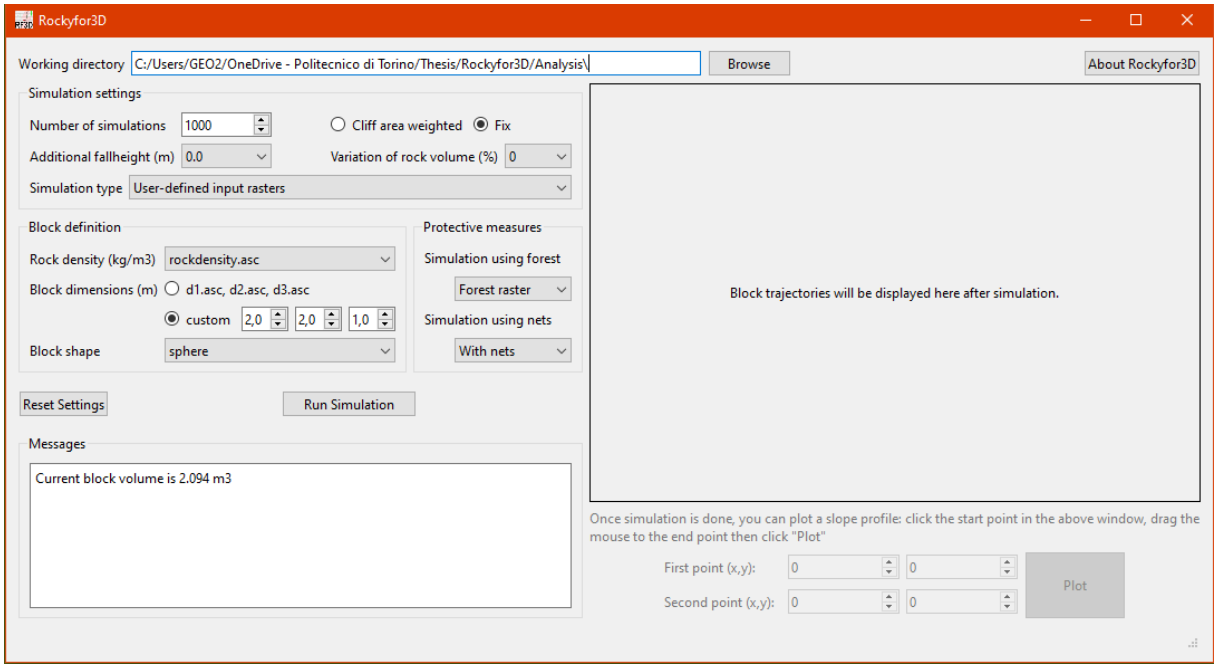

Figure 5.6 - Graphical User Interface of Rockyfor3D.

Simulation settings

- Number of simulations: defines the number of individual rockfall trajectories that will be simulated from each source cell.
- Option Fix/Cliff area weighted: Fix simulates the defined number of trajectories from all defined release cells. Cliff area weighted calculates the number of simulations per cell based on the cliff area with the ceil function, rounding the result up to the nearest integer, ensuring that the number of simulated trajectories is always a whole number:

$$Nr\_simulations_{cell} = ceil\left(\frac{0{,}5 \cdot Nr_{simulationsGUI}}{\cos(Slope_{cell})}\right) \qquad \textit{(Eq. 5.6)}$$

- Variation of rock volume (%): the percentage with which the three defined block dimensions will be randomly varied during each single trajectory simulation. The default value is 0%.
- Additional initial fall height (m): this is the height above the DEM surface from which the block will be released. This allows for an increase in the initial vertical velocity of the simulated block.
- Simulation type
  - Using input rasters: the simulation will run based on the raster files present in the working directory, *rg70.asc*, *rg20.asc*, *rg10.asc*, and *soiltype.asc*.
  - Rapid automatic simulation: Rockyfor3D will create the required input rasters of roughness and soil type based on the slope gradient and the following rules:

Terrain	Soil type	Low roughness			Medium roughness		
		rg70	rg20	rg10	rg70	rg20	rg10
source area	6	0	0	0	0	0	0
slope > 38°	5	0,05	0,05	0,10	0,05	0,10	0,10
slope 32°-38°	4	0,05	0,10	0,20	0,10	0,20	0,30
slope 20°-32°	3	0,05	0,10	0,15	0,10	0,15	0,25
slope 10°-20°	2	0	0	0,10	0	0,10	0,10
slope < 10°	1	0	0	0	0	0	0

Block definition

- Rock density (kg/m^3): the rock density can be defined either by the input raster *rockdensity.asc*, which also defines the source areas location, or by inputting a value in the GUI. In the latter case, the start positions will be defined automatically on those cells exceeding a slope gradient threshold. This threshold, after the studies conducted by ARPA Piamonte, *et al.* (2008), is only dependent on the resolution of the *dem.asc*:

$$\alpha = 55 \cdot cellsize^{-0{,}075}$$

- Block dimensions (m): these can be defined by the user input rasters *d1.asc*, *d2.asc*, *d3.asc*, or by an input values on the GUI.
- Block shape: can be defined either with an input the raster *bl_shape.asc* or in the GUI.

Protective measures

- Simulation using forest: defines if forest is accounted for in the simulation or not. If selected input forest raster files should be present in the working directory.
- Simulation using nets: defines if nets, or calculation screens, are taken into account in the simulation or not. If activated, necessary raster files should be available.

Other initial parameters fixed by Rockyfor3D are the initial horizontal velocity V_h*=0,5 m/s* and the vertical velocity V_h*=-0,5 m/s*. The vertical velocity component at the first impact can be increased by rising the additional fall height.

Simulation with Forest

If a simulation that considers the effect of a forest present at the studied site is required, Rockyfor3D has two options for integrating forest data in the input. The first option consists in using a text tree file, containing the *x* and *y* coordinates of each and every single tree, as well as the stem diameter measured at breast height (DBH) in cm, presented in tree columns without a header. This tree file needs to be called *treefile.txt* and should be available in the working directory along with the minimum required input files. In addition to the *treefile.txt*, a raster called *conif_percent.asc*, with their cells representing the percentage of coniferous trees on each forest zone, also needs to be available in the working directory, with values ranging from 0 to 100%.

The second option to represent the forest in the simulation is by means of four raster maps, these being:

(9) *nrtrees.asc*: the cell values represent the number of stems per hectare, with values from 0 to 10000 stems/ha.
(10) *dbhmean.asc*: each cell represents the mean stem diameter measured at breast height, values range between 0 and 250 cm.
(11) *dbhstd.asc*: each cell represent the standard deviation of the DBH values, from 0 to 250 cm.
(12) *conif_percent*.asc: the cell values represent the mean percentage of coniferous trees within each forest area, value range from 0 to 100%.

Figure 5.7 shows a workflow for creating the forest raster maps required for this option. All forest rasters need to have the same map extent and same cellsize as the raster *dem.asc*. Based on these four raster files, the model randomly places the given number of trees within each pixel with given diameters. The attribution of the DBH is based on the gamma distribution with its shape and scale parameters defined by the mean value and standard deviation data given. Finally, it creates a tree file containing the *x* and *y* coordinates of all trees and their DBH.

Step 1: Digitise a polygon vector forest map

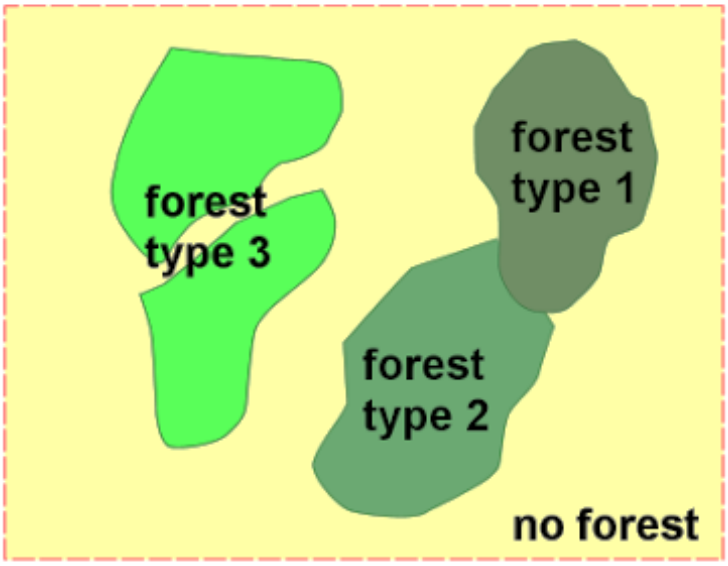

Step 2: Enter forest attribute data

stand	nrtrees	dbhmean	dhbstd	conif_percent
1	290	32	11	56
2	400	27	9	26
3	800	20	5	0

Step 3: Convert the vector map into rasters using the different attribute fields

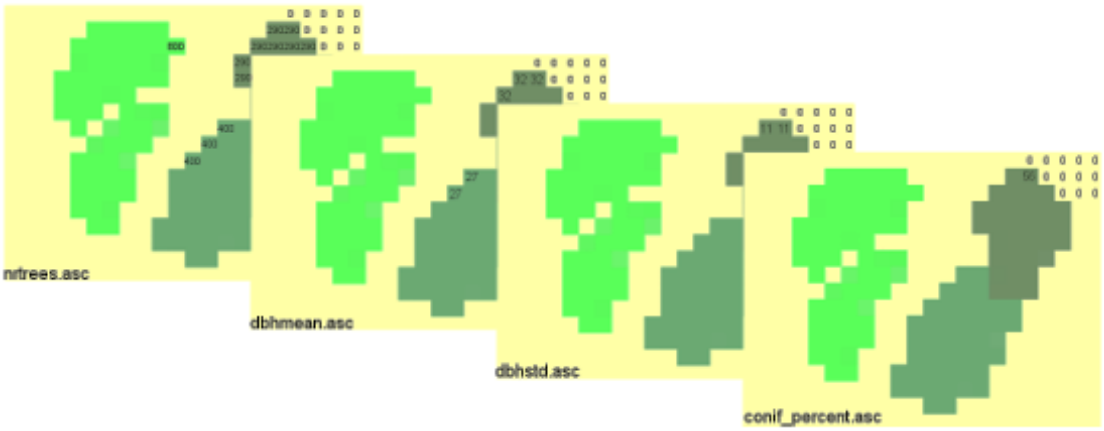

Figure 5.7 - Workflow for creating the forest maps required in option 2.

The advantage of the first option is that a horizontal forest structure is well represented, this means that the important rockfall corridors and large dominant trees are captured in a more precise way. On the other hand, an extensive *in situ* survey is needed to consider all trees location and diameter. The second option required very accurate and time-extensive digitalizing work to achieve a similar structural precision, but it better shows the smaller trees, which, even though small, still help protect the slope along with the large dominant trees.

Simulation with Rockfall Nets and Control Screens

If a simulation with rockfall nets is required, the following three raster files should be available in the working directory:

(13) *net_number.asc*: constitutes an identification number for each one of the nets.
(14) *net_energy.asc*: represents the energy absorption capacity of the net, with a maximum value of 20.000 kJ.
(15) *net_height*: vertical dimension of each net up to 10 m, measured normal to the slope surface.

These files can be created using vector to raster conversion of one or multiple lines, which have as attribute their identification number, energy capacity and height. It is important to remark that these lines should not intersect each other. Again, all rockfall net rasters need to have the same map extent and same cellsize as the raster *dem.asc*.

When a simulation with rockfall nets is carried out, relevant and detailed data of the rockfall kinematics are collected when blocks intersect the nets, which act as control screens. This data is saved in a text file called *Rockyfor3D_v6_ CalC_SCR_dd-mm yy_HHhMM.txt*. The following data is recorded for each block arriving in the net:

(a) velocity (m/s)
(b) kinetic energy, both translational and rotational (kJ)
(c) vertical passing height (m)
(d) rotational velocity (rad/s)
(e) impact angle, angle between a horizontal plane and the trajectory of the block the moment the block arrives in the net; negative value means a descending block, positive value means an ascending block (degrees)
(f) passing height, normal to the slope surface (m)

In addition, the total number of blocks arriving in the net is recorded. The output text file contains both post-processed and raw simulated data for each calculation screen. The post-processed data include the median as well as the 90%, 95%, and 98% values (respectively x50, x90, x95, and x98) of the probability density function for variables (a) to (e) described above, for each calculation screen.

By using a rockfall net having both energy level and height equal to zero, the data can be efficiently collected along a given line, allowing for the representation of a rockfall event in the absence of intersecting elements.

5.4.2 Dynamic Characteristics of the Model

Block Motion Dynamics

The selected block shape determinates the block volume, and consequently its mass, and the moment of inertia. Both values are calculated based on the three defined block dimensions following the code from Figure 5.8.

For calculating the block position, the rebound on the slope surface and impacts against trees, Rockyfor3D always considers a spherical shape. Two characteristic diameters are defined for this sphere: the smallest of the three dimensions *d1*, *d2*, and *d3*, which is used to compute impacts against trees; and a larger diameter, defined as the mean of the two largest dimensions among *d1*, *d2*, and *d3*.

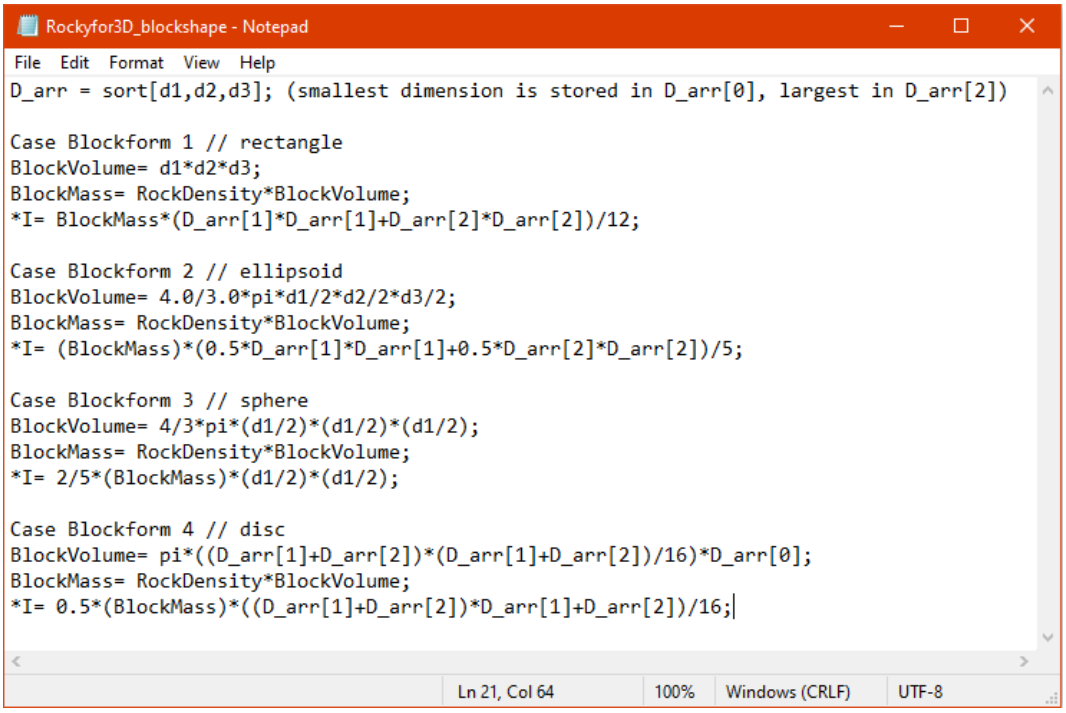

Figure 5.8 - Block physical parameters calculation in Rockyfor3D.

The parabolic free fall is computed with a standard algorithm or a uniformly accelerated parabolic movement through the air, it allows for determining the position and the velocity at the intersection with the slope, represented by the DEM. Rockyfor3D simulates fully three-dimensional trajectories by calculating the position along the *x*, *y*, and *z* axes. The *x*-axis corresponds to the East-West direction, the *y*-axis to the North-South direction, and the *z*-axis to its vertical position.

The velocity after a rebound on the slope surface, or simply bounce, is mainly calculated with ten functions. As illustrated in Figure 5.9, the first step is the conversion of the incoming velocity in the horizontal plane *x*-*y* (V_h) and the one in the vertical plane *z* (Vv) into an incoming normal V_n and tangential V_t velocities.

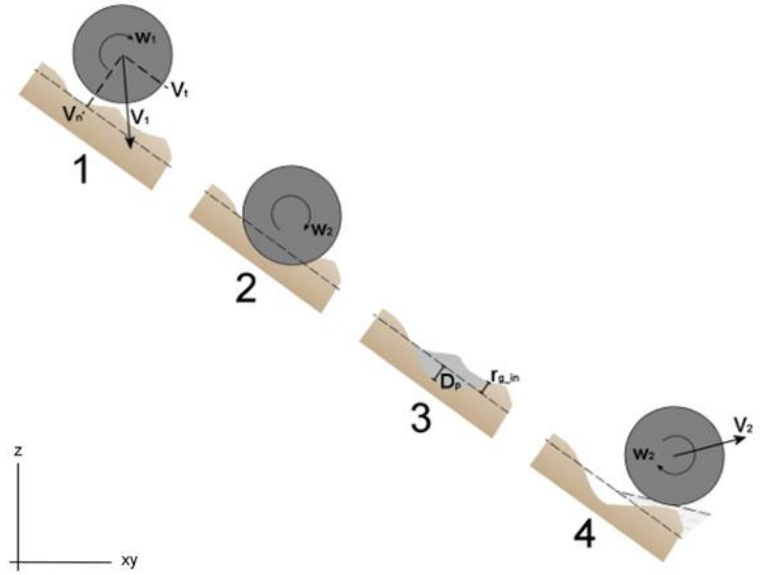

Figure 5.9 - The rebound as represented by the algorithms used by Rockyfor3D.

Then, the penetration depth of the block at the impact location is calculated in accordance to Picher, *et al.* (2005), with the required input data being:

- The normal coefficient of restitution (R_n)
- The diameter of the block in m (d)
- The mass of the rock in kg (*RockMass*)
- The impacting velocity of the falling block in m/s (V)

The constants used are:

- k = 1,207, dimensionless constant accounting for the spherical block shape.
- B = 1,2, dimensionless compressibility parameter of the impacted material, which varies little for different surface materials.

The main penetration depth (D_p) functions are:

$$\frac{D_p}{d} = \frac{2}{\pi} N \, ln\left(\frac{1 + I_e/N}{1 + k\pi/4N}\right) + k \quad \text{for } \frac{D_p}{d} > k \qquad \textit{(Eq. 5.7)}$$

$$\frac{D_p}{d} = \sqrt{\frac{1 + k\pi/4N}{1 + I_e/N}} \frac{4k}{\pi} I_e \qquad \text{for } \frac{D_p}{d} \leq k \qquad \textit{(Eq. 5.8)}$$

where, the moment of inertia,

$$I_e = \frac{RockMass \cdot V^2}{R_i \cdot d^3} \qquad \textit{(Eq. 5.9)}$$

where R_i is the identation resistance of impacted material in MPa, calculated as following:

$$R_i = 55 \cdot 10^9 \cdot R_n^7 \qquad \textit{(Eq. 5.10)}$$

The N function ranges between 1 and 5 MPa for fine soil and 200 to 250 MPa for bedrock.

$$N = \frac{RockMass}{\rho_{soil} \cdot d^3 \cdot B \cdot 0{,}5} \qquad \textit{(Eq. 5.11)}$$

where ρ_{soil} is the density of the impacted material in kg/m^3, which is calculated with:

$$\rho_{soil} = \max(1000; 1200 \cdot \ln(R_n) + 3300) \qquad \textit{(Eq. 5.12)}$$

This function provides values between 1400 kg/m^3 for fine soil and 2650 kg/m^3 for bedrock.

In Rockyfor3D, the maximum penetration depth D_p equals the simulated block radius. After the penetration depth is calculated, the calculation of the block velocity after rebound can be initiated. An important parameter for calculating the velocity of the block after the rebound is the tangential coefficient of restitution (R_t). Many authors showed that R_t is determined by the composition and size of the material covering the surface and the radius of the falling block itself. Dorren, *et al.* (2006) proposed the following calculation method for this coefficient:

$$R_t = \frac{1}{1 + ((MOH + D_p)/R)} \qquad \textit{(Eq. 5.13)}$$

where, *MOH* is the representative obstacle height at the slope surface, D_p is the penetration depth, and *R* is the radius of the falling block, with all dimensions expressed in meters. Three *MOH* classes, representative for the mean obstacle height a falling block can encounters during 70%, 20% and 10% of the rebounds, are mapped. For each rebound, the model selects the *MOH* randomly based on these classes, the resulting values from *rg70*, *rg20* and *rg10* are used in the 70%, 20% and 10% of rebound calculations, respectively. Also, prior to compute R_t, the model randomly varies it by ±10% to account for natural variations in surface roughness. The obtained R_t is used for calculating the tangential velocity component of the block after the rebound (V_{t2}) following Pfeiffer, *et al.* (1989) and Nöel, *et al.* (2021):

$$V_{t2} = \sqrt{\frac{R^2 \cdot (I \cdot V_{rot1}^2 + RockMass \cdot V_{t1}^2) \cdot F_f \cdot S_f}{1 + RockMass \cdot R^2}} \qquad \textit{(Eq. 5.14)}$$

where, V_{t1} is the tangential velocity component of the block before the rebound, V_{rot1} is the rotational velocity before the rebound and *I* is the moment of inertia of the defined block form.

$$F_f = R_t + \frac{1 - R_t}{1.5 + \left(\frac{V_{t1} - V_{rot1} \cdot R}{3{,}048}\right)^2} \qquad \textit{(Eq. 5.15)}$$

$$S_f = \frac{R_t}{1 + \left(\frac{V_{n1}}{15{,}24}\right)^2} \qquad \textit{(Eq. 5.16)}$$

The normal coefficient of restitution (R_n) is used for calculating the normal velocity component of the block after the rebound V_{n2} following Pfeiffer, *et al.* (1989):

$$V_{n2} = \frac{-V_{n1} \cdot R_n}{1 + \left(\frac{V_{n1}}{9{,}144}\right)^2} \qquad \textit{(Eq. 5.17)}$$

where, V_{n1} is the normal velocity component of the block before the rebound. The factor $(V_{n1}/9{,}144)^2$ adjusts for the decrease in normal coefficient of restitution as the impact velocity increases. This factor represents a transition from more elastic rebound at low normal velocities to much less elastic rebound caused by increased fracturing of the block and cratering of the slope surface at higher normal velocities.

The rotational velocity after the rebound V_{rot2} is calculated as:

$$V_{rot2} = min\left[\frac{V_{t2}}{R};\ V_{rot1} + \frac{2 \cdot (V_{t1} - V_{t2})}{5 \cdot R}\right] \qquad \textit{(Eq. 5.18)}$$

The maximum value of V_{rot2} in radians finally depends on the block shape,

$$V_{rot2} = min\left[V_{rot2};\ S \cdot RockMass^{-\frac{1}{3}} \cdot \pi/180\right] \qquad \textit{(Eq. 5.19)}$$

where, for blocks where one block dimension is at least 50% smaller than both other dimensions *S=12.480*, and for all other blocks, *S=9.278*.

The last steps of the rebound calculation consist of verifying if sufficient energy has been lost during the rebound. This checking is done on the basis of the relationship between the total deviation angle (TOT_{dev}) and the total energy loss by Nöel, *et al.* (2023). If the total deviation is larger than 55°, then the ratio between the total kinetic energy before and after the rebound (E_{ratio_impact}) cannot be larger than:

$$E_{ratio\_impact}: -0{,}01 \cdot TOT_{dev} + 1{,}3 \qquad \textit{(Eq. 5.20)}$$

If required, the E_{ratio_impact} value is used to scale down the tangential, normal, and rotational energy components such that their proportions remain unchanged with respect to the total kinetic energy after the rebound.

Following Pfeiffer, *et al.* (1989), the slope angle at the rebound location is uniformly randomly reduced at each rebound; however, the maximum reduction in the slope angle is limited to 4°. Rolling motion is represented as a sequence of short-distance rebounds, with the spacing between successive rebounds equal to the block radius and an absolute minimum distance of 0,2 m. This minimum distance condition applies only to slopes with gradients lower than 30°.

Impact against Trees

Due to the fact that the model uses analytical solutions instead of time step iterations, the exact position of the simulated block is constantly known. Therefore, the impact position on the digitally generated tree stems and its influence on the energy dissipation during such impacts can be calculated. In addition to the impact position on the tree stem, the model uses the diameter of the impacted tree, the tree type, coniferous or broadleaved, and the block energy. If an impact against a tree takes place, the block loses a fraction of its kinetic energy according to four main functions, which are visualised in Figure 5.10.

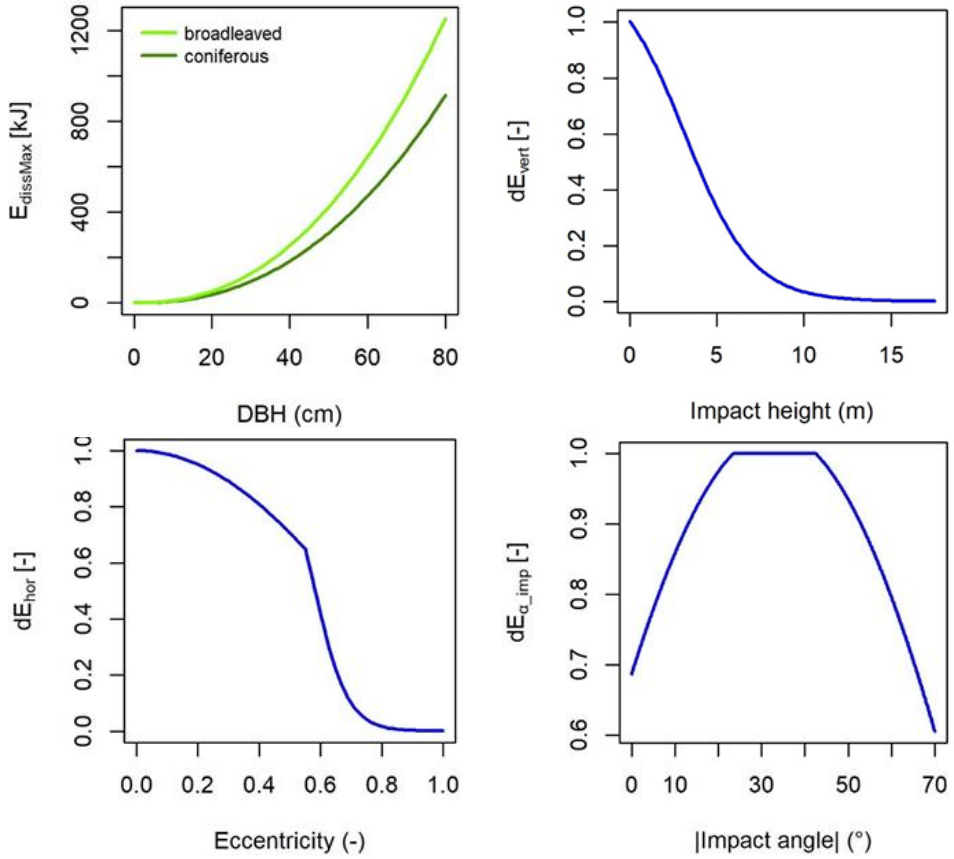

Figure 5.10 - Functions for calculating the energy dissipation during a block-tree impact.

Following Dorren, *et al.* (2005), the maximum amount of kinetic energy ($E_{dissMax}$) that could be absorbed and consequently dissipated by a tree impact is determined by the stem diameter and the tree type following:

$$E_{dissMax} = FE_{ratio} \cdot 38{,}7 \cdot DBH^{2{,}31} \qquad \textit{(Eq. 5.21)}$$

where, $E_{dissMax}$ is the maximum amount of kinetic energy that can be dissipated by the tree J, FE_{ratio} is the fracture energy ratio of the tree type and the stem diameter at breast height (DBH) in cm. Rockyfor3D uses only two standard values for the $FE_{ratio,}$ 0,95 for coniferous trees and 1,3 for broadleaved trees. There is also an option to provide custom tree energy dissipation factor for every single tree in the treefile.txt. To do so, the tree factors should be given after the *x*-coordinate, *y*-coordinate and the DBH of each tree. Whether this maximum amount of energy is indeed dissipated during the impact depends on the horizontal and the vertical position of the impact on the tree stem, classified according to Figure 5.11.

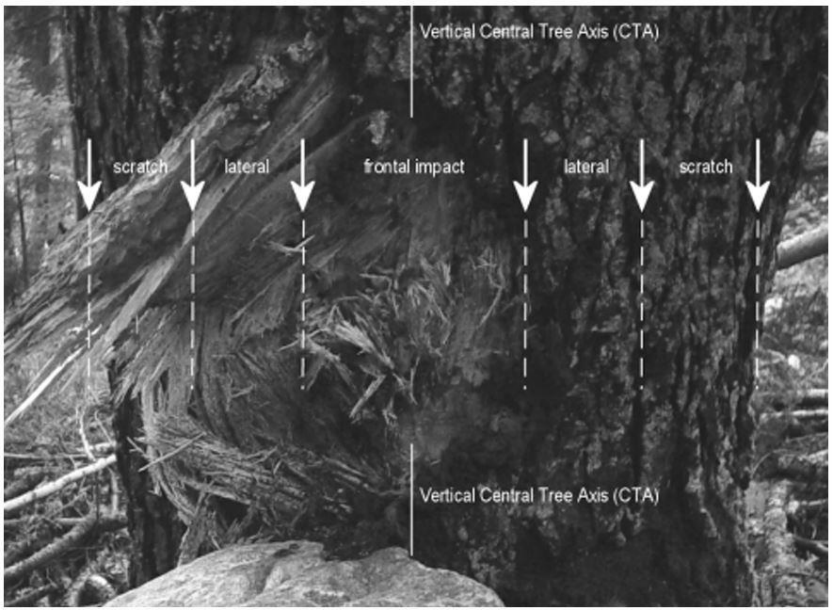

Figure 5.11 - Impact types based on the horizontal distance between the block centre and the tree axis.

The effect of the horizontal position (dE_{hor}) is determined by following the functions (Dorren, *et al.*, 2005):

$$Dist_{IPCT} = \frac{\overline{P_i\ CTA}}{0{,}5 \cdot DBH} \qquad \textit{(Eq. 5.22)}$$

$$dE_{hor} = cos\left(Dist_{IPCT} \cdot \frac{\pi}{2}\right) \qquad \text{for } Dist_{IPCT} < 0{,}543 \qquad \textit{(Eq. 5.23)}$$

$$dE_{hor} = max\left[0, \frac{0{,}98+0{,}046}{1+10^{(-8\cdot(0{,}58-Dist_{IPCT}))}}\right] \qquad \text{for } Dist_{IPCT} \geq 0{,}543$$

where, dE_{hor} is the maximum amount of energy that can be dissipated by the tree, related to the horizontal position of the impact, P_i-*CTA* is the horizontal distance between the tree canter point and the impact point projected on the normal line from the tree canter to the fall direction before impact and the DBH in m.

The effect of the vertical position, or impact height, is calculated with the three following equations. Firstly, the theoretical height of the tree (H_{tree}) is calculated on the basis of the DBH:

$$H_{tree} = 1{,}22 \cdot DBH^{0{,}8} \qquad \textit{(Eq. 5.24)}$$

Then, the percentage of maximum amount of energy that can be dissipated by the tree (dE_{vert}), related to the vertical position of the impact (Z_i) is calculated following:

$$dE_{vert} = 1.2\left(\frac{1}{1+e^{18{,}04\cdot\left(\frac{Z_i}{H_{tree}}\right)+0{,}02\cdot DBH-2{,}35}} - \frac{1}{1+e^{15{,}69+0{,}02\cdot DBH}}\right) \quad \textit{(Eq. 5.25)}$$

The percentage of maximum amount of energy that can be dissipated by the tree, related to the impact angle (α_{imp}) of the block with respect to the vertical standing tree (dE_{α_imp}) is calculated following Jonsson (2007):

$$dE_{\alpha_{imp}} = min\left[1; (1{,}03 \cdot sin\left(1{,}46 \cdot \frac{min[\alpha_{imp}; 70]}{180°} \cdot \pi + 0{,}73\right)\right] \quad \textit{(Eq. 5.26)}$$

Finally, the total amount of energy dissipated during the tree impact ($E_{dissTree}$) is calculated:

$$E_{dissTree} = E_{dissMax} \cdot dE_{vert} \cdot dE_{hor} \cdot dE_{\alpha_{imp}} \quad \textit{(Eq. 5.27)}$$

Calculation of the Fall Direction

The fall direction of the simulated block is initially determined by the aspect of the source cell. Then, the direction of the falling block changes due to rebounds on the slope surface or impacts against trees. The deviation angle after a rebound on the slope surface is determined by the topography, the fall direction of the block before the rebound and the velocity of the falling block.

During each rebound, the model deviates the block from its original direction before rebounds towards the direction of the aspect of the raster cell in which the rebound takes place, as illustrated in Figure 5.12. The aspect represents the steepest slope direction in each neighbouring cell and is calculated following Zevenbergen, *et al.* (1987).

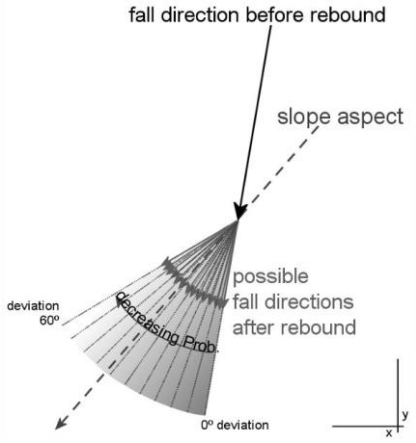

Figure 5.12 - Principle of the fall direction calculation after rebound on the slope surface.

How much the block deviates from its fall direction before the rebound towards the slope aspect in the raster cell is finally determined by a random number and the velocity of the block. The random number determines whether the block deviates from its original direction within angular intervals of 5°, ranging from 0° up to 55°. All these cases have predefined accompanying probabilities of occurrence, which are determined by the velocity of the block before the rebound as presented in Table 5.6. These values are based on statistical analysis of rockfall trajectories and velocities observed during rockfall experiments presented in Dorren, *et al.* (2006). If the block moves upslope during the simulation, the deviation ranges described here are allowed for both directions lateral to the direction before rebound. If the block enters a small depression in the digital elevation model, the direction before and after rebound remains unchanged.

Table 5.6 - Rebound deviation angle probabilities for three velocity classes.

Deviation Angle (°)	0 - 5	5 - 10	10 - 15	15 - 20	20 - 25	25 - 30	30 - 35	35 - 40	40 - 45	45 - 50	50 - 55
V < 10 m/s	49	15	9	6	5	4	3	3	3	2	2
10 ≤ V ≤ 15 m/s	53	15	8	6	4	4	3	3	2	2	2
V > 15 m/2	46	16	10	7	5	4	4	3	3	2	0

If on its trajectory the simulated block encounters a tree, the trajectory of the block can be deviated laterally up to 76° from its initial fall direction due to de impact according to the observations made during the experiments described in Dorren, *et al.* (2005). This accounts for the incoming and outgoing direction in a circle with a radius of 5 m around the impacted tree. Close to the tree stem, this deviation between the fall direction before and after the impact can be even 180°. The deviation of the block after a tree impact depends on the position of the block centre with respect to the tree stem axis at the time of impact. On that basis, the three main impact types, shown in Figure 5.11, have been defined. Based on these three types, the probabilities given in Table 5.7, in combination with a uniformly distributed random number, are used to calculate the deviation.

Table 5.7 - Probabilities for deviation in the fall direction due to a tree impact.

Impact type	Probabilities (%)		
	0 – 22,5 ° deviation	22,5° - 67,5° deviation	67,5° - 76° deviation
Frontal	44	50	6
Lateral	11	84	5
Scratch	72	24	4

5.4.3 Output Data

All outputs of Rockyfor3D are therefore given in raster format, having the same extent, cellsize and format as the input rasters. Each time a simulated block surpasses or rebounds in a given raster cell, the maxima of different variables simulated in that cell are recorded in separate rasters in the concerning cell. The output raster files created by Rockyfor3D are:

(1) *E_50.asc*, *E_90.asc*, *E_95.asc*, *E_98.asc*, *E_99.asc*: these rasters represent respectively the median, the 90th, 95th, 98th and 99th percentile of the simulated kinetic energy per cell. The output is given in integers and corresponds to the following energy class limits: 3, 6, 9, 12, 15, 18, 21, 24, 27, 30, 40, 50, 60, 70, 80, 90, 100, 110, 120, 130, 140, 150, 200, 250, 300, 500, 750, 1000, 1500, 2000, 3000, 5000, 8000, 10000, 15000, 20000, 50000, 99999, in kJ. In these rasters, the value 99999 represents all values larger than 50000 kJ.
(2) *Ph_50.asc*, *Ph_90.asc*, *Ph_95.asc*, *Ph_98.asc*, *Ph_99.asc*: these rasters represent respectively the median, the 90th, 95th, 98th and 99th percentile of the simulated passing heights of the centre of gravity of the block, measured in normal direction to the slope surface per cell. The output is given in integers and corresponds to the following height class limits: 0.5, 1, 2, 3, 4, 5, 10, 20, 99 in m. In these rasters, 99 represents all values larger than 20 m.
(3) *Nr_passages.asc*: the number of blocks passed through each cell.
(4) *Nr_sourcecells.asc*: this map shows, for each cell, the number of different source cells from which the blocks arrived.
(5) *Reach_probability.asc*: this map shows whether it is probable, higher values in the map, or improbable, lowest values higher than zero in the map, that a rock arrives in a given cell.

$$Reach_{probability} = \frac{Nr\_passages \cdot 100}{Nr\_sourcecells \cdot Nr\_simulations\_from\_source\_cells} \ (\%) \quad \textit{(Eq. 5.28)}$$

(6) *Propag_probability.asc*: this map can be used for the calculation of the spatial occurrence probability, which is needed in risk analyses.

$$Propag_{probability} = \frac{Nr_{passages} \cdot 100}{Total_{Nr_{simulations}}} \ (\%) \qquad \textit{(Eq. 5.29)}$$

(7) *Nr_deposited.asc*: the number of blocks stopped in each cell.
(8) *Rvol_deposit.asc*: the maximum block volume in cubic meters stopped in each cell.
(9) *EL_angles.asc*: a raster with the minimum recalculated energy line angles per cell. The energy line angle is the slope angle of a virtual direct line between the stopping location and the source location of a fallen block.
(10) *Traj_time.asc*: minimum time needed to reach a raster cell from the defined source areas in seconds.
(11) *V_max.asc*: the absolute maximum simulated velocity per raster cell in m/s. This data should be used with caution as there is no further information on the statistical distribution of the block velocities; the output was added on request.

In case of a "with-forest" simulation, the following two rasters are additionally created:

(12) *Tree_impact_heights.asc*: maximum tree impact height per raster cell in m.
(13) *Nr_tree_impacts.asc*: number of tree impacts per raster cell.

All the output raster maps are in ESRI ASCII Grid raster format and can be directly opened and visualised in most GIS software. In order to digitize an intensity or hazard map in a given study area on the basis of the output data of Rockyfor3D, the output rasters *Reach_probability.asc* and *Nr_deposited.asc* are most useful for delineating realistic rockfall runout zones.

After each simulation, Rockyfor3D creates a log file, called "Rockyfor3D_vx_x_logfile_dd-mm-yyyy_HHhMM.txt", which contains the information shown in Figure 5.13.

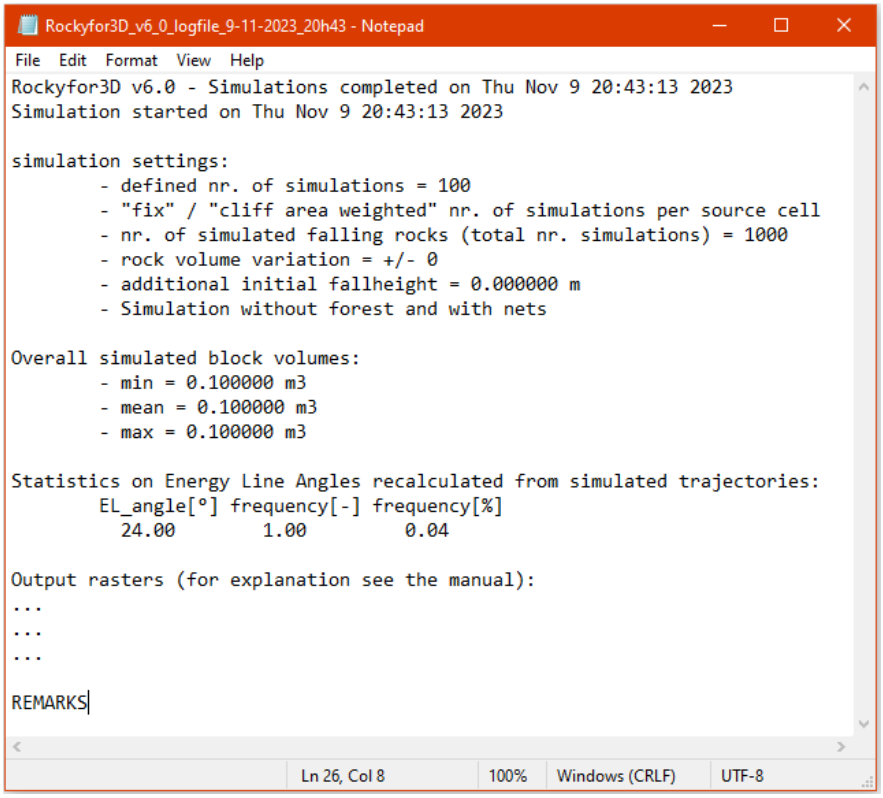

Figure 5.13 - Logfile output of Rockyfor3D.

5.1 Rocfall2

RocFall2 is a two-dimensional statistical analysis program designed to assist in the assessment of slopes susceptible to rockfalls. The model is used to evaluate the kinematic behaviour of individual rock blocks moving along a slope profile, allowing the estimation of parameters such as energy, velocity, and bounce height envelopes for the entire profile, as well as the location of the endpoints. In addition, the program provides statistical distribution of these variables. Rocfall2 supports lumped mass, hybrid, and rigid body approaches.

The first essential setting for initiating the setup of the event under consideration is the analysis method, *i.e.*, weather to perform a lumped mass, hybrid, or rigid body analysis. Other general settings like probability, and scaling functions can be changed in the GUI. Project settings should always be set at the start of the modelling, since some of the settings determine the availability of the next modelling options.

Following, the slope profile has to be added to the file, in Rocfall2, a slope may consist of any number of segments that cannot intersect each other for being considered valid. The first and last segments must not be located below any slope segment, this means that the initial and terminal segments cannot form an overhang sector at the limits of the slope. However, overhang zones are permitted elsewhere on the slope. It is important to remark that slopes having an excessive number of vertices lead to complex geometries and high computational costs during the analysis, especially if it is a rigid body simulation.

The following step is to define the materials that form the slope, these can be defined in the *Slope Material Library* by the user or can be selected from the set of predefined materials. The available parameters to define a new material depend on the analysis method previously selected, lumped mass or rigid body. For the rigid body method, the following slope materials can be defined, for each of them it is also possible to add statistical distributions with their respective parameters:

- normal and tangential restitution coefficients
- dynamic and rolling friction
- forest/vegetation damping
- slope roughness
- advanced friction parameters

To account for the presence of forest, the model has the option to define two forest damping coefficients, the mean effective height of the trees and the drag coefficient. The effective height represents the vertical dimension of an obstacle, it represents the portion of the tree or vegetation that effectively interacts with and dissipates the energy of the moving block. Complimentary, the drag coefficient defines the intensity of resistive force opposing the motion of the simulated block, a higher drag coefficient corresponds to greater resistance and energy dissipation, resulting in reduced velocities and shorter runout distances.

In Rocfall2 source areas are simulated through seeders, these elements can be punctual or linear and are characterized by the mass velocity and shape of the falling blocks, these characteristics can be specified as an exact number or possess one of the available statistical distribution types. When using the line seeders, a uniform distribution along the length of the line, *i.e.*, there is an equal probability that the rock will start falling from any point along the length of the seeder. Along with the rock type selected, seeder properties include the initial horizontal, vertical and or rotational velocities to be set as a fixed number or having a statistical distribution.

Another important feature is the *Rock Type Library*, it is used to define and store the properties of the blocks that will be simulated. For rigid body analysis, these properties include mass density and shape of the block.

A barrier in Rocfall2 can be simulated as a line segment that can be placed on the slope in order to stop falling blocks or absorb part of the energy as they move downslope. When adding barriers, the user can enter a custom one by defining their energy absorption capacity, and elongation, or use the ones available in the *Barrier Properties Library*. Another useful line segment element are the data collectors, they are elements that gather information about the rocks that pass through them, without affecting their dynamics. Data collectors, and also barriers, record the velocity, kinetic energy, vertical impact location, and horizontal location of all the passing or impacted blocks. Data collectors are used when the user requires to determine information about a certain location but do not want to alter the paths the rocks take as they travel down the hill.

Once the analysis is completed, the information gathered in barriers and data collectors can be visualized in graphs and raw data. In addition the trajectories of all the simulated blocks, end points locations, and kinematic parameter along the slope can be also be perceived as output.

Chapter 6

Rockfall Stabilization and Protection Measures

Rockfall hazard mitigation strategies can be classified in stabilization and protection works. These measures are not mutually exclusive, but rather complementary to each other in order to achieve a higher level of safety. Stabilization techniques act at the source, preventing rock detachment either by reducing the driving forces or increasing the resistance. Protective measures, by contrast, are designed to intercept blocks that are already in motion before they reach the elements at risk. The most common measures are classified in the following chart.

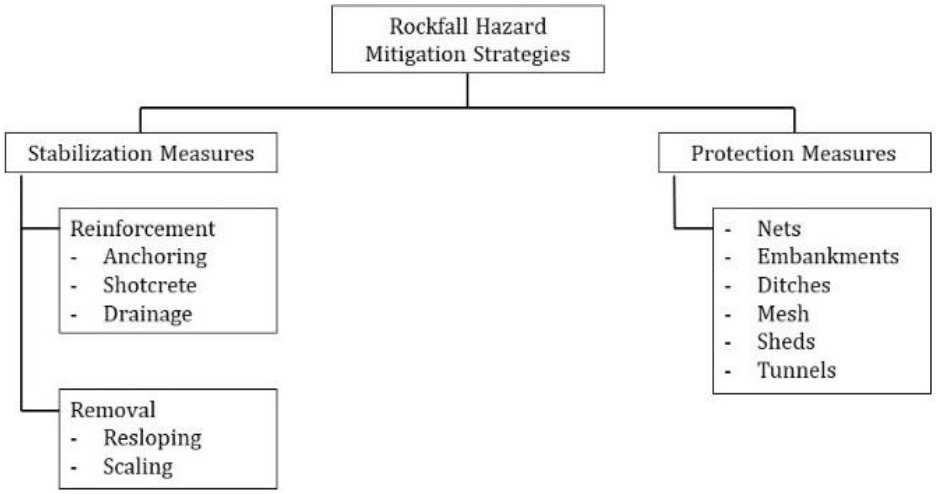

6.1 Stabilization Measures

These measures include scaling and trimming to remove loose or irregular blocks and obtain more stable slope geometries. Further methods include improving drainage to reduce water pressures, applying shotcrete to limit weathering and erosion, and mechanically securing unstable masses through rock bolts, dowels and anchors.

Anchoring

This category includes different reinforcing systems that add strength to the rock mass by increasing the tensile strength and the shear resistance along the discontinuities. The most common systems used are dowels, rock bolts, and rock anchors, illustrated in Figure 6.1.

Rock bolts and anchors are generally short low capacity reinforcement consisting of a steel tube or bar fixed into the rock and tensioned to a determined load. Most of the anchor types are fully bonded along their free length using grout or resin to protect them against corrosion. Dowels are steel reinforcing bars cemented into boreholes, opposing to bolts and anchors, these are not subjected to any pretensioning forces. This system increase the shearing capacity of the rock mass across potential failure surfaces, for the reinforcement to be effective the bolt or anchor must be fixed beyond the assumed failure surface.

The reinforcement force is usually designed busing limit equilibrium approaches. The main advantage of using tensioned bars is that they develop their full capacity immediately after installation. A further advantage of these systems is that a known anchor force is applied and the tension on the bar can be verified at any time, and re-tensioned if necessary.

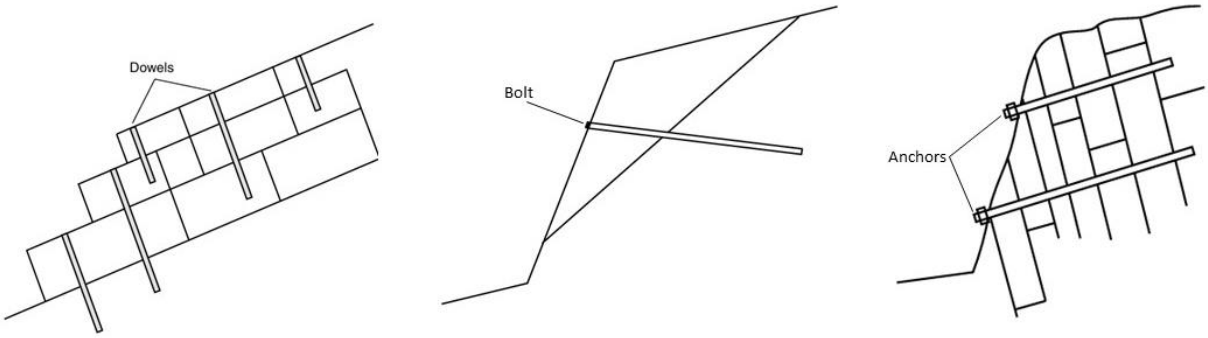

Figure 6.1 - Typical applications or rock anchoring.

Shotcrete

A technique that consists in spraying concrete on the rock wall to stabilize small volumes of rock. The sprayed concrete contribute to attach small blocks in place by means of its bond to the adjacent stable parts of the rock. The result is a smooth surface ranging between 8 to 10 cm thick of a rock-concrete structure on the surface of the slope. There is no transfer of load from the rock mass to the concrete layer, therefore, it acts as a reinforcement and not as a support. Shotcrete in combination with steel wire mesh and rock bolts can be used to give structural support to the rock wall, if necessary.

Prior to spraying the concrete, the face should be scaled and trimmed to remove blocks that are at their limit of detachment. Initially, dry rock surface are preferred in the sprayed concrete practice, although the use of additives and control of the nozzle water can give successful applications even on wet surfaces. Alteration filling products should be removed from the discontinuities openings, by means of air or water jet before the concrete spraying to ensure a good bond between the concrete and the rock. To prevent the development of water pressure behind the wall surface, drainage measures should be designed along the sprayed area.

Re-sloping and Scaling

Re-sloping involves the geometric stabilization of the slope, which include the removal of loose weathered superficial material together with the re-shaping the slope profile. By creating benches and reducing the local slope angle, the driving forces of the unstable material are decreased, preventing collapse under gravity and, therefore, reducing the risk of a rockfall event. This intervention also improves long-term stability of the slope material by limiting erosion and surface degradation process. Re-sloping operations often require the use of large construction machinery; consequently, the slope must be accessible and provided with adequate working platforms and access roads or at least have the adequate site conditions for creating them.

Scaling is the process of removing medium-large unstable blocks using small hand tools. The objective is to induce a controlled detachment of the block, or a portion of it, before it can fail spontaneously. This operation is typically performed by trained personnel working directly on the rock face and is suited for localized instabilities that cannot be efficiently treated by large-scale geometric modifications. Prior to scaling, the potential runout zone of the detached material should be evaluated and, if necessary, temporarily protected to ensure the safety of workers, infrastructure, and people. Figure 6.2 illustrates many of the available removal options for slope surface stabilization.

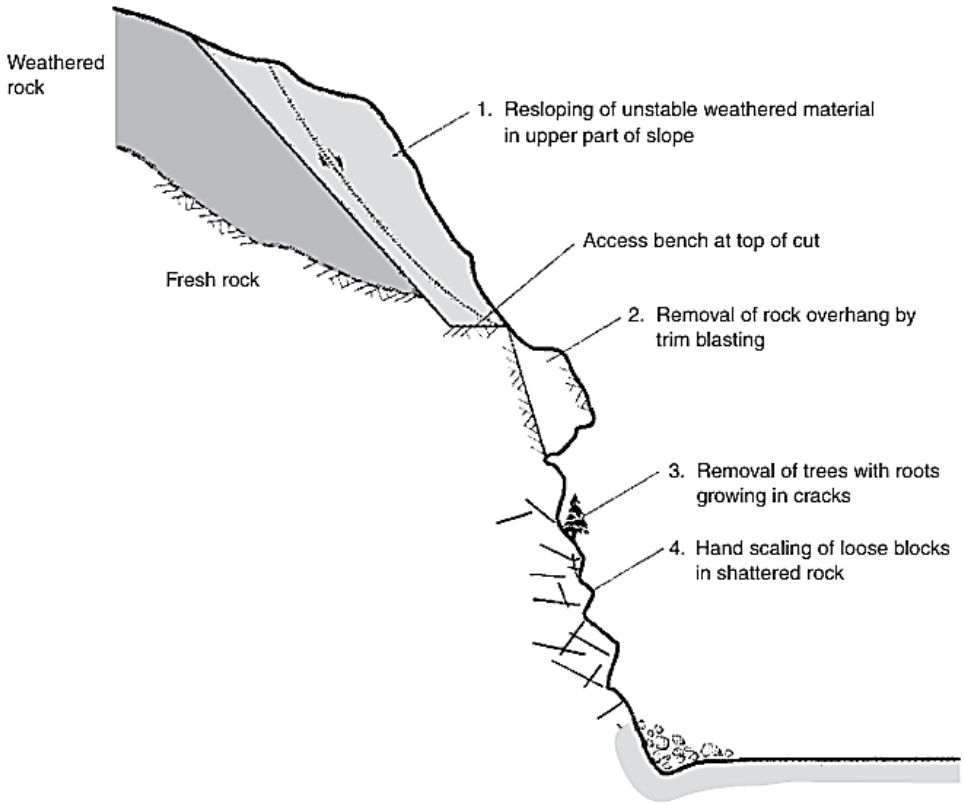

Figure 6.2 - Removal methods for slope stabilization (Wyllie, *et al.,* 2005).

6.2 Protection Measures

These structures are designed to intersect, deflect and stop the falling blocks to safeguard infrastructure and human life. Their design depends on the kinetic energy of the falling blocks as well as the bouncing height they can reach.

Embankments and Ditches

A variety of barriers types can be constructed, either to enhance the performance of ditches, or to form catchment zones at the base of the slope. The required type of barrier and its dimensions depend on the energy of the falling blocks, the available space, and the availability of construction materials.

A fundamental requirement for embankments is flexibility upon impact; they must be able to absorb kinetic energy through deformation. These systems are designed for high impact energy capacity and are constructed with materials capable of withstanding the impact of sharp and angular blocks without suffering significant damage or loss in their functionality. These barriers are particularly useful at the toe of flatter slopes where falling rock rolls and spins down the face but

does not bounce significantly. Their effectiveness generally require the addition of a ditch or catchment area behind the barrier to accumulate the stopped blocks.

Gabions and concrete blocks are effective protection barriers for rolling falling blocks, the advantage of gabions are their sustainability, the ease of construction on irregular bases, and their capacity to sustain considerable impacts. On the other hand, barriers constructed with pre-casted concrete are also widely used even though concrete blocks are in some way less resilient than gabions, they have the advantages of wide availability and rapid installation process, flexibility must be provided by allowing movement at the joints between the blocks.

Reinforced-soil barriers, are constructed alternating geotextiles and soil layers, in this way, it is possible to construct an embankment; the face subjected to impact can be additionally protected from damage with elements like gabions or rubber tires. The capacity of this type of barriers depends on their mass in relation to the impact energy, the shear resistance along each contact layer, and the material deformation capacity. A disadvantage of these barriers is that a considerable amount of space is required for both, the barrier itself and the catchment area behind it.

Catch Fences

A widely used system on steep slopes where the available space is reduced are the rockfall catch fences or nets, named also as dynamic barrier. It is a flexible system, able to withstand high impact levels due to their construction without rigid components. The system consists of a deformable mesh arranged in modules attached to lateral posts with a concrete foundation, the upperpart of the barrier is fixed to the slope using anchored cables that can be supplemented with sink breakers to improve energy dissipation.

The moment in which the block impacts the net, there is a deformation activating energy absorption components over an extended time of collision, which dissipates the kinetic energy of the block. Regular inspection and maintenance are essential to ensure the mesh and energy absorption components remain functional, particularly after significant rockfall events.

Draped Mesh

A draped wire mesh is hung on the slope face and is particularly effective on highly steep slopes for containing falling blocks close to the slope face, thereby preventing high bounce levels. The upper edge of the mesh should be placed to contain the rockfall release area, ensuring that unstable blocks are contained in the mesh from the moment of detachment. The mesh is not anchored at intermediate points or at the base, allowing blocks follow a controlled path down the slope. At the base, a ditch is required to collect the fallen material; since the mesh absorbs the energy of the falling blocks, the required dimensions for the ditch at the base are considerably reduced in comparison with unprotected slopes.

Sheds and Tunnels

In corridors subjected to extreme rockfall hazard, where other measures can be ineffective, the construction of a rock shed or even relocation of highways may be justified. A shed is a rigid protective structure placed over a road or railway to shield it from falling blocks, the shed upper surface is covered with a layer of energy absorbing material, typically sand or gravel. These structures are constructed in reinforced concrete or steel, designed to resist the wort-case scenario of an impact on the edge of the roof, while also ensuring the stability of the foundations and columns.

A critical feature of sheds is the weight and energy absorption capacity of the cushioning layer that should both absorb energy by compression, and disperse the punctual impact energy

so that the energy transmitted to the structure occurs over a large area. Furthermore, the cushion material should remain intact after the impact so it does not need to be replaced. In locations where neither rock sheds are practical, it may be necessary to relocate the corridor or to drive a tunnel to bypass the hazard zone.

Figure 6.3 illustrates the above described protection measures.

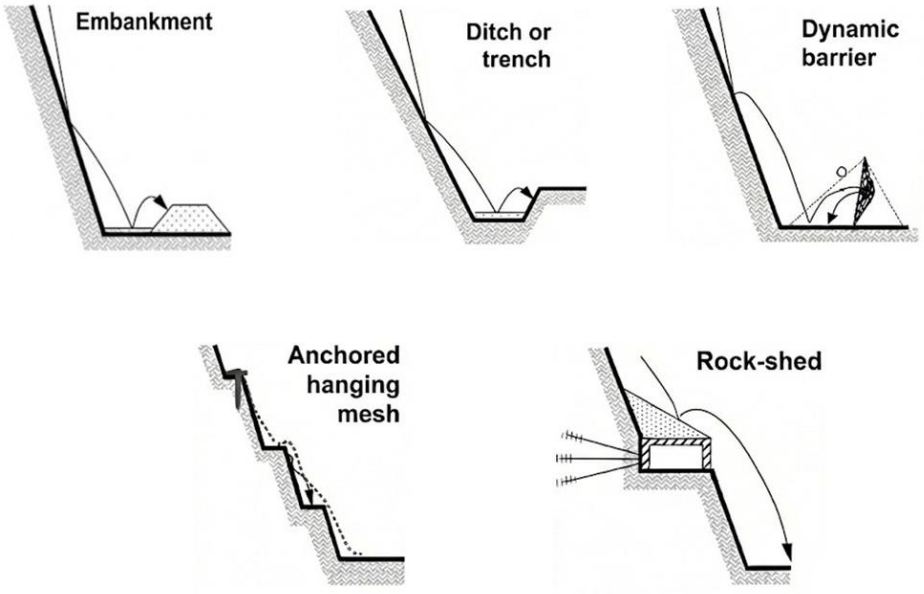

Figure 6.3 - Protection measures.

Chapter 7

Case Study: Venaus (TO)

The presented case study forms part of a project concerning the safety measures implemented at the Enel hydroelectric power plant in Venaus (TO). The objective of the project is to identify and design the most suitable rockfall protection systems to safeguard the existing buildings and infrastructure located at the base of the slope.

7.1 Description of the Case Study

In April 2025, the slope behind the hydroelectric plant was affected by a rockfall event that reached the company's facilities, causing structural damage of varying severity. Two blocks, each with an approximate volume of 4 m^3, propagated downslope and impacted one of the plant's building. Figure 7.1 represents the trajectories of the fallen blocks. This event highlighted both the deteriorated condition of the slope and the vulnerability of the hydroelectric complex and downstream structures.

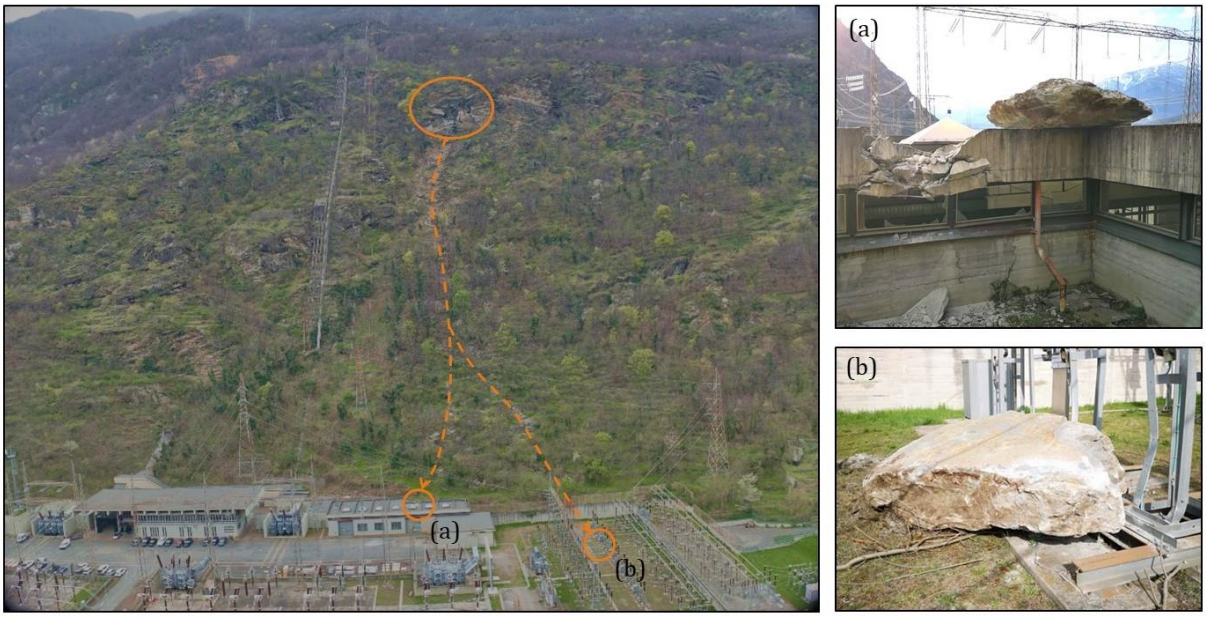

Figure 7.1 - Trajectory representation of the rockfall event on April 2025.

Following the rockfall event, the slope was considered unsafe, and the company implemented an urgent installation of rockfall stabilization mesh along the wall from which the detachment had occurred. Subsequently, the company also evaluated the installation of a series of rockfall barriers downstream of the rock walls to protect both, the hydroelectric plant and the adjacent electrical distribution substation.

For these purposes, the company commissioned GEODES S.r.l. to carry out an assessment of slope stability and the residual susceptibility to further block detachments, and the design and engineering of protective measures in order to prevent additional damage.

7.1.1 Geographical Setting

The study area is located in the Municipality of Venaus, in the Province of Turin, in the western sector of the Piedmont Region, close to the French-Italian border. Placed at the middle portion of the Cenischia Valley, a tributary valley of the larger Susa Valley, it has an elevation ranging approximately from 620 to 850 m a.s.l. This sector of the Alps is characterized by a sharp transition from the high mountain environment of the Mont Cenis Massif to the more open and populated Susa Valley floor. The Cenischia Valley itself is deeply incised, with strong lateral confinement, producing steep, highly dissected slopes particularly on the orographic right side where the study site is located.

Upstream the hydroelectric power plant affected by the collapse, the slope exhibits an average inclination of about 40°, although locally it features steeps rock walls reaching maximum inclinations of up to 89°. The rock face from which the rockfall originated, which extends for more than 150 m with an approximate SW-NE orientation and lies between 780 and 820 m a.s.l., is characterized by rugged morphology and surfaces exhibiting inclinations exceeding 70°.

Figure 7.2 - Geographical context of the study area.

7.1.2 Geological Setting

According to the official geological cartography provided by the *Servizio Geologico d'Italia*, the area of interest, situated along the right orographic slope of the Cenischia Valley, is documented in the Geological Sheet No. 153-Bardonecchia and No. 154–Susa at a scale 1:50.000 (Figure 7.4). From consultation of the official cartography, it is evident that the study area lies entirely within the Ambin Complex, which forms part of the pre-Triassic basement of the Ambin tectonostratigraphic unit.

The Ambin Complex mainly consists of albitic-chloritic garnet gneisses and leucocratic jadeite-bearing gneisses. These rocks are of magmatic, volcanic, and/or volcanoclastic origin and belong to the same magmatic complex. Among these rocks, metapelites are present, including chlorite-bearing quartz-mica schists, rare boudins of glaucophanic schists, and, in smaller amounts, quartz-rich mica schists with occasional layers of metaconglomerates, quartzites, and carbonates. Ortho- and para-derivatives do not extend laterally and have highly variable thicknesses, likely due to original heterogeneity (Elettri, *et al.*, 2025). Specifically, where the study area is located, the following units have been recognized:

- Quartz-mica schists, quartzites, and marbles (AZM): para-derivatives characterized by quartz-mica schists laterally passing into quartzite beds, ranging from decimetre to meter scale. These are interbedded with layers of similar thickness composed of schists containing glaucophane, light mica, chlorite, and carbonates.
- Eye-gneisses with albite and chlorite (AZD): light green in colour, mainly composed of quartz, albite, white mica, and chlorite, with subordinate relic cloritoid, late biotite, and carbonates. This lithotype represents the dominant component of the Ambin complex.

Above the bedrock, there are several Quaternary deposits, predominantly of detrital nature.

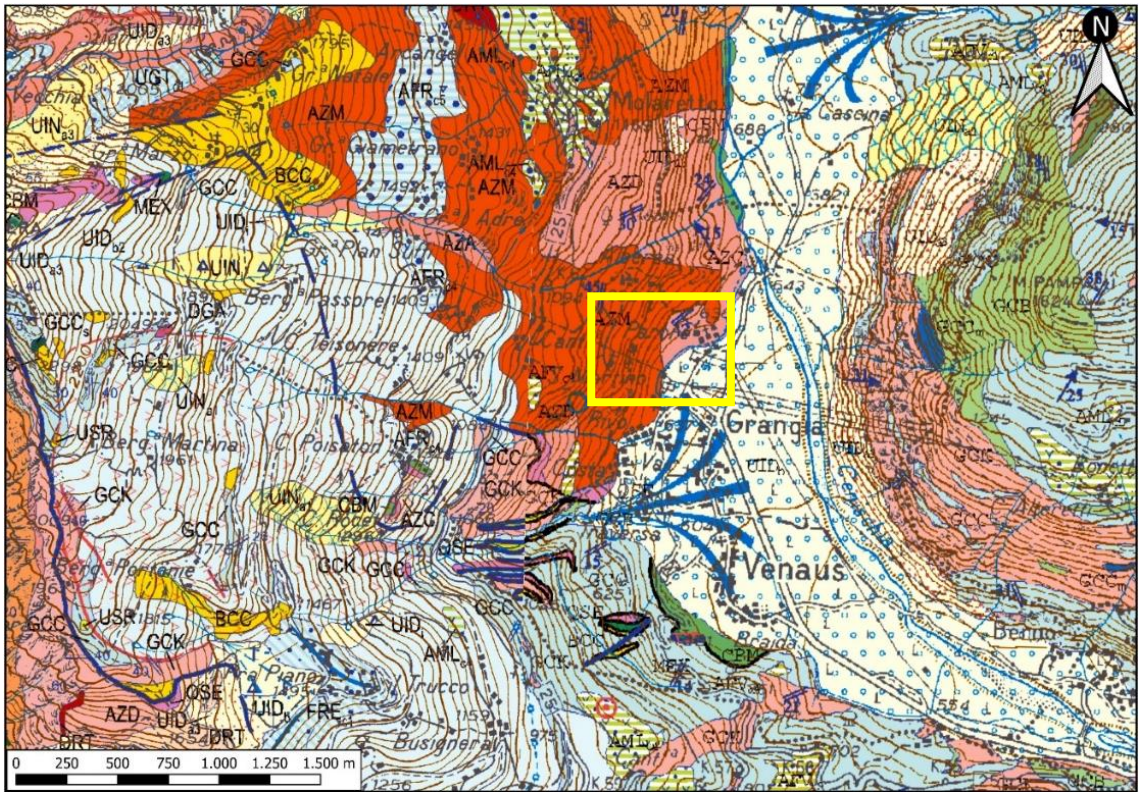

Figure 7.3 - Extract from Geological Sheets No. 153-Bardonecchia and 154-Susa at a scale of 1:50.000 of the CARG from the Servizio Geologico d'Italia, framed in yellow, the study area.

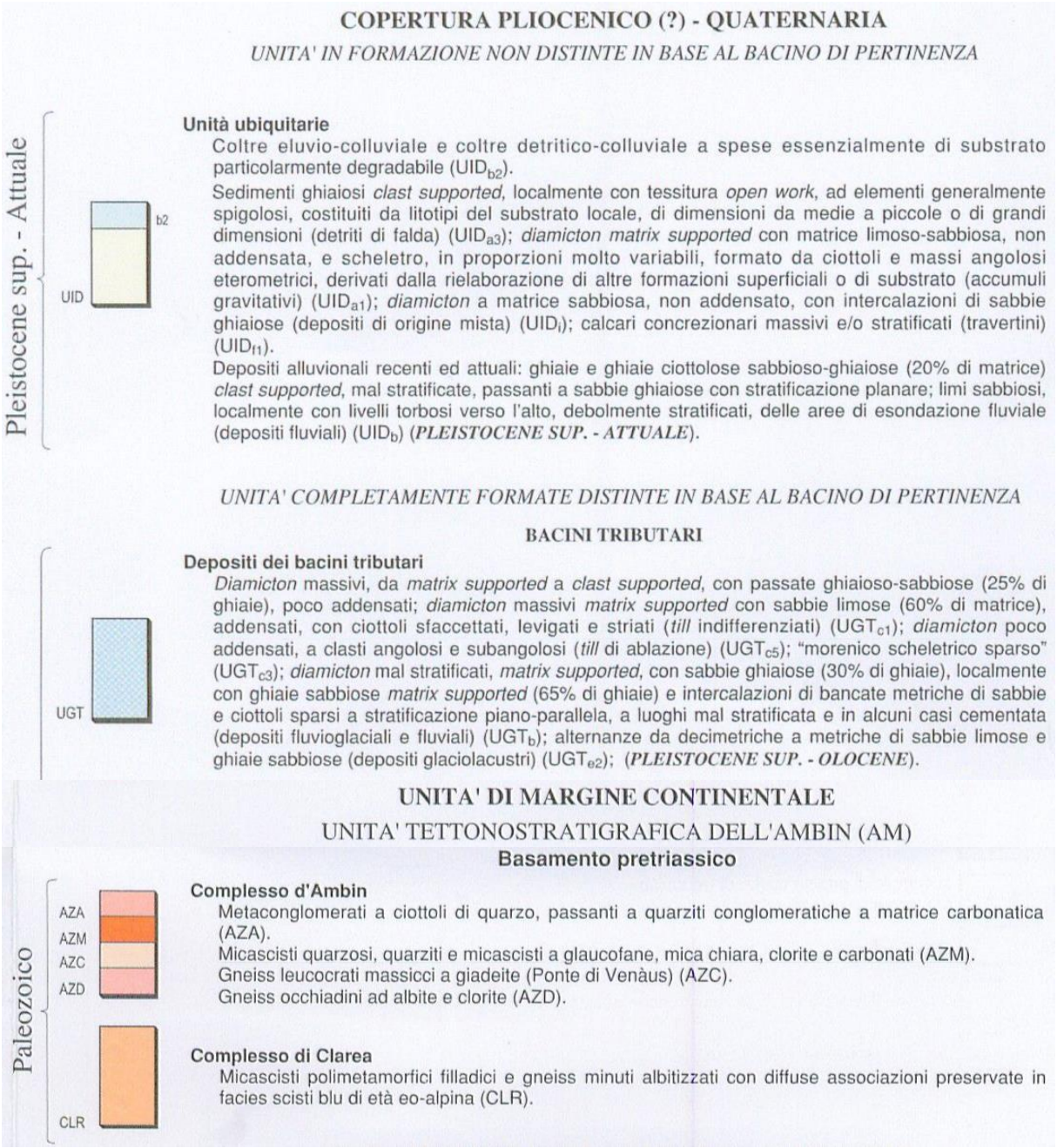

Figure 7.4 - Extract of references from Geological Sheets No. 153-Bardonecchia and 154-Susa at a scale of 1:50.000 of the CARG from the Servizio Geologico d'Italia.

7.2 Site Investigation

Following the event, on 8 April 2025, a detailed aerial photogrammetric survey of the slope behind the power plant was carried out in order to obtain an updated topographical base of the site immediately upstream of the hydroelectric power plant. In addition, the survey allowed the identification of potential detachment zones, unstable blocks and deposit areas.

On 9 April, a detailed geological-geomechanical survey was conducted, with the aim of: (i) characterizing the degree of fracturing of the rock mass and the nature of the discontinuities present on its walls, on the detachment zone and along to the accessible areas; (ii) estimate the

minimum volume, size and shape of potentially unstable blocks; and (iii) identify the discontinuity sets and the geometric conditions that favour instabilities. The inaccessible portions of the slope were instead examined through visual inspection and drone conducted survey.

To support this thesis analysis, a further site investigation was conducted on December 5. These site measurements were aimed to assess the characteristics of the forest and its components, and determine the macro-roughness of the different slope areas, in order to carry out an accurate three dimensional rockfall runout analysis.

7.2.1 Aerial Photogrammetric Survey

The drone conducted survey was performed and the acquired data confirmed that the slope is characterized by an abundant amount of debris, consisting of clasts of varying composition and size, distributed all along the slope and concentrated below the rock walls. In addition to the rock debris, the slope is covered by a forest with medium to high density. The hydroelectric power plant and the distribution centre, along with their facilities and offices, are located immediately at the base of the slope, below large portions of rock outcrops on the slope (Figure 7.5).

Figure 7.5 - Panoramic view of the right slope of the Val Cenischia (Google Earth).

The rock walls were identified and categorized to facilitate their recognition and characterization (Figure 7.6). The aerial images evidenced locally unstable blocks, which could be subjected to further rockfall events affecting the downstream sectors of the slope. The drone flight also revealed the presence of already existing stabilization interventions on a portion of intensely fractured rock mass located at an elevation between 755 and 765 m a.s.l., consisting of adhered mesh fixed with steel cables, in addition to those installed after the event.

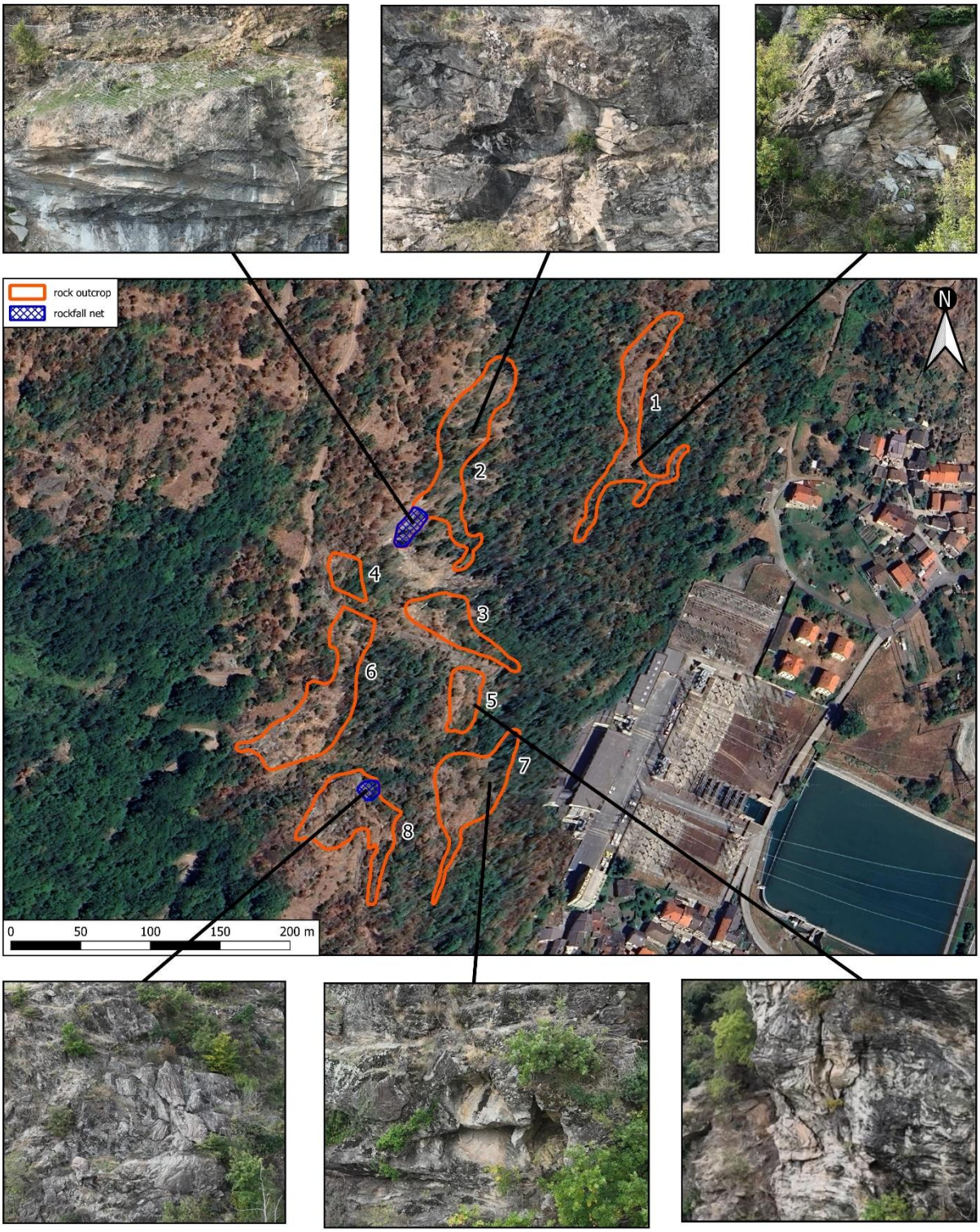

Figure 7.6 - Delineation of rock walls, highlighting unstable blocks and existing stabilization structures identified through aerial imagery.

7.2.2 Geological-Geomechanical Survey

The geological field investigation consisted of three complete geomechanical surveys, which allowed for the structural characterization of the exposed bedrock, and by a block-metric survey of the blocks located along the slope in terms of dimensions and shape, useful for the subsequent stability analysis.

Along the entire slope, several outcrops of the bedrock were identified, mainly composed of mica schists characterized by a very prevalent millimetre-thick schistosity, dipping towards NW at a moderate angle, between 22° and 50°. Within these schists, micaceous minerals, particularly light-coloured mica, and green-coloured minerals, likely chlorite, were recognized. Additionally, the bedrock is characterized by the presence of quartz veins of variable length and up to 5 cm thickness, subparallel to the schistosity.

Figure 7.7 - Geomechanical survey photos; (a) schiststocity, (b) and (c) quartz veins.

The rock mass is intensely fractured, with portions of blocks overhanging the slope. The terrain at the base of the rock walls is covered by a layer of detrital deposits of indeterminate thickness, consisting of angular clasts and blocks with a wide range of sizes, from centimetres up to multi-metre blocks. It can be stated that these detrital bodies are of different ages, as some are vegetated and embedded in the fine sandy-silty matrix below the surface, characteristic of colluvial-detrital deposits, while others lack herbaceous vegetation and exhibit clean, brightly coloured surfaces, likely dating back to the landslide event of April.

Block-metric Survey

Blocks deposited along the slope were characterized in terms of volume through a dedicated block survey. The results obtained from this survey were subsequently used in the global stability analysis of the slope, as an indication for the definition of rock volumes susceptible to collapse from the rock walls present on the slope. The measurements from the block survey are reported in Table 7.1.

Table 7.1 - Block dimensions recorded along the slope.

ID	Height (cm)	Width (cm)	Length (cm)	Volume (m^3)
1	90	210	75	1,418
2	154	60	90	0,832
3	28	18	7	0,004
4	80	20	40	0,064
5	30	25	10	0,008
6	150	100	40	0,600
7	20	25	15	0,008
8	45	23	8	0,008
9	150	100	20	0,300
10	50	40	10	0,020
11	150	70	30	0,315
12	250	70	80	1,400
13	110	130	15	0,215
14	45	30	20	0,027
15	300	180	60	3,240
16	500	150	450	33,750

Based on the measurements carried out on site, the average block volume is approximately 0,564 m^3. In the calculation of the mean volume, block No. 16 was excluded, as it does not represent a block susceptible to collapse. Instead, it corresponds to a large isolated unstable block identified during field investigations. If detached, this block is expected to undergo fragmentation due to the highly fractured nature of the site rock mass; therefore, it was not included in the statistical evaluation of blocks susceptible to collapse.

Geomechanical Survey

The geomechanical surveys were carried out in accordance with the International Society for Rock Mechanics (IRSM) data collection guidelines (1978), enabling for discontinuity characterization on the basis of the following parameters:

(a) orientation (dip and dip direction)
(b) persistence
(c) mean spacing
(d) aperture
(e) roughness
(f) infilling
(g) weathering
(h) water condition
(i) mean block size
(j) GSI

In addition, sclerometer tests were performed on the main discontinuity sets observed on site. The geostructural data was obtained at three survey stations, locations of which are shown in Figure 7.8, with the aim of defining the geometry and characteristics of the discontinuities affecting the rock mass along the slope from different positions. The survey data and analysis is reported in Appendix I.

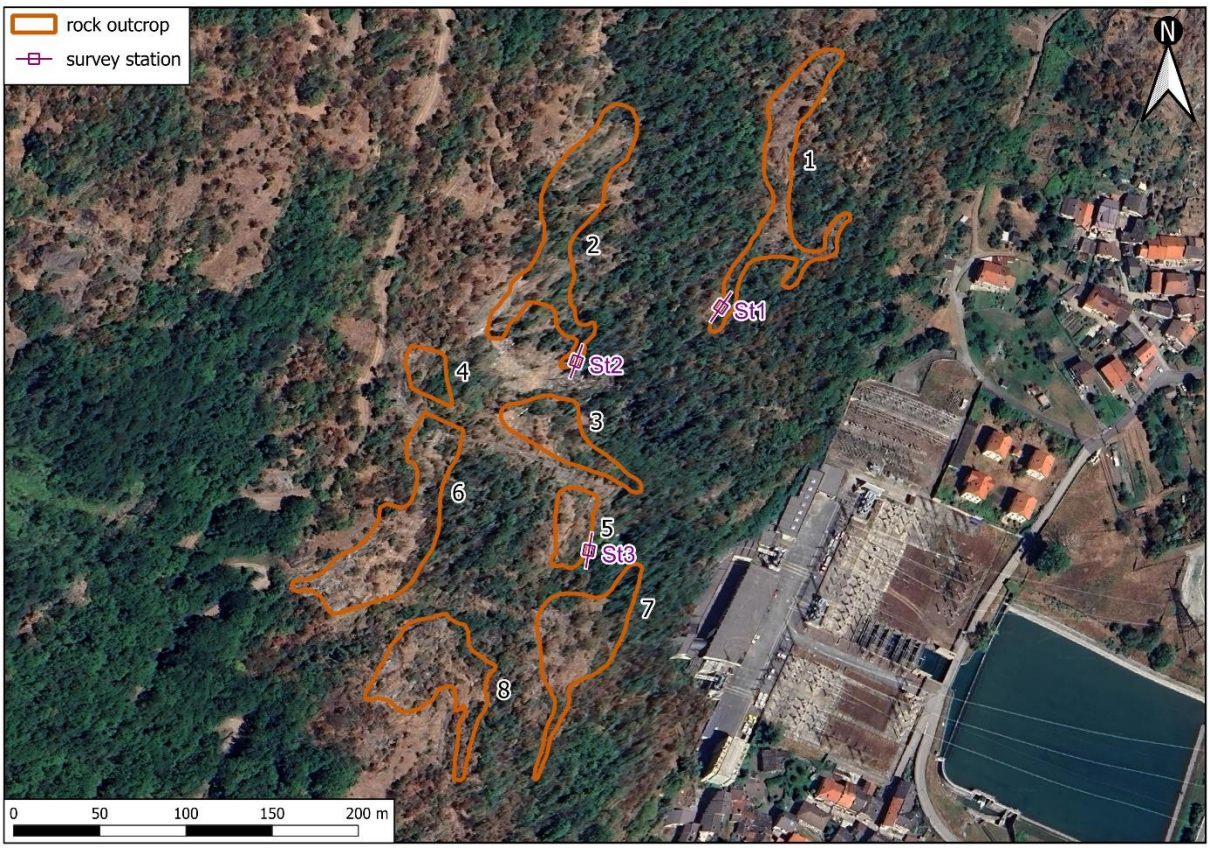

Figure 7.8 - Geo-Structural stations location.

Following the acquisition of these measurements, the orientation data were analysed using Dips 7.018 from the Rockscience Inc., with a Schmidt equal-angle stereonet method on the lower hemisphere.

The structural station St1 is characterized by schistosity planes dipping toward WNW with an average inclination angle ranging between 24° and 50°, and a large-scale undulating trend. The rock mass (Figure 7.9) consists of grey quartzic mica-schists with lenticular quartz veins ranging from centimetre to multi-centimetre scale, subparallel to the schistosity. The mass is intensely fractured, and a total of n.6 discontinuity families have been identified in addition to the schistosity. The joints observed show fillings ranging from absent to soft, of a sandy-silty nature, with a thickness of less than 5 mm, and generally a weak degree of surface weathering. Along the wall, a fault plane is also present, where kinematic indicators, consisting of movement striations and calcite steps have been observed, allowing the classification of the fault kinematics as a normal fault. The minimum volume of blocks found on site is approximately 0,225 dm^3, the maximum is 1,912 m^3, while the average volume is around 24,375 dm^3. The rock mass is characterized by a GSI of 55-60.

Figure 7.9 - Rock outcrop on survey station St1.

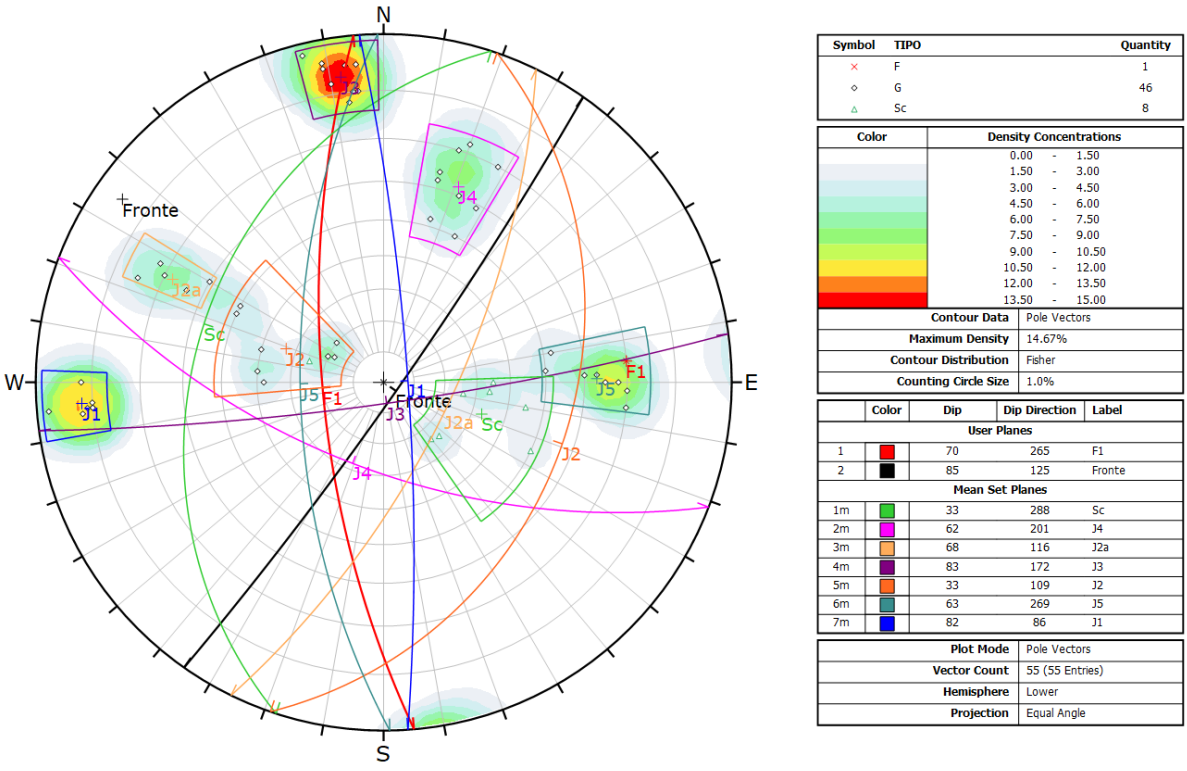

Symbol	TIPO	Quantity
×	F	1
◇	G	46
△	Sc	8

Color	Density Concentrations
	0.00 - 1.50
	1.50 - 3.00
	3.00 - 4.50
	4.50 - 6.00
	6.00 - 7.50
	7.50 - 9.00
	9.00 - 10.50
	10.50 - 12.00
	12.00 - 13.50
	13.50 - 15.00
Contour Data	Pole Vectors
Maximum Density	14.67%
Contour Distribution	Fisher
Counting Circle Size	1.0%

	Color	Dip	Dip Direction	Label
User Planes				
1		70	265	F1
2		85	125	Fronte
Mean Set Planes				
1m		33	288	Sc
2m		62	201	J4
3m		68	116	J2a
4m		83	172	J3
5m		33	109	J2
6m		63	269	J5
7m		82	86	J1

Plot Mode	Pole Vectors
Vector Count	55 (55 Entries)
Hemisphere	Lower
Projection	Equal Angle

Figure 7.10 - Sterographic representation St1.

The structural station St2 is characterized by schistosity planes dipping toward NW, with an average inclination ranging between 30° and 45°, and exhibiting a large-scale undulating pattern. The rock mass (Figure 7.11) located at the base of the slope from which the collapse landslide occurred in April 2025, consists of grey quartzic mica-schists with lenticular quartz veins ranging from centimetre to multi-centimetre scale, subparallel to the schistosity. The mass is intensely fractured, and five families of discontinuities have been identified in addition to the schistosity. The observed joints exhibit fillings varying from absent to soft, of a sandy-silty composition, generally less than 5 mm thick, and display a surface weathering ranging from absent to weak. The minimum volume of blocks is approximately 0,900 dm^3, the maximum is 0,300 m^3, while the average volume is 24,750 dm^3. The rock mass is characterized with a GSI of 55-60.

Figure 7.11 - Rock outcrop on survey station St2.

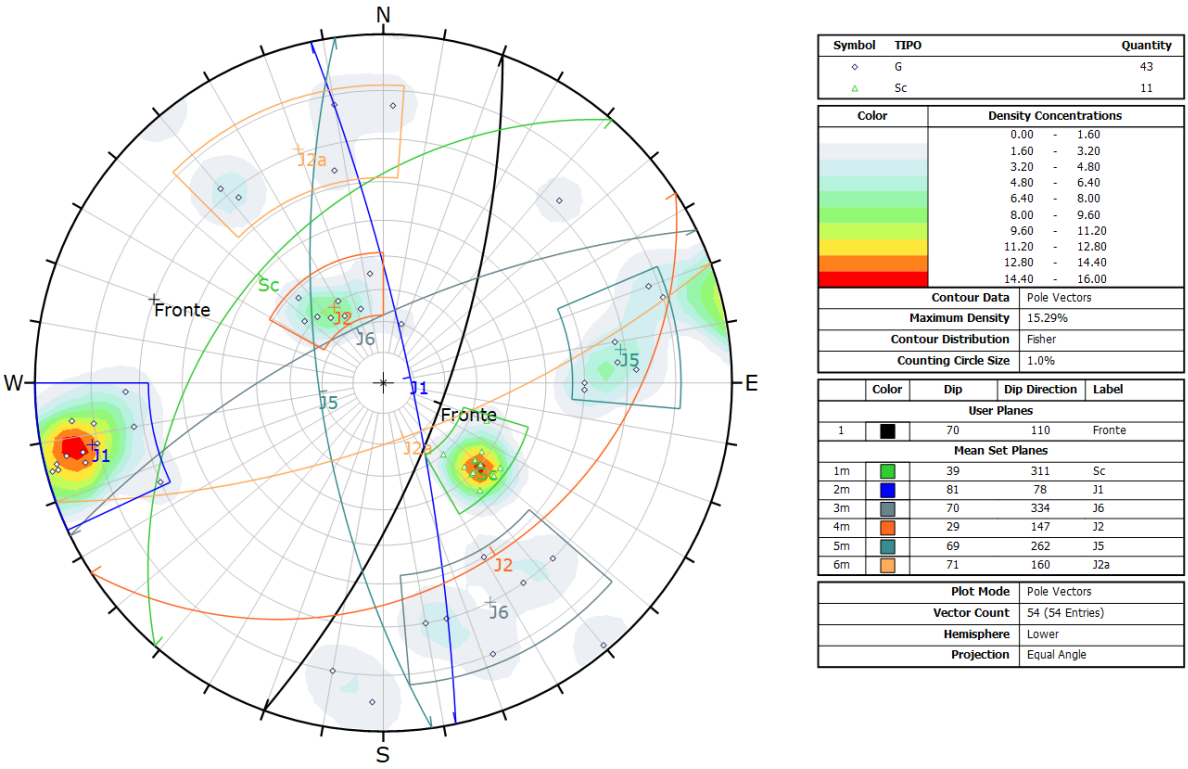

Symbol	TIPO	Quantity
◇	G	43
△	Sc	11

Color	Density Concentrations
	0.00 - 1.60
	1.60 - 3.20
	3.20 - 4.80
	4.80 - 6.40
	6.40 - 8.00
	8.00 - 9.60
	9.60 - 11.20
	11.20 - 12.80
	12.80 - 14.40
	14.40 - 16.00

Contour Data	Pole Vectors
Maximum Density	15.29%
Contour Distribution	Fisher
Counting Circle Size	1.0%

	Color	Dip	Dip Direction	Label
User Planes				
1		70	110	Fronte
Mean Set Planes				
1m		39	311	Sc
2m		81	78	J1
3m		70	334	J6
4m		29	147	J2
5m		69	262	J5
6m		71	160	J2a

Plot Mode	Pole Vectors
Vector Count	54 (54 Entries)
Hemisphere	Lower
Projection	Equal Angle

Figure 7.12 - Sterographic representation St2.

The structural station St3 is characterized by schistosity planes dipping toward WNW, with a medium-to-high average inclination ranging between 30° and 50°, and exhibiting a large-scale undulating pattern. The rock mass (Figure 7.13) consists of grey quartzic mica-schists with lenticular quartz veins ranging from centimetre to multi-centimetre scale, subparallel to the schistosity. The mass is intensely fractured, and six families of discontinuities have been identified in addition to the schistosity. The observed joints exhibit fillings varying from absent to soft, of a sandy-silty composition, generally less than 5 mm thick, and display a surface weathering ranging from absent to weak. The minimum volume of blocks found on site is approximately 1,000 dm^3, the maximum is 130,000 dm^3, while the average volume is around 15,000 dm^3. The rock mass in this station is characterized with a GSI value of 50-55.

Figure 7.13 - Rock outcrop on survey station St3.

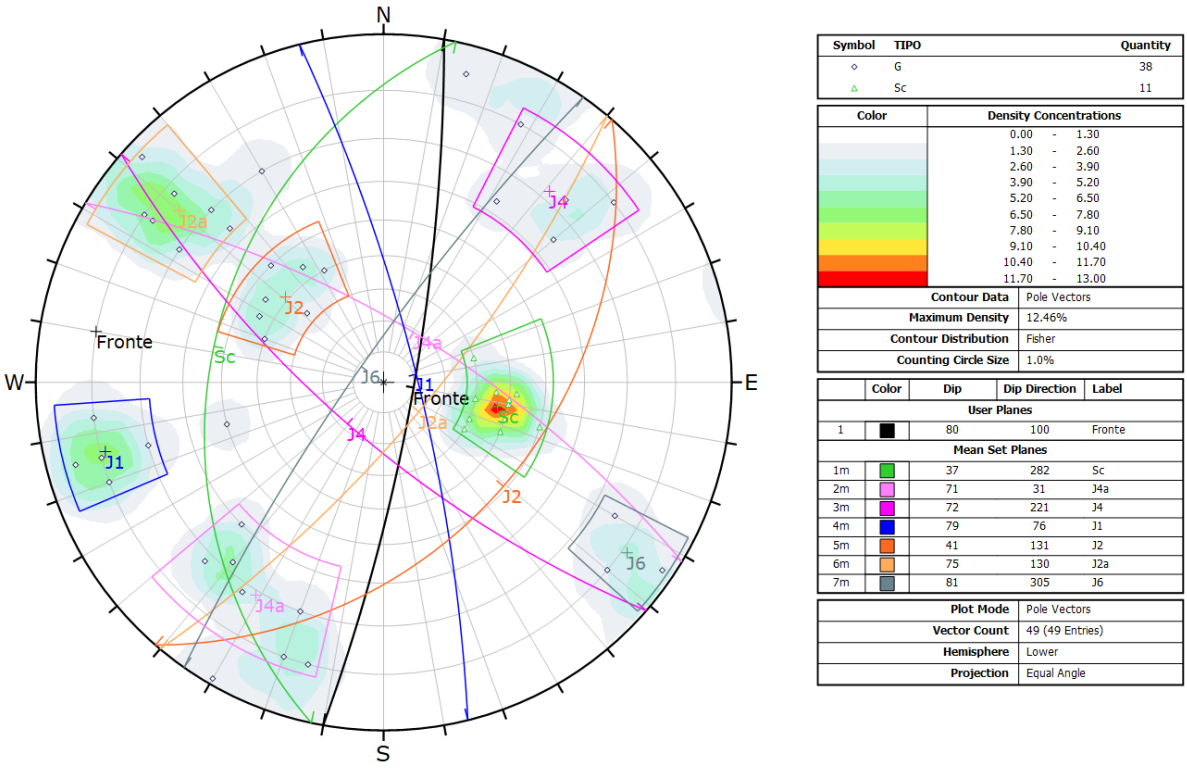

Symbol	TIPO	Quantity
◇	G	38
△	Sc	11

Color	Density Concentrations
	0.00 - 1.30
	1.30 - 2.60
	2.60 - 3.90
	3.90 - 5.20
	5.20 - 6.50
	6.50 - 7.80
	7.80 - 9.10
	9.10 - 10.40
	10.40 - 11.70
	11.70 - 13.00

Contour Data	Pole Vectors
Maximum Density	12.46%
Contour Distribution	Fisher
Counting Circle Size	1.0%

	Color	Dip	Dip Direction	Label
User Planes				
1		80	100	Fronte
Mean Set Planes				
1m		37	282	Sc
2m		71	31	J4a
3m		72	221	J4
4m		79	76	J1
5m		41	131	J2
6m		75	130	J2a
7m		81	305	J6

Plot Mode	Pole Vectors
Vector Count	49 (49 Entries)
Hemisphere	Lower
Projection	Equal Angle

Figure 7.14 - Sterographic representation St3.

7.2.3 Forest Survey

In order to perform a complete 3D analysis, the characteristics of the vegetation on the site are required. A total of six survey areas were inspected on site, recording the number of trees, species and stem diameter. The survey areas, shown in Figure 7.15, were selected based on their accessibility, following existing trails along the slope. All of these areas are located below the rock walls; therefore, it can be affirmed that the forest characteristics influencing the analysis were correctly measured and taken into consideration. The raw data obtained from the forest survey are presented in Appendix II.

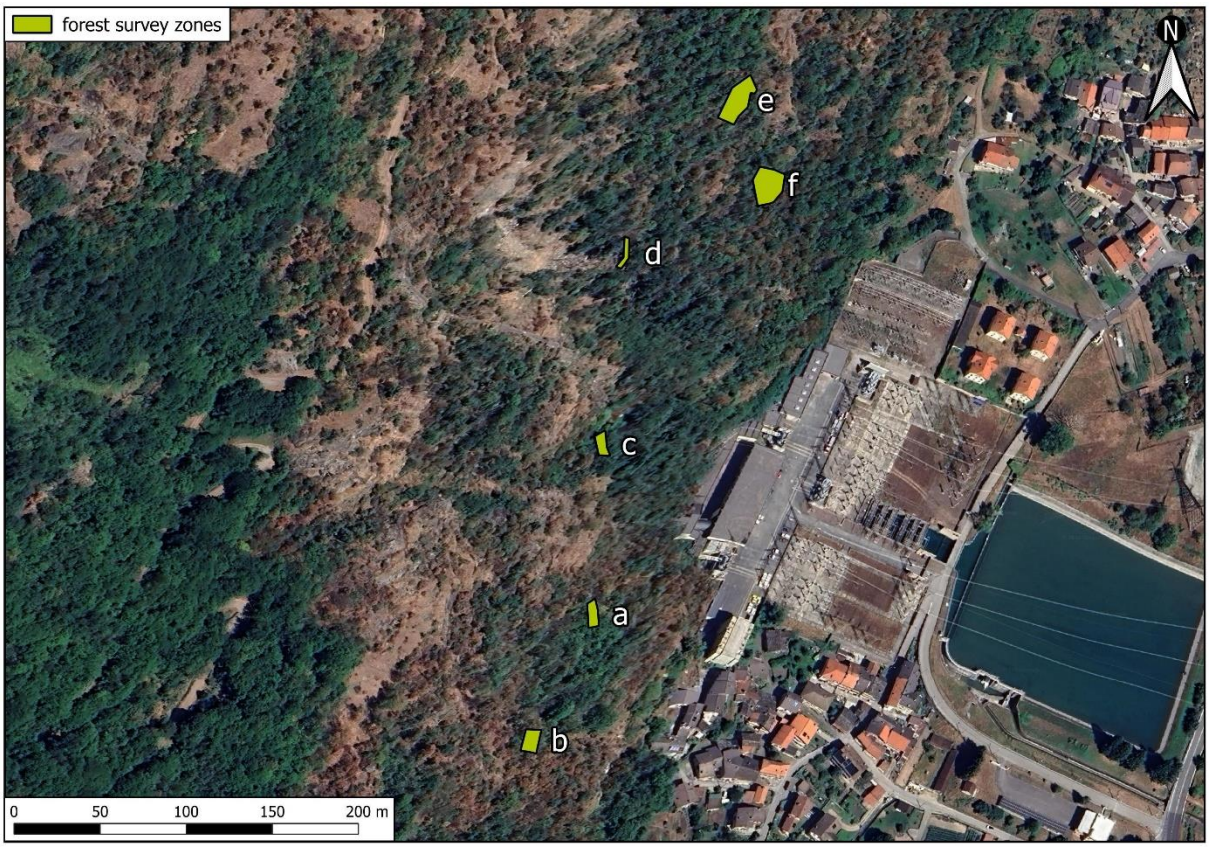

Figure 7.15 - Location of the surveyed zones.

A probabilistic analysis was subsequently carried out to obtain the mean value and standard deviation of the diameter data, as well as the tree density. Survey results are shown in Table 7.2.

Table 7.2 - Forest survey results.

Zone	Area		Count	Density	DBH (cm)	
	m^2	Ha	No.	(trees/Ha)	mean	std.dev
a	120	0,012	37	3083	19	7
b	89	0,009	30	3371	16	10
c	81	0,008	40	4938	9	4
d	56	0,006	40	7143	16	7
e	310	0,031	75	2419	12	5
f	308	0,031	46	1494	21	12

The forest survey revealed a significant variability in tree density and stem diameter across the six zones, while the percentage of coniferous species is null for this side of the valley. Zones *c* and *d* exhibit the highest tree densities but relatively smaller mean diameters, indicating a dense stand of younger or smaller trees. Conversely, zones *a* and *f* have lower densities but larger mean diameters, suggesting the presence of fewer, more mature trees.

Considering that this survey was conducted nine months after the rockfall event, it is possible that the trees measured over a narrow long area, like zone *d*, might not be fully representative of the portion of slope below the rock wall No. 2, from where the mass of rock detached and partially deposited immediately below it. Figure 7.16 and Figure 7.17 are evidence that the area below the detachment zone has a lower tree density with respect to the others.

Figure 7.16 - Downslope view from the detachment area.

Figure 7.17 - Aerial view of the zone below rock wall No.2.

7.3 Release Area Characterization

After concluding all the required surveys, the office-based analysis is performed. First, the information needed to determine each one of the parameters required for the definition of the Susceptibility Index to Failure (SIF), described in Section 3.3.1, is compiled.

The base for the analysis is the selection of the Digital Terrain Model (DTM) to be used. In this study case, the DTM was extracted from the Italian Ministry of Environment geoportal (*SIM - Sistema Informativo Multimediale*), with a spatial resolution of 1 x 1 m and referenced in the coordinate system ESPG:32632 (WGS 84/UTM zone 32N).

Subsequently, using a dedicated tool from the Geospatial Data Abstraction Library (GDAL) utility in QGIS, a XYZ ASCII file is generated from the DTM raster, containing the coordinates of the centre of each pixel. Following this file is imported into QGIS as a vector layer, generating a point for each DTM cell.

The resulting point cloud is clipped using the delimitation polygons of the rock walls, yielding a set of points corresponding exclusively to the potential detachment areas. These points can then be directly selected, either wholly or partially for each rock wall and attributed with the corresponding factors required for the computation of the SIF.

Each factor is then carefully evaluated and its corresponding class assigned in accordance with Table 3.2. The report of the weighting values attributed to each factor for the different rock walls is presented in Table 7.3, forming the input data for the subsequent computation of the SIF value.

Table 7.3 - Weighting values assigned to each factor at the rock walls.

Factor, f \ Rock wall		1	2	3	4	5	6	7	8
F1	Slope angle	pixel based	pixel based	pixel based	pixel based	pixel based	pixel based	pixel based	pixel based
F2	Rock mass structural conditions *	3,0	2,0	-	-	3,0	-	-	-
F3	Condition of discontinuities *	0,5	0,5	-	-	2,0	-	-	-
F4	Stability conditions	1,5	1,5	1,5	1,5	1,5	1,5	1,5	1,5
F5	Fracturing level of the rock mass **	-	-	0,5/2,0	1,0	-	1,0	1,0	1,0
F6	Lithology sensitivity	0,5	0,5	0,5	0,5	0,5	0,5	0,5	0,5
F7	Expected rockfall events	1,0	1,0	1,0	1,0	1,0	1,0	1,0	1,0
F8	Water	0,0	0,0	0,0	0,0	0,0	0,0	0,0	0,0
F9	Seismicity	0,0	0,0	0,0	0,0	0,0	0,0	0,0	0,0
F10	Unstable blocks and/or overhanging sectors	2,0	2,0	2,0	2,0	2,0	2,0	2,0	2,0
F11	Aggravating conditions	0,0/0,5	0,0/0,5	0,0	0,0	0,0	0,0	0,0	0,0
F12	Lateral or foot erosion	0,0	0,0	0,0	0,0	0,0	0,0	0,0	0,0
F13	Stabilization works	0,0	-0,5/0,0	0,0	0,0	0,0	0,0	0,0	-0,5/0,0
F14	Freeze-thaw cycles	0,0	0,0	0,0	0,0	0,0	0,0	0,0	0,0

The slope angle factor (F1) was assigned using a range-based classification code implemented in the attribute calculator in QGIS, reported in Appendix III. Previously, a slope analysis was derived from the DTM and, for each point within the detachment area, the local inclination angle was assigned and classified according to the ranges defined on Table 3.2.

The weighting factors of the rock mass structural conditions (F2) were assigned with basis on the geomechanical surveys for the investigated walls, following J_n values. The assignation of this factor is only for the rock faces that underwent detailed site characterization, as indicated in Table 3.2.

The discontinuity condition factor (F3) was determined using the detailed data obtained from the geostructural surveys, including roughness, persistence, opening, infilling and wall alteration.

The stability conditions (F4) was assigned on the basis of field evidence and geomorphological indicators of instability, such as open fractures, detached blocks, fresh scar surfaces, and local rockfall accumulations. This features are at a greater or lesser extent present in every zone of the considered detachment areas, hence a potentially unstable class was considered.

The fracturing level of the rock mass (F5) was evaluated by integrating geostructural survey data from the neighbouring rock outcrops with visual comparison of exposed rock faces considering GSI values.

For the lithology sensitivity factor (F6), a medium-to-good rock quality was assigned to the entire rock mass on the slope, considering the rock formation, in terms of mineral composition, as a relatively homogeneous lithological setting without weak or highly altered sectors.

As for the expected rockfall events factor (F7), an occasional frequency corresponding to approximately three events per year was adopted. This estimate takes into account the detachment of April 2025 and an additional reported event in the subsequent months, as well as qualitative evidence collected during field surveys.

Hydrological conditions (F8) of the site were defined assessing data from the *Agenzia Regionale per la Protezione Ambientale* (ARPA) (Regional Agency for Environmental Protection), monitoring network, which indicate an average rainfall intensity of approximately 6,2 mm/h during precipitation events, with peak values reaching about 100 mm in rare annual occurrences. Furthermore, no moisture was observed along discontinuities during the surveys, and no rivers or streams intersect the analysed area.

The seismicity factor (F9) was selected according to data from the *Istituto Nazionale di Geofisica e Vulcanologia* (INGV) (National Institute of Geophysics and Volcanology), which classifies the area as having low seismic activity, with peak ground acceleration values lower than 0,15 g.

Unstable blocks and overhanging sectors (F10) were identified at several locations along the slope through the analysis of aerial imagery acquired during the drone survey, complemented with field verification.

The only aggravating condition (F11) considered is a possible fault crossing rock walls No. 1 and 2. Given its uncertain nature, a low criticality level was assigned to the points surrounding the fault, considering that this sector might be more fractured or altered locally than the surrounding mass.

No evidence of lateral or foot erosion (F12) was observed during the field surveys. In particular, the absence of active streams at the slope toe and the lack of undercutting processes justify the attribution of a null weight to this factor.

Regarding the stabilization works (F13), two areas with anchored mesh systems were identified, as shown in Figure 7.6. This structures are considered to have a partially effective effect to the susceptibility of detachment; therefore, a reduced negative value was attributed to the corresponding sectors.

Finally, the annual thermal and hydrological conditions of the site does not favour the occurrence of freeze-thaw cycles. Temperatures rarely fall below freezing and there are no frequent alternating periods of below-zero and above-zero temperatures throughout the year. Consequently, factor (F14) is considered null for the analysed area.

After each column of the attribute table of the point cloud is filled with the assigned weighting factors, the SIF index is computed directly on the attribute table using the field calculator with the codes presented in Appendix III. The Susceptibility Index to Failure as a new attribute value can be rasterized to create a colour map indicating different levels of susceptibility to detachment, (Figure 7.18). Raster resolution was set to 2 x 2 m to optimize subsequent software simulations.

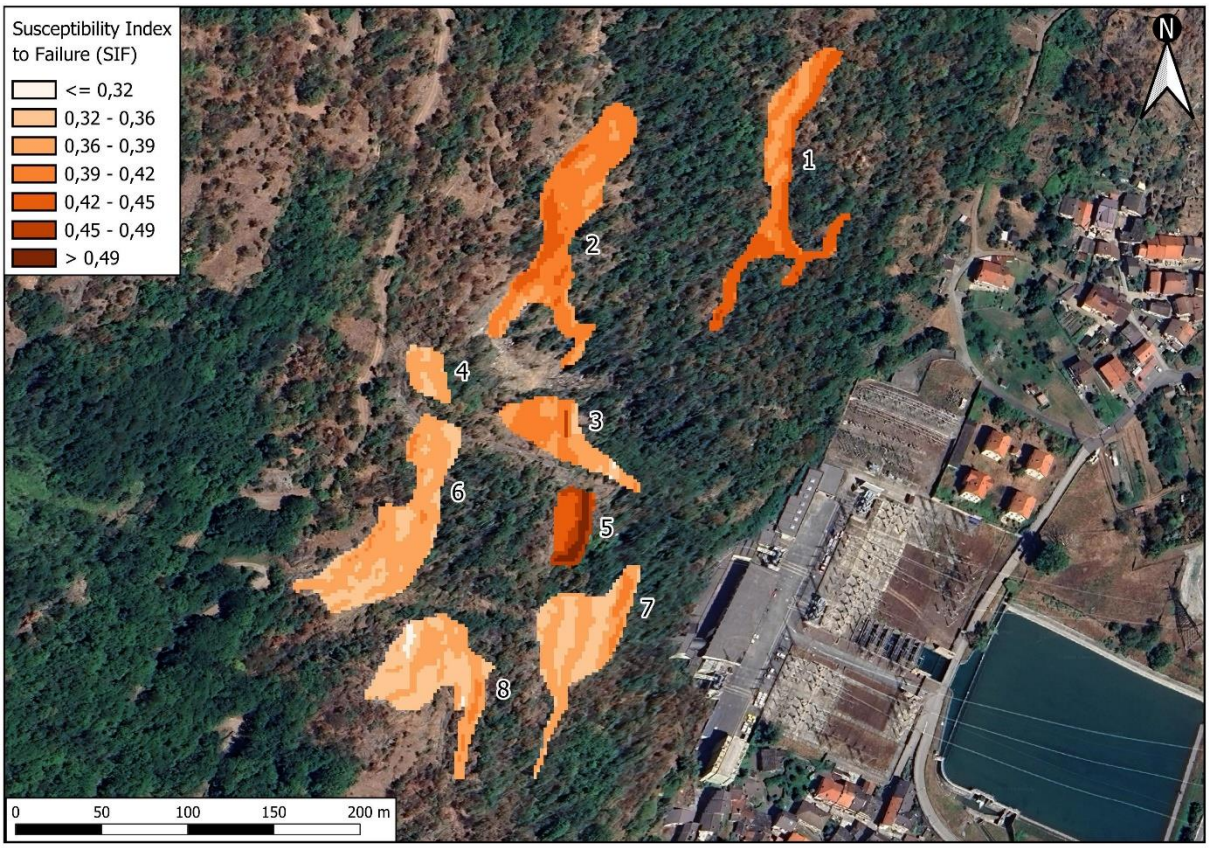

Figure 7.18 - SIF analysis result.

From the SIF map, it can be stated that the rock walls with the highest level of susceptibility to detachment are walls No. 1, 2, 3, and 5, with wall No. 5 exhibiting the highest SIF value of 0,52. This outcome can be related to the steeper inclination of wall No. 5 and its high degree of fracturing, which results in a higher level of hazard potential.

The result is directly comparable with the rockfall event of April 2025, which affected the Venaus hydroelectric power plant at the base of the slope. The detachment originated from the uppermost part of rock wall No. 2, for which a high mean value of SIF was obtained, with the steeper upper sectors of the wall characterized by values ranging between 0,40 and 0,44.

The rest of the rock walls, No. 4, 6, 7, and 8, together with the lower portion of wall No. 3, exhibit the lower values of SIF compared to the others. This corresponds to a lower level of susceptibility to detachment and, consequently, to a reduced hazard associated with the rockfall phenomena.

From a numerical point of view, it is worth emphasizing that the relative homogeneity of some parameter involved in the determination of the SIF index among the different walls implies that the factors having the greatest influence on the differentiation on the level of susceptibility are those that characterize each portion of the rock wall to their specific weight, such as the slope inclination (F1) and the geostructural conditions (F2, F3, F5).

The definition of the SIF index therefore allowed for an objective quantification of the hazard level, in terms of susceptibility to detachment, of the rock walls along the slope upstream of the Enel hydroelectric power plant and the adjacent substation in Venaus. On the basis of these data, it was possible to identify with greater precision the source areas of potential rockfall events, which will subsequently be used in the computation of block trajectories in the 3D analyses, with the aim of defining appropriate mitigation measures for the protection of the existing structures.

7.4 Numerical Analysis

The numerical analysis is structured into three main stages. First, the results of the SIF analysis, together with the other input parameters, are implemented in the QPROTO plugin to perform a simplified three-dimensional runout analysis. Among other results, this step provides weighted trajectory frequency map and enables the computation of the Source Affecting Index for the detachment areas.

Subsequently, a detailed 3D probabilistic rockfall model is implemented using Rockyfor3D, which accounts for the effects of forest cover and slope macro-roughness. This analysis allows for the validation of the QPROTO results and more detailed information of the runout process.

Finally, in order to obtain the parameters required for the design of protection measures, two-dimensional analysis are carried out in Rocfall2 along sections corresponding to a highest trajectory frequency.

7.4.1 Three-dimensional Weighted Runout Analysis

The base of the analysis is a cloud of points identifying the detachment areas, this vector file must have the attributes presented in Table 5.1. The values regarding ID, elevation and aspect are obtained from raster analysis of the DTM and assigned as attribute to the vector file containing the source points. The boulder mass is set to 8100 kg, regarding a 3 m^3 rock block, to represent blocks with sufficient energy to reach the base of the slope and analyse the invasion area. Furthermore, the visibility distance was set to 1000 m in order to extend the analysis to include the areas containing the elements at risk.

The energy line angle was defined following Castelli, *et al.* (2021), this approach allows estimating energy angles for any slope inclination ranging between 30° and 60° approximating them as isometric shapes, and rock volumes between 0.1 and 10 m^3. The energy line charts derived from the analysis are presented in Figure 7.19, (a) refers to slopes without forest cover while

(b) is related to a forest of approximately 400 trees/Ha. Intermediate forest density can be associated to interpolated values between the two sets of curves.

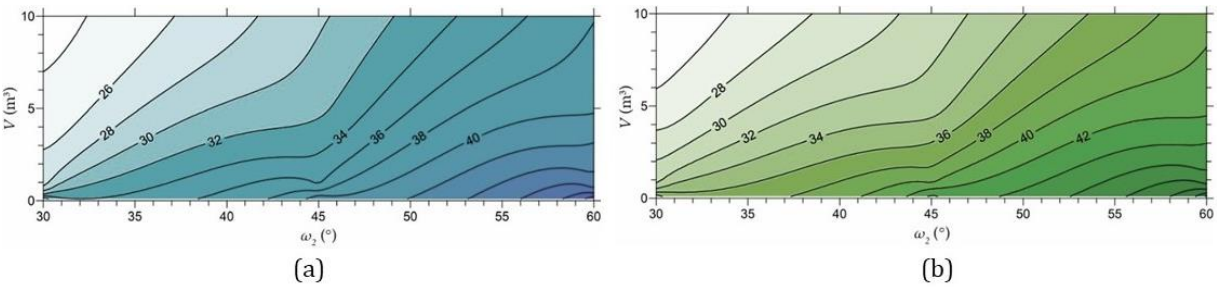

Figure 7.19 - Energy line angle estimation chart for (a) non-forested slope and (b) densely forested slope (Castelli, *et al.,* 2021).

In order to assign a value of energy angle to each rock outcrop, a study of the slope morphology below each homogeneous area was carried out based mainly on the average slope inclination. A dense forest is considered based on previous survey and a block volume of 3 cubic meters. Figure 7.20 exhibits the distribution of the homogeneous zones on the rock outcrops and the assigned energy line angles.

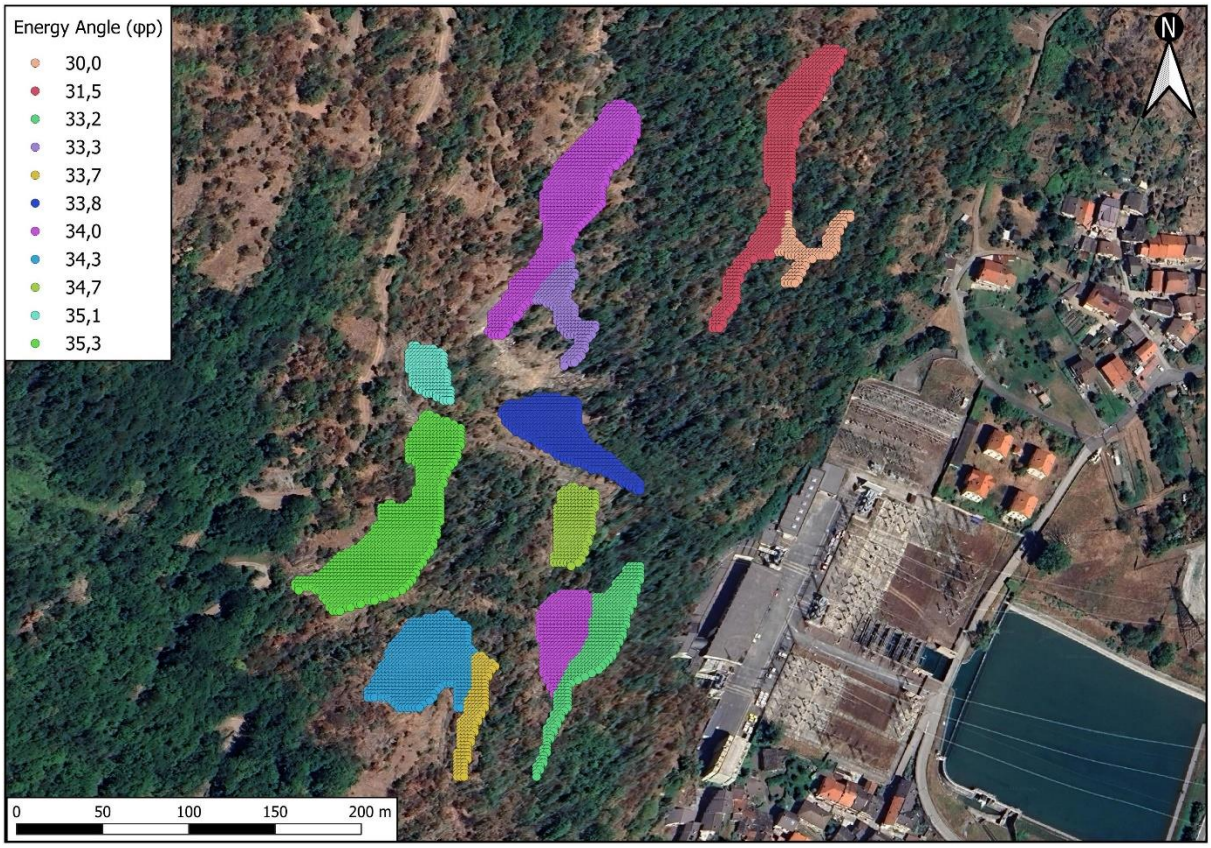

Figure 7.20 - Energy line angle association to each source point.

The last attribute required as input is the lateral dispersion angle, representing the aperture of the cone for the analysis. This parameter is defined following Azzoni *et al.* (1995) that stated that lateral dispersion usually corresponds to 20% of the slope length. From a set of sections equally spaced transversal to the slope direction, displayed in Appendix IV, the slope length was measured from the uppermost part to the base of the slope, resulting in an average slope length of 344,24 m. The lateral dispersion angle (α), assigned to each rock outcrop is computed as follow:

$$\alpha = \tan^{-1}\left(\frac{344{,}24 \cdot 20\%}{344{,}24}\right) = 11{,}3°$$

After defining all the input parameters as attributes of the source points, the analysis was carried out, obtaining all the results listed in Table 5.2 in raster format. Among these outputs, the present study focuses on the *susceptibility*, *i.e.* the weighted passing frequency, *w_en*, the maximum weighted kinetic energy, and *e_max*, the maximum computed kinetic energy, presented in Figure 7.21 to Figure 7.23 respectively. These maps also show the delineation of the rock outcrops and the boundaries of the critical area, where the elements at risk are located.

The susceptibility highlights a clear concentration of high-intensity values in the central and southern parts of the slope, directly downslope of rock walls No. 2, 3 and 7. This area can be interpreted as a deposit zone, where large volumes of rock blocks tends to accumulate. The spatial correspondence between the highest susceptibility corridors and the delimited critical areas demonstrates that a rockfall event is likely to intersect the elements at risk.

The weighted maximum kinetic energy map reveals that the highest energy levels are concentrated below rock walls No. 1, 2, 5 and 7. This parameter considers the energy that the blocks possess during their runout, simulated by QPROTO as an equivalent sliding motion. The spatial coincidence between the critical areas and energy values up to 2.500 kJ indicates that a potential rockfall event might reach the elements at risk with considerable impact energy, stressing the need for protective measures designed to withstand impacts of high levels of energy. As for the protective measures, these are installed a few to some tens of meters behind the boundaries of the critical areas, where topographic conditions and normative space requirements allows their installation, in this sectors, the energy levels are even higher.

The maximum computed kinetic energy is presented to enable comparison with a model that reproduces the phases of motion with more accuracy. This non-weighted parameter also highlights a considerable gap between the weighted kinetic energy of almost triple its value. The results demonstrate that neglecting the Susceptibility Index to Failure may lead to an overestimation of the potential hazard, as non-weighted parameters do not consider the detachment propensity of each source area.

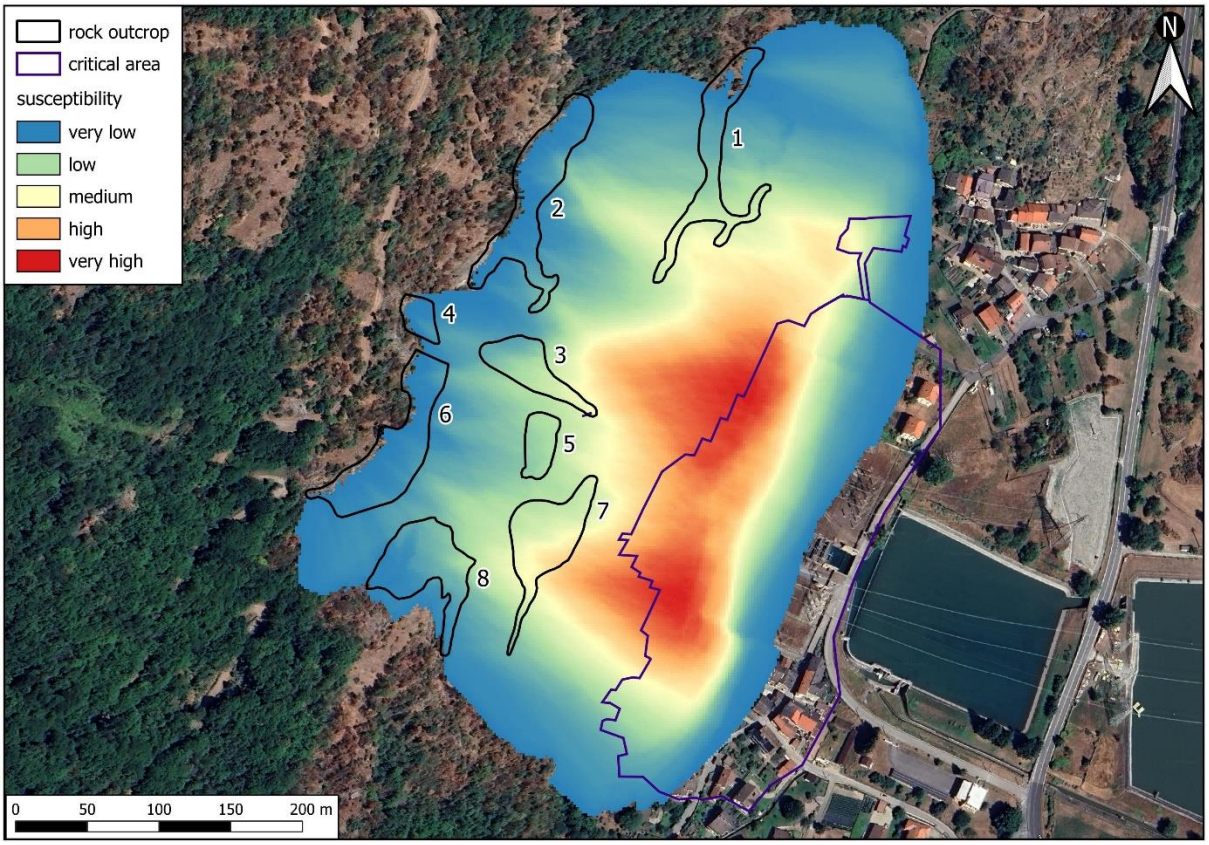

Figure 7.21 - Susceptibility map, 3 m³ block.

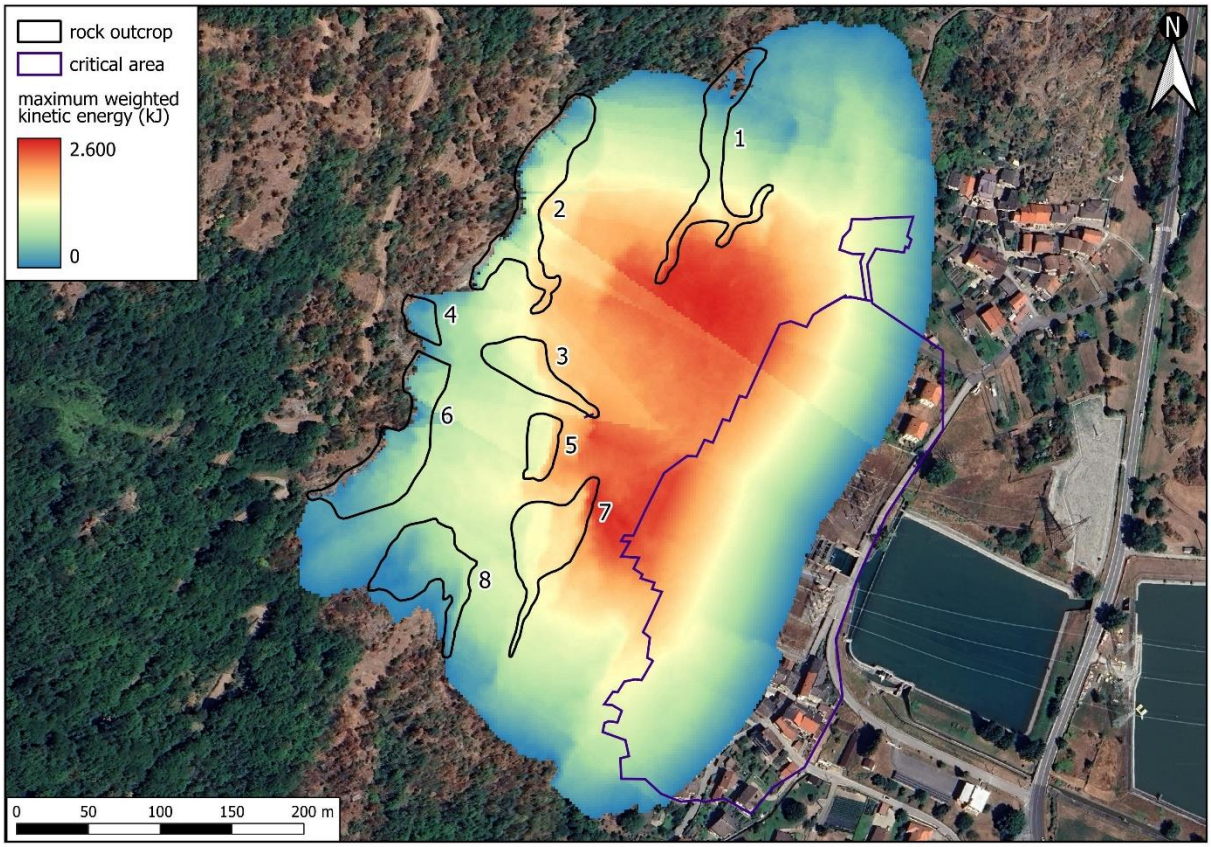

Figure 7.22 - Maximum weighted kinetic energy, 3 m³ block.

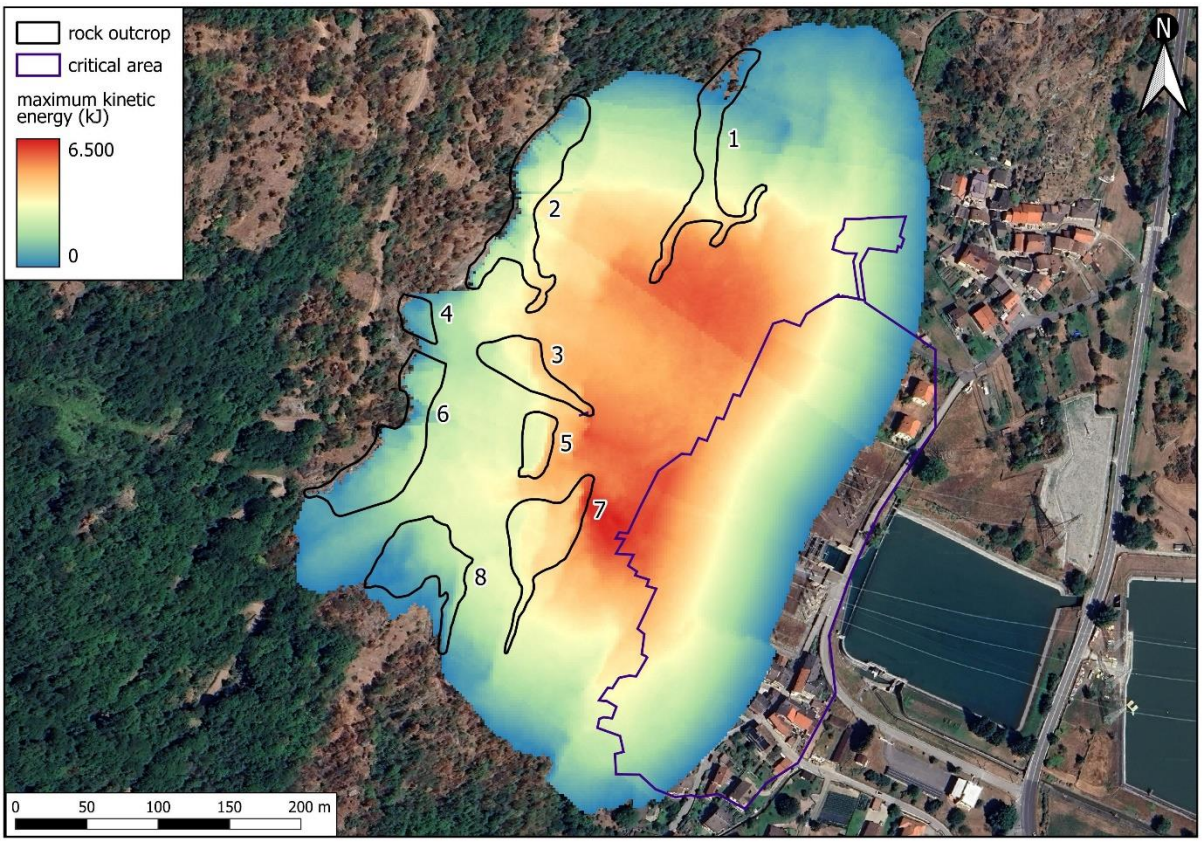

Figure 7.23 - Maximum kinetic energy, 3 m^3 block.

Following the QPROTO analysis, in order to identify the most hazardous sectors within the detachment areas, the next step is to apply the RADAR plugin with the output files from QPROTO. The result, shown in Figure 7.24, reveals that the highest SAI values are associated with rock walls No. 2, 4, and 6; which is consistent with the event of April 2025 regarding the rock wall No. 2. In contrast, parts of rock outcrops No. 3, 5 and 8 exhibit a moderate level of impact on the critical areas, while the remaining rock walls present values lower than 4%. This result evidence that blocks detaching from the upper part of the slope are those that mostly affect the elements at risk, likely due to the greater potential energy accumulated at higher elevations, which results in higher velocities and impact energies along the runout paths.

The overall result indicates that 29,75% of the 4.951 source points do not affect the critical areas. Furthermore, 28,05% of the source points have a SAI value ranging from 0% to 2%, meaning that they can hit up to 2% of the elements at risk. A total of 30,52% of the source points range between 2% and 6%. Finally, only 363 source points, representing 4.34% of the total, have a Source Affecting Index greater than 8%, with only 1,07% exceeding the 10% threshold. The chart on Figure 7.25 shows a frequency distribution of the SAI ranges.

These results highlight that the areas most susceptible to detachment are not necessarily the most hazardous ones, blocks detaching from the weakest rock walls might not necessarily reach the critical areas. This indicated that the morphological characteristics of the slope play a fundamental role in controlling the rockfall hazard.

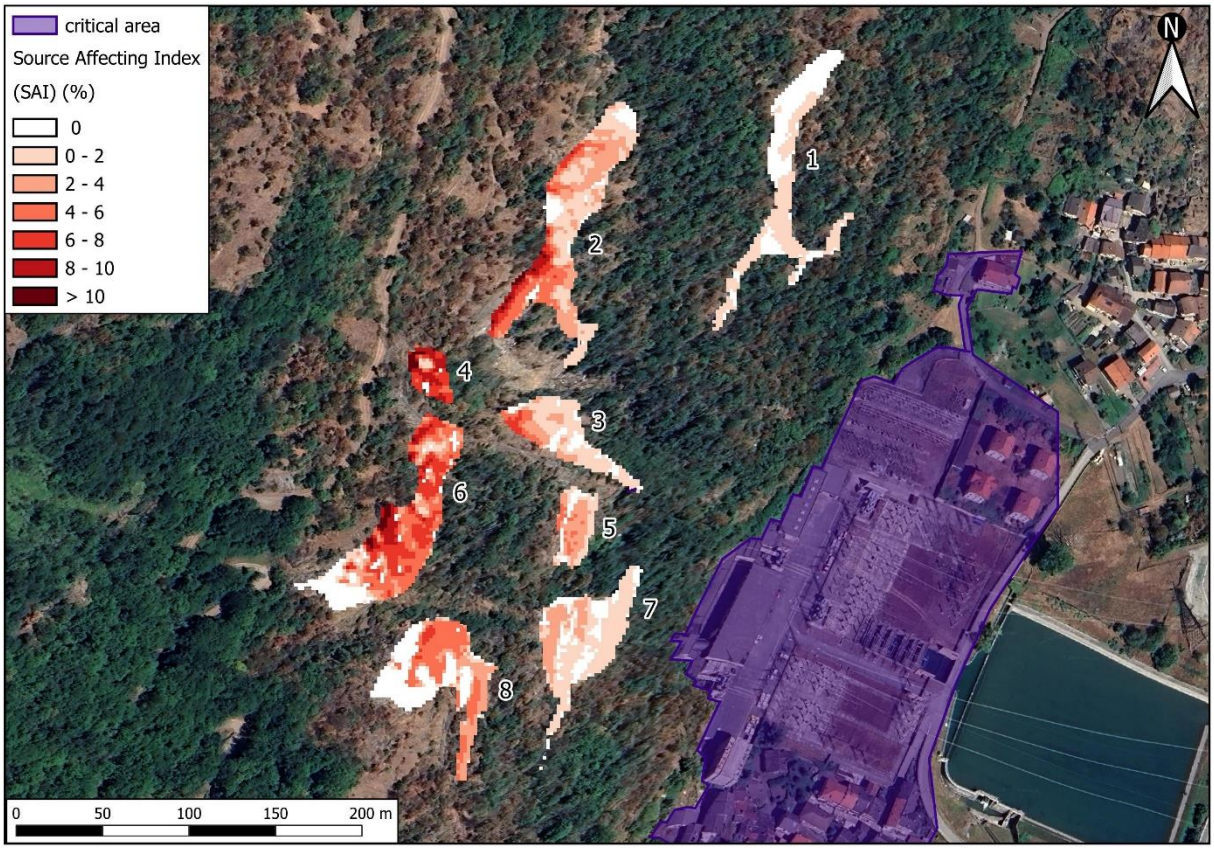

Figure 7.24 - SAI analysis result.

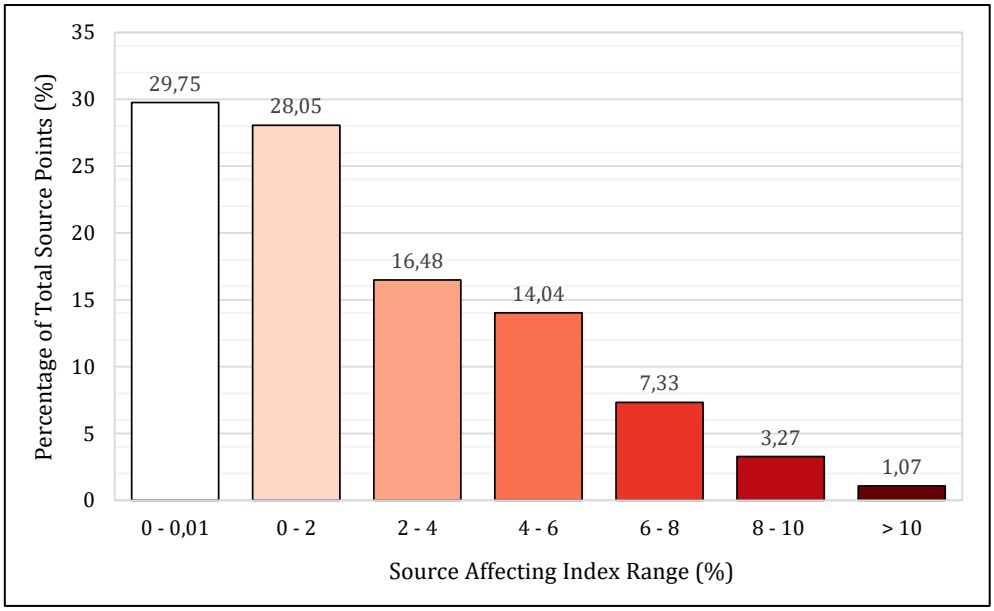

Figure 7.25 - Frequency distribution of the SAI.

7.4.2 Three-dimensional Predictive Runout Analysis

A Rockyfor3D model will be implemented in order to obtain results that better reproduce the runout trajectories of the falling blocks, with a more detailed representation of the different phases of motion. The parameters required to run the analysis have already been described in Section 5.4.1.

Following an extensive analysis of geological maps, aerial photogrammetry and background site-specific information, the different types of surface cover of the slope were identified and discretized for further parameter association. Figure 7.26 shows the terrain characterization of the slope.

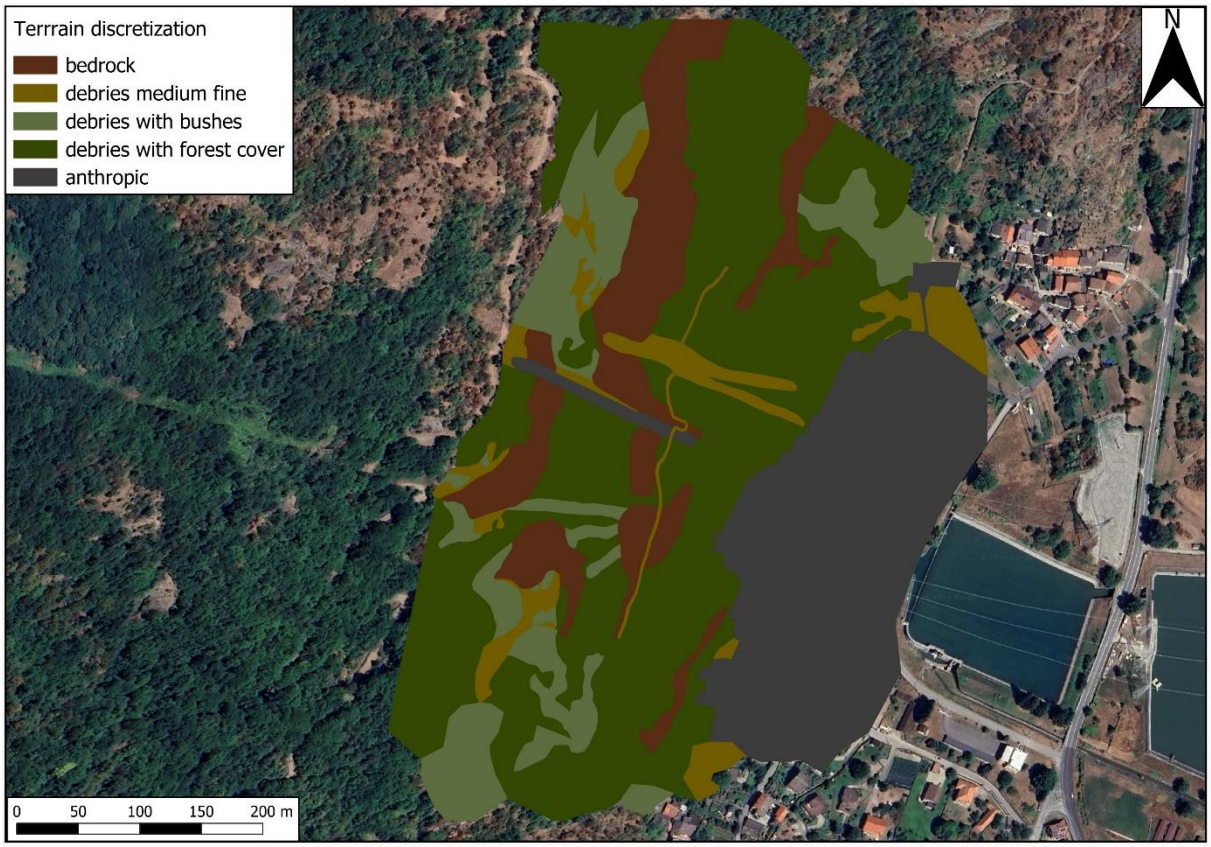

Figure 7.26 - Soil type discretization.

The parameters needed for the terrain characterization were initially obtained through a comparison between photographs taken during the different surveys and examples from the software manual presented in Appendix V, together with the forest data from Section 7.2.3.

Back Analysis

In order to adjust the initial characteristic parameters of the terrain, a back analysis is performed considering the event of April 2025. For the input, the DTM with 2 x 2 m resolution was used as a base for the analysis. An ellipsoidal shaped block having 4 m^3 was considered and the cells contained within the rock outcrops delimitations were characterized with a rock density value of 2.700 kg/m^3. A total of 4.951 cells are characterized as source points, therefore, with a number of simulations per cell set to 1.000, a total of 4.951.000 trajectories were simulated.

From the data in Table 7.2, the surveyed areas were extrapolated based on satellite imagery to define and delineate larger forest zones. The forest density result in zone *d* is considered to be inconsistent with site observations. In order to address this, an average of the adjacent zones was taken to characterize the number of trees per hectare on zone *d*.

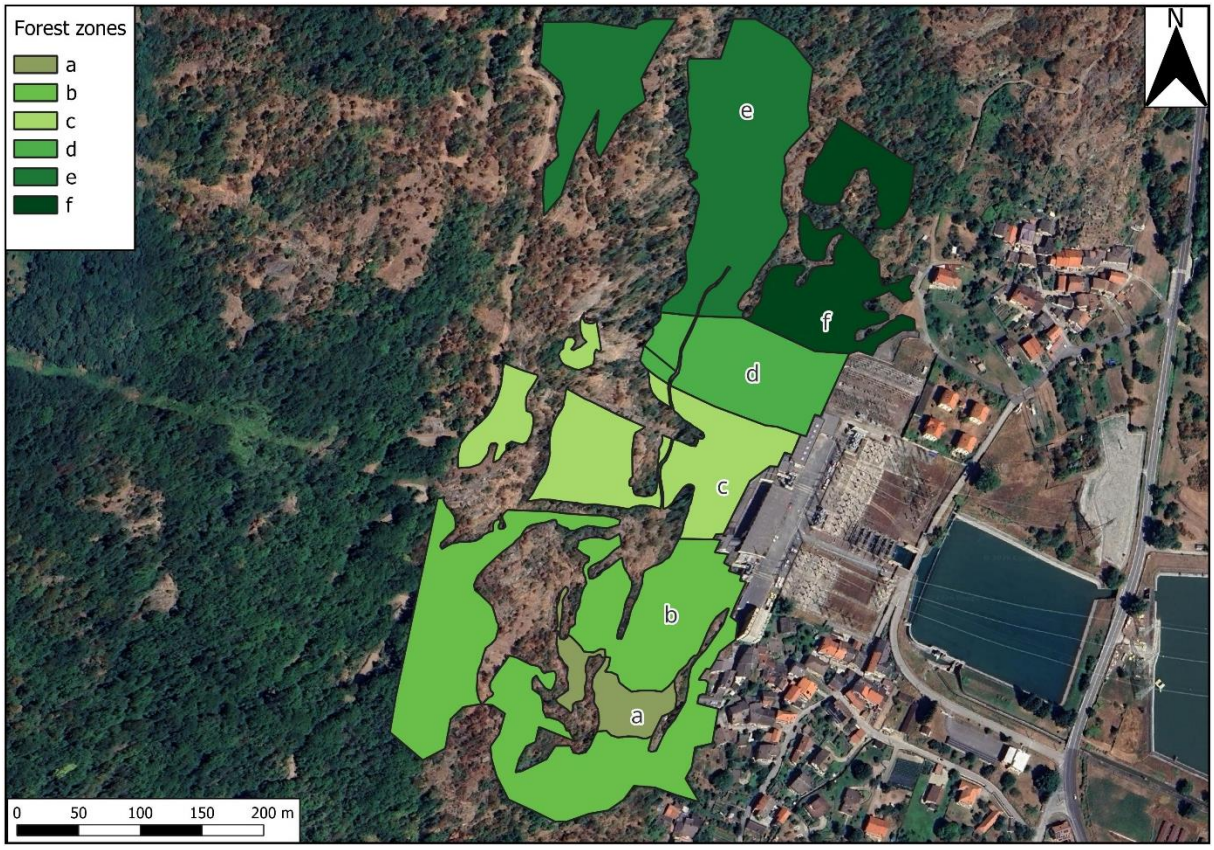

Figure 7.27 – Forest zones for Rockyfor3D analysis.

After several attempts of parameter characterization, a considerable block accumulation is perceived on the electric distribution centre, whereas fewer blocks accumulate where the building was hit. This last event can be classified as a rare, corresponding to trajectories with a low probability of occurrence. In any case, the accumulation and runout outputs serve as validation for the back analysis. Table 7.4 summarizes the roughness and soil type derived from the back analysis, while Figure 7.28 presents a map illustrating the most probable trajectories and stopping points with block accumulations higher than 500 units, representing 0,01% of the total number of simulations.

Table 7.4 – Roughness and soil type parameters obtained through back analysis.

Terrain characterization	Roughness			Soiltype
	rg70	rg20	rg10	
anthropic	0	0	0	1
bedrock	0	0	0,70	6
debris medium fine	0,05	0,10	0,20	4
debris with bushes	0,05	0,10	0,20	4
debris with forest	0,05	0,10	0,20	4

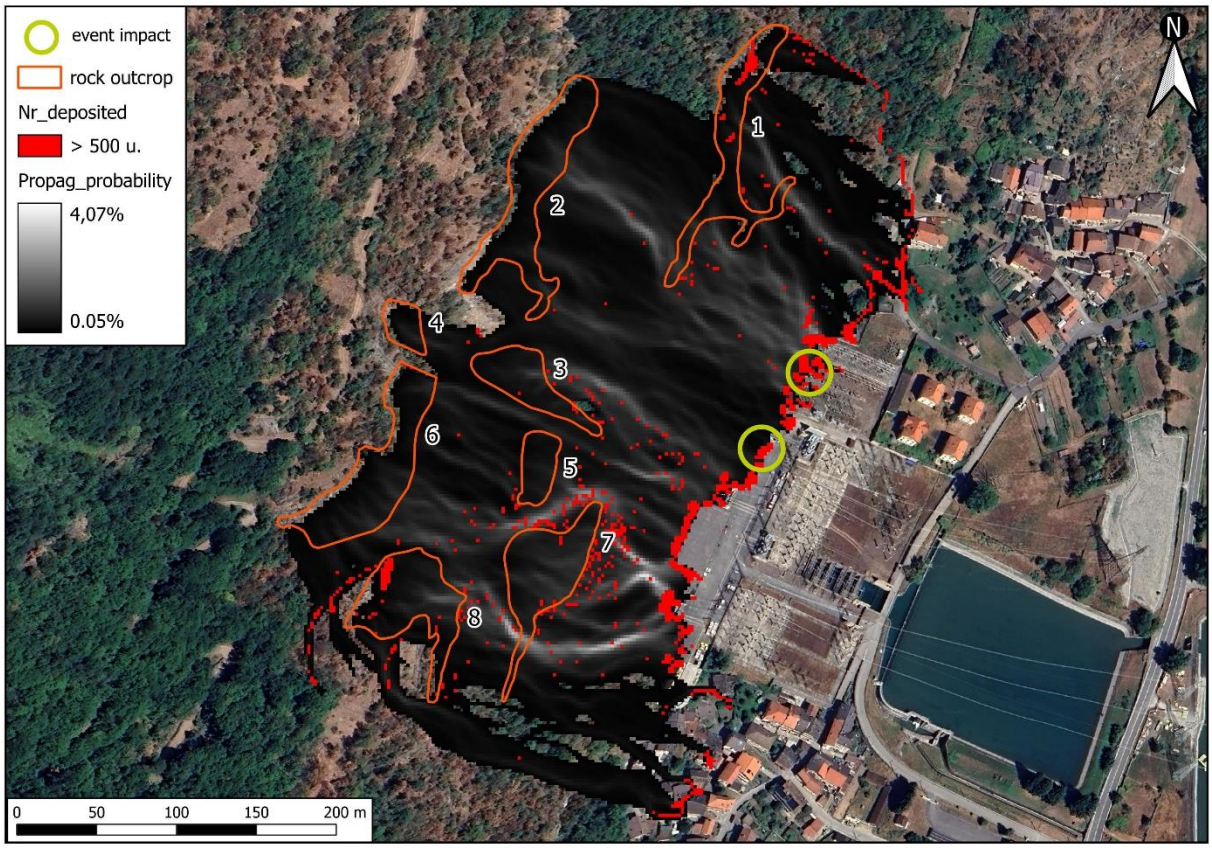

Figure 7.28 – Propagation probability and stopping points (>500 units) from back analysis.

Predictive Runout Analysis

This set of analyses was performed in order to analyse the behaviour of rock blocks falling along the slope. The main outputs are the preferred trajectories paths, the distribution of the stopping points along the slope, and the associated kinetic energy and passing height. In particular, two-dimensional sections will be derived from the main trajectories to perform 2D analyses for the design of rockfall protection barriers.

For the main analysis of the actual conditions, the forest density on zone *d* was reduced by 30%, resulting in 2065 trees/Ha, to be cautious and account for the previous event damage, for the same reason, the soil type characterized with medium fine debris below the event detachment area increased its roughness. Two deterministic scenarios of block volumes were analysed, considering rock blocks having 1 and 3 m^3, respectively.

Table 7.5 - Roughness and soil type parameters for the predictive analysis.

Terrain characterization	Roughness			Soiltype
	rg70	rg20	rg10	
anthropic	0	0	0	1
bedrock	0	0	0,70	6
debris medium fine	0,15	0,15	0,25	4
debris with bushes	0,05	0,10	0,20	4
debris with forest	0,05	0,10	0,20	4

The predictive analysis results are presented in terms of propagation probability, stopping point distribution, and kinetic energy and passing heights classes at the 99th percentile, in order to capture values approaching the maximum for each scenario.

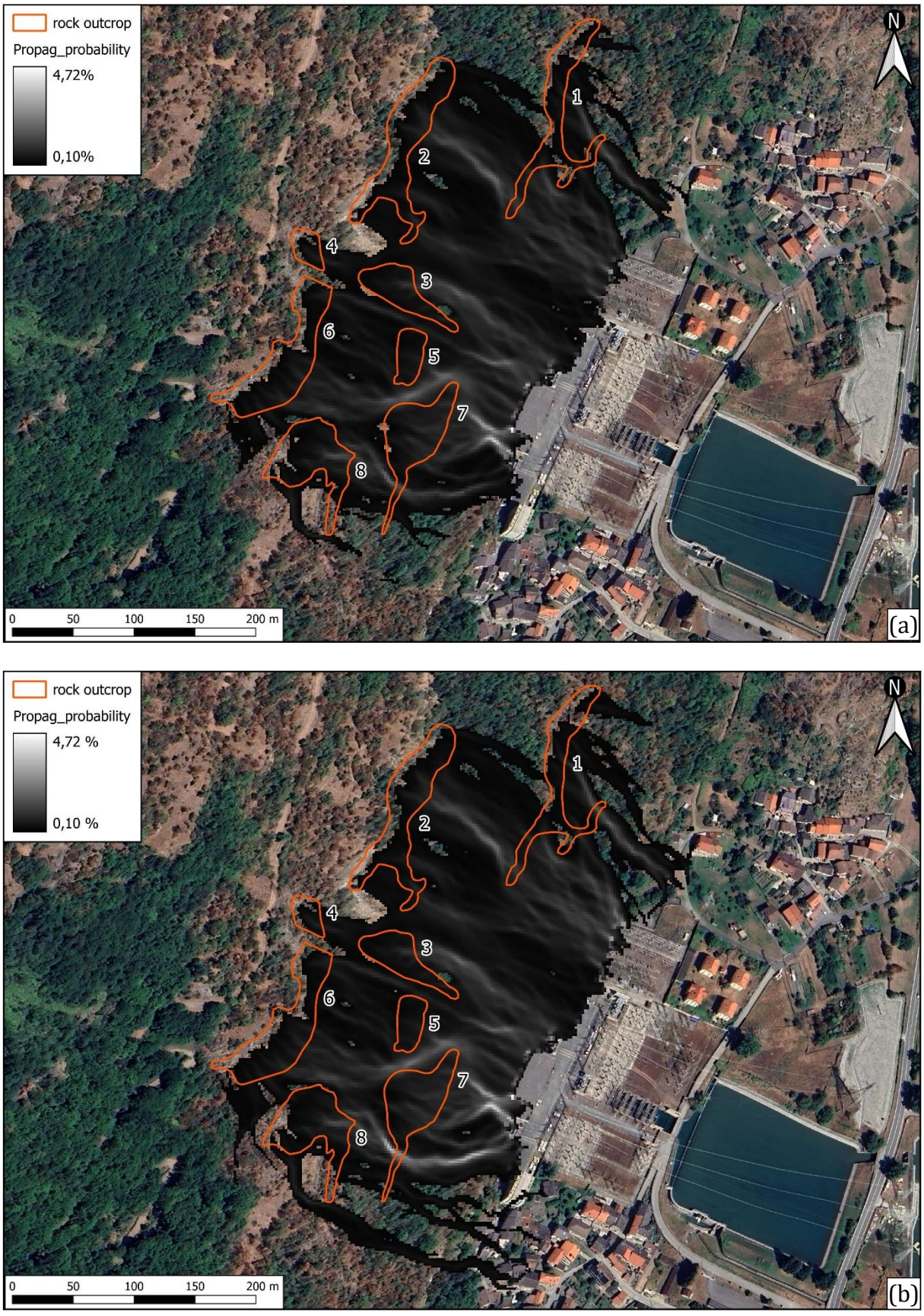

Figure 7.29 - Propagation probability; (a) 1 m^3; (b) 3 m^3.

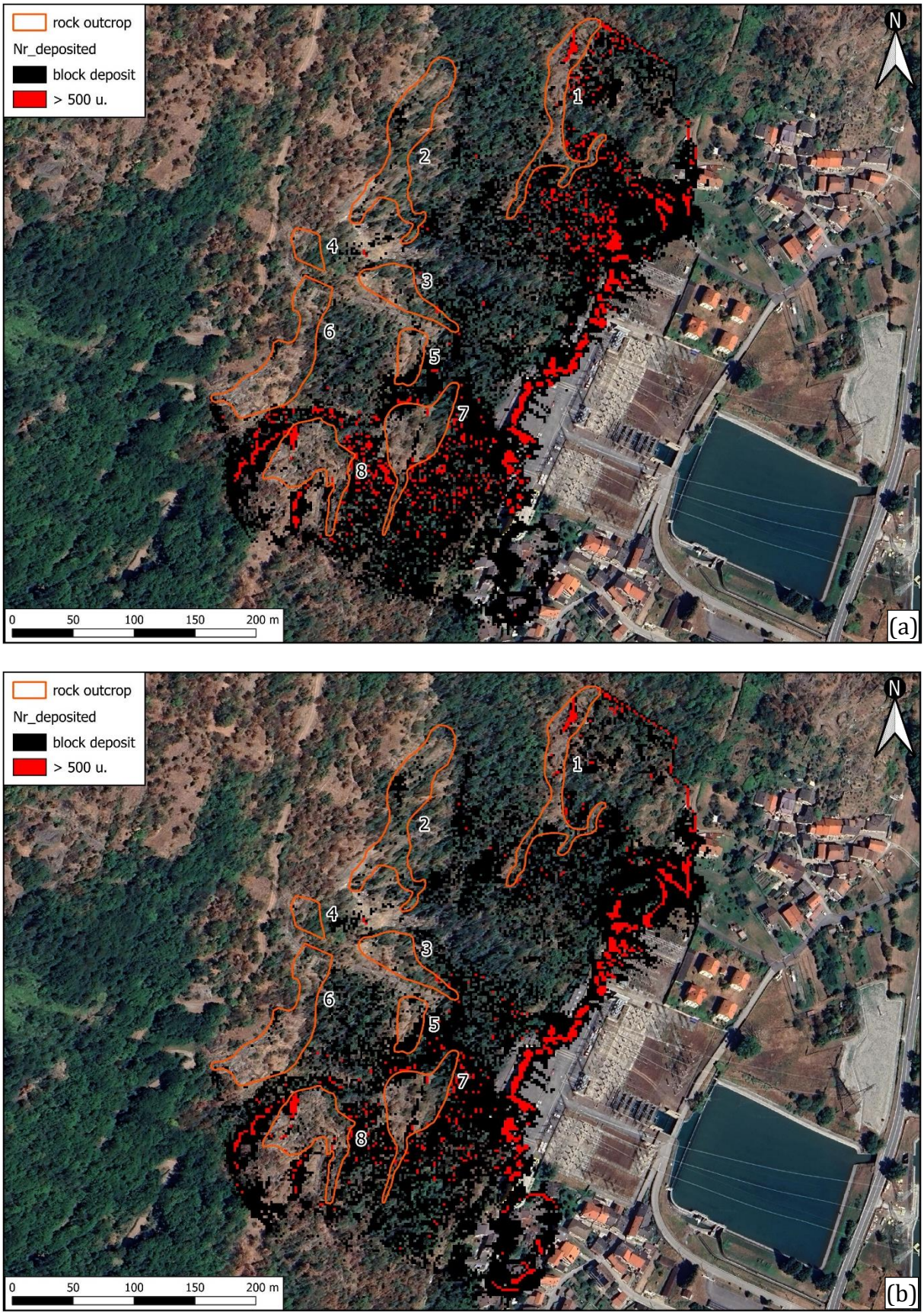

Figure 7.30 - Deposited blocks; (a) 1 m^3; (b) 3 m^3.

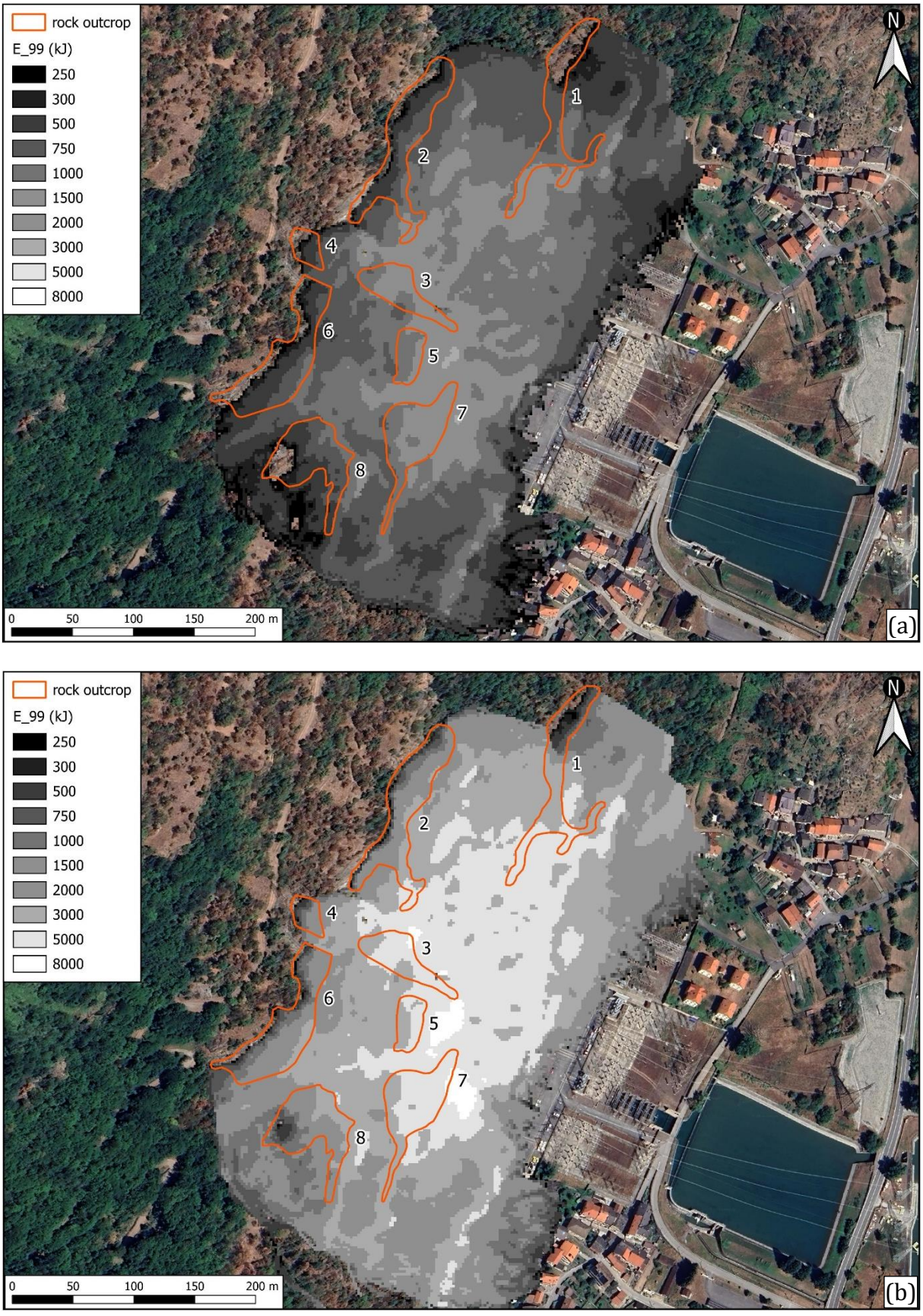

Figure 7.31 - Kinetic energy at the 99th percentile; (a) 1 m^3; (b) 3 m^3.

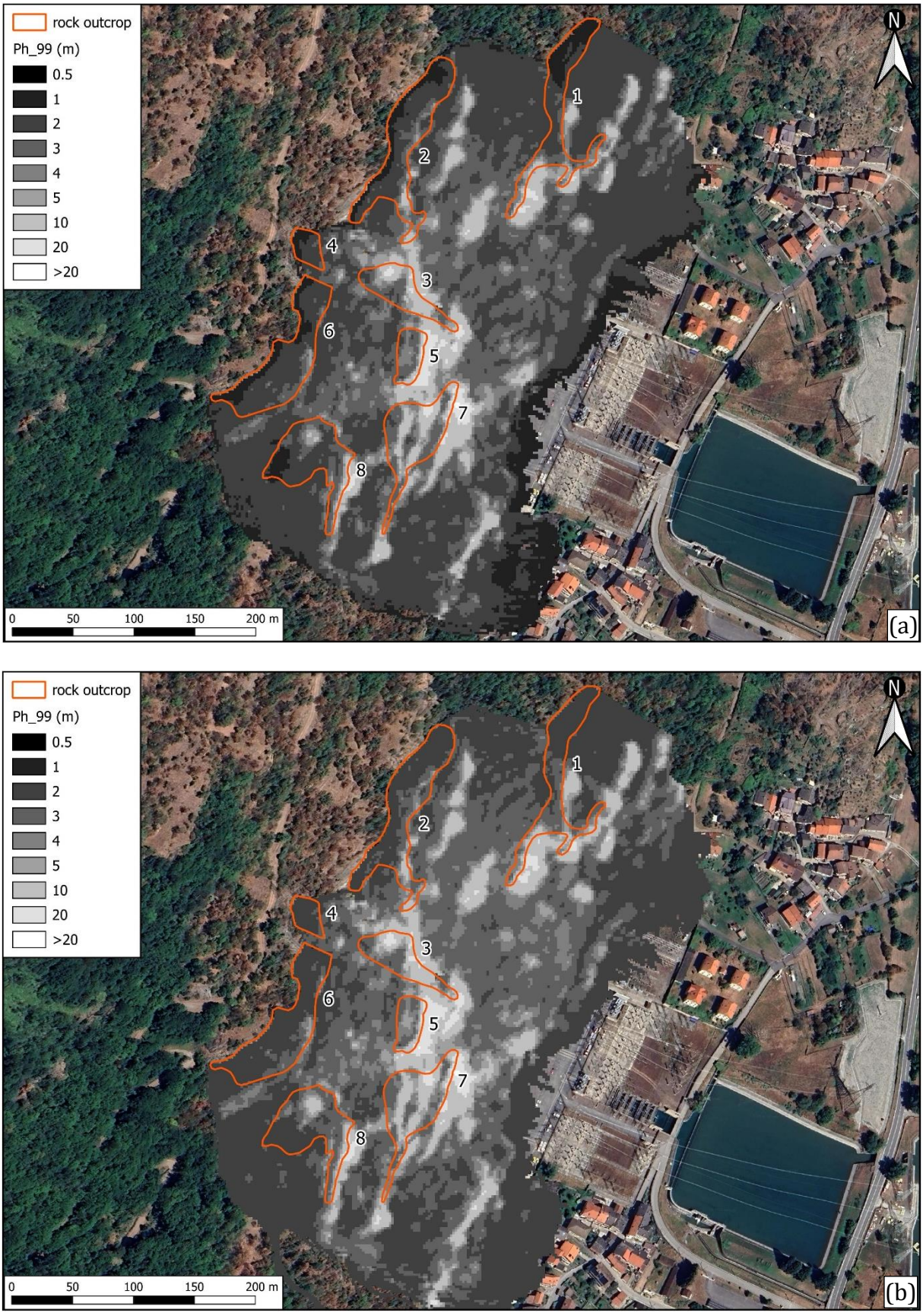

Figure 7.32 - Passing height at the 99th percentile; (a) 1 m³; (b) 3 m³.

Conclusions

In comparison with back analysis results, Figure 7.29 shows a consistent dispersion of the most frequent runout paths, not changing the trend in the middle part of the analysing area for neither of the scenarios considered. The main difference between the scenarios is that blocks having larger volumes tend to arrive farther and extend the invasion area on the NE and SW of the slope.

Likewise, in comparison with the back analysis results, Figure 7.30 exhibits a wider dispersion of blocks stopping points along the slope. Between scenarios, a small increase in deposit zones before reaching the slope is presented with 1 m^3 blocks. In any case, a predominant accumulation area concentrates at the base of the slope. Consequently, blocks with volume ranging between 1 and 4 m^3 systematically reach the base of the slope, representing a potential hazard to the exposed elements in this area. Therefore, reinforcing the need for protection measures along the entire base of the slope.

In addition, the maximum values of propagation probability and spatial distribution of the stopping points from Figure 7.29 and Figure 7.30 suggests that, although the overall runout is comparable, slight differences occur at the southern extreme of the analysed area. In this sector, longer and denser preferential paths are observed when larger volumes of blocks are involved, whereas in the predictive runout analysis with smaller blocks (1 to 3 m^3) show less runout concentration on this path.

Furthermore, the physical properties that characterize the runout, kinetic energy and passing heights, exhibited in Figure 7.31 and Figure 7.32, a clear correspondence between high energy levels and elevated bounced heights, particularly pronounced downslope rock walls No. 5 and 7. Rock walls No. 2 and 1 are also a source of blocks that achieve high levels of energy and passing height along their runout paths. Meanwhile the areas where maximum kinetic energy values occur are spatially consistent for both scenarios. However, a clear increase to higher energy levels is observed for larger blocks. In contrast, passing heights do not exhibit a significant step increase, maintaining similar values across most areas and comparable maximum values in both scenarios. This behaviour suggests a strong topographic control, where the highest values likely correspond to free-fall trajectories originating from the upper parts of steep rock faces.

It is worth noting the similarities between the analyses conducted with Rockyfor3D and QPROTO. Although magnitudes differ, the zones having the higher levels of energy spatially coincide. This indicates that, even when using a simplified method, the general patterns of block runout and energy concentration are reliably captured. This supports for a two-step approach, first QPROTO can be used for identify areas at risk, while Rockyfor3D provides precise energy data of the runout.

7.4.3 Two-dimensional Analysis

A further analysis is conducted on sections with the higher values of propagation probability (Figure 7.33) in order to get more detailed information on kinetic energy and bouncing heights. This analysis will also serve for the calculation and design of the retaining structures.

A new back analysis is required as restitution coefficients respond different in 2D and 3D models due to the distinct representation of the block geometry and the associated degrees of freedom, which affect energy dissipation and rebound behaviour during impacts. Furthermore, variations between models numerical simulations and assumptions can have an influence on these parameters.

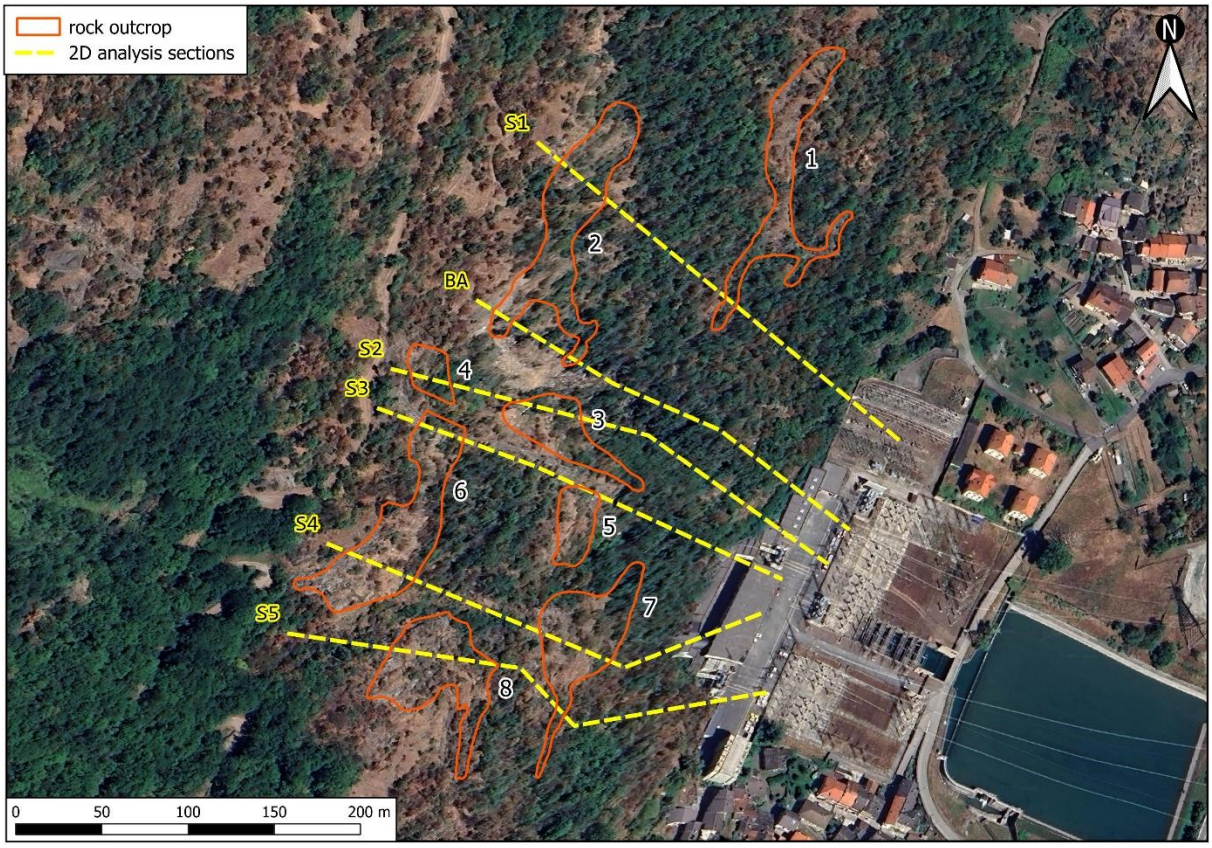

Figure 7.33 - Rocfall2 analysis sections.

The trajectory from the April 2025 event was derived from the conducted surveys and the 2D profile following that trajectory was derived from the DTM. The surveys also indicate that the detachment occurred on the southern upper part of rock wall No. 2, and that the block that collided with the building was estimated in about 4 m³. Table 7.6 exhibits the parameters that characterize the slope cover material derived from a back analysis procedure, while Figure 7.34 shows the trajectories derived from the simulation with a close in of the building area on the upper-right corner, depicting the several possibilities of blocks arriving to the roof of the building.

Table 7.6 - Terrain coefficients obtained from back analysis.

Material Name	Color	Normal Restitution	Tangential Restitution	Dynamic Friction	Rolling Friction	Effective Forest Height (m)	Forest Drag (kg/s)
bedrock		Normal Mean: 0.46 Std Dev: 0.04 Rel. Min: 0.12 Rel. Max: 0.12	Normal Mean: 0.7 Std Dev: 0.03 Rel. Min: 0.09 Rel. Max: 0.09	Normal Mean: 0.31 Std Dev: 0.04 Rel. Min: 0.12 Rel. Max: 0.12	Normal Mean: 0.1 Std Dev: 0.02 Rel. Min: 0.06 Rel. Max: 0.06		
debries medium fine		Normal Mean: 0.35 Std Dev: 0.04 Rel. Min: 0.12 Rel. Max: 0.12	Normal Mean: 0.65 Std Dev: 0.04 Rel. Min: 0.12 Rel. Max: 0.12	Normal Mean: 0.35 Std Dev: 0.04 Rel. Min: 0.12 Rel. Max: 0.12	Normal Mean: 0.25 Std Dev: 0.02 Rel. Min: 0.06 Rel. Max: 0.06		
debries with bushes		Normal Mean: 0.35 Std Dev: 0.04 Rel. Min: 0.12 Rel. Max: 0.12	Normal Mean: 0.6 Std Dev: 0.04 Rel. Min: 0.12 Rel. Max: 0.12	Normal Mean: 0.35 Std Dev: 0.04 Rel. Min: 0.12 Rel. Max: 0.12	Normal Mean: 0.3 Std Dev: 0.03 Rel. Min: 0.09 Rel. Max: 0.09		
debries with forest cover		Normal Mean: 0.35 Std Dev: 0.04 Rel. Min: 0.12 Rel. Max: 0.12	Normal Mean: 0.6 Std Dev: 0.04 Rel. Min: 0.12 Rel. Max: 0.12	Normal Mean: 0.35 Std Dev: 0.04 Rel. Min: 0.12 Rel. Max: 0.12	Normal Mean: 0.3 Std Dev: 0.03 Rel. Min: 0.09 Rel. Max: 0.09	3.5	250
concrete		0.2	0.3	0.55	0.1		

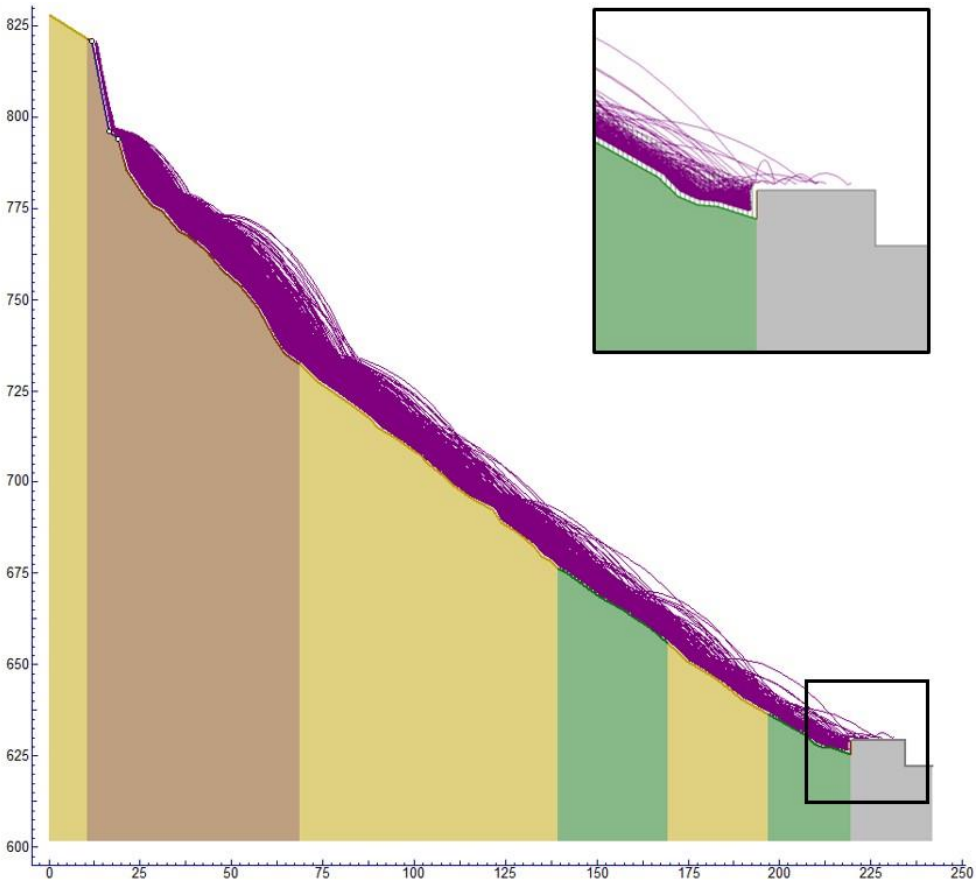

Figure 7.34 - Back analysis block trajectories (4m^3).

The representative rock block for the predictive runout analysis was selected considering the worst known case scenario, a 4 m^3 rock block. Rockyfor3D results indicates that, in this case, higher energy values are associated to bigger blocks (Figure 7.31). For the case under study, the largest block registered corresponds to the event of April 2025 and was therefore adopted as the reference scenario. The sources of detachment were set on the most vertical sectors on the slope sectors characterized with rock outcrops.

The number of simulations was defined at 25 rock blocks per meter of source line in order to get a homogeneous analysis in all sections. Table 7.7 lists the number of seeders placed per section, their length, and the associated number of simulations for each model.

Table 7.7 - Seeders and number of simulations associated.

Section	Source		No. of simulations
	#	length (m)	
S1	1	45,3	1133
	2	21,2	530
	3	20,5	513
	total	87,0	2175
S2	1	13,3	333
	2	13,6	340
	3	18,2	455
	4	18,7	468
	total	63,8	1595
S3	3	45,3	1133
	4	16,3	408
	total	61,6	1540
S4	1	15,5	388
	2	12,5	312
	3	32,3	808
	4	13,5	338
	5	15,2	380
	6	12,7	318
	total	101,7	2542
S5	1	20,8	520
	2	20,3	508
	3	11	275
	total	52,1	1303

In all the considered sections, collectors were placed at different quotes to gather data on trajectories dynamics. For each section, the runout trajectories, the percentage of blocks stopped along the slope, the translational velocity, and the passing height, reported at their 95th percentile, were extracted for analysis.

Following, the runout trajectories and stopping points along the slope profile are presented for each of the considered sections.

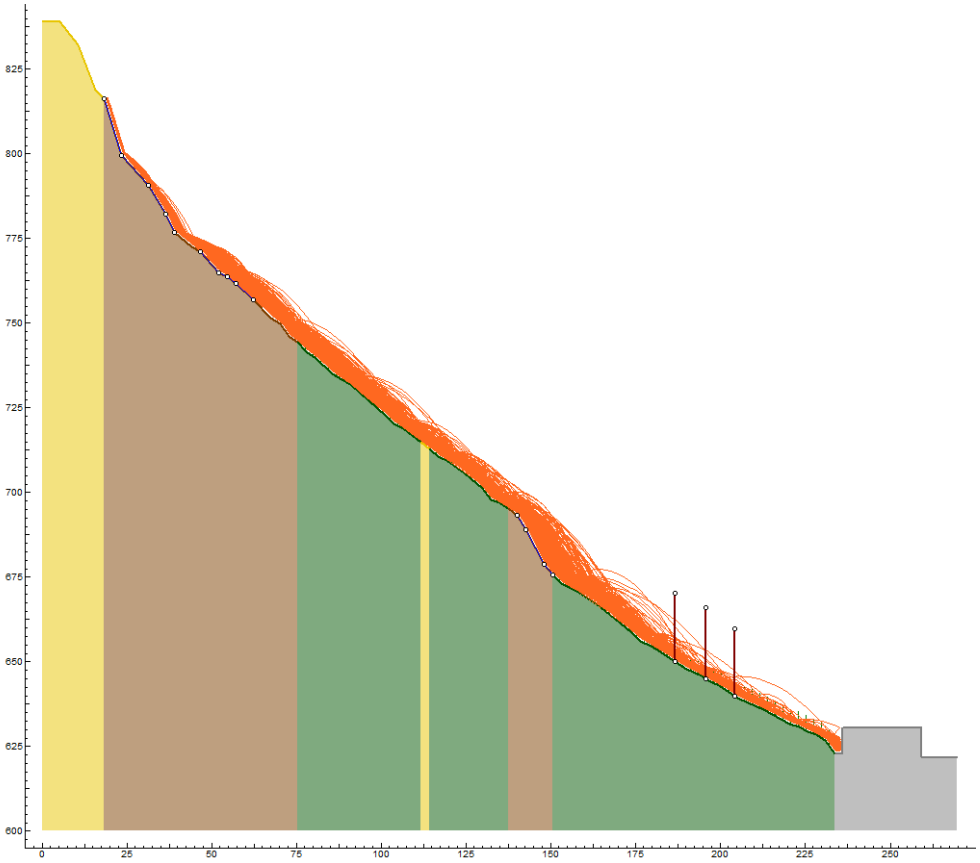

Figure 7.35 - Section S1, trajectories and collectors.

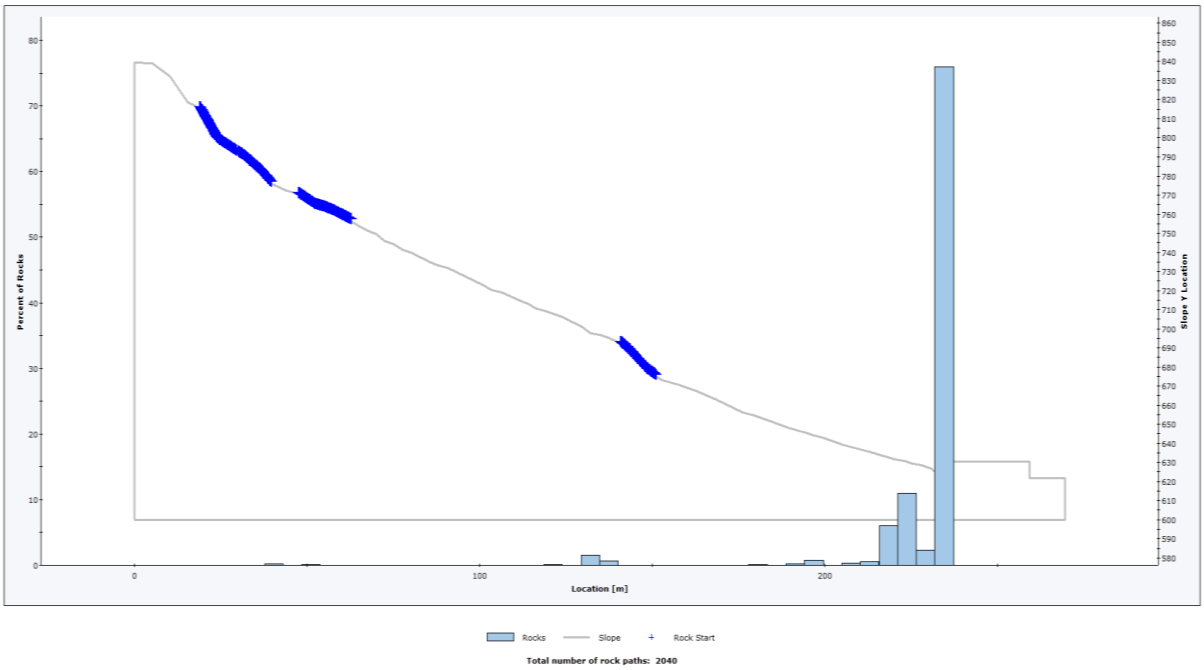

Figure 7.36 - Section S1, stop points along the slope.

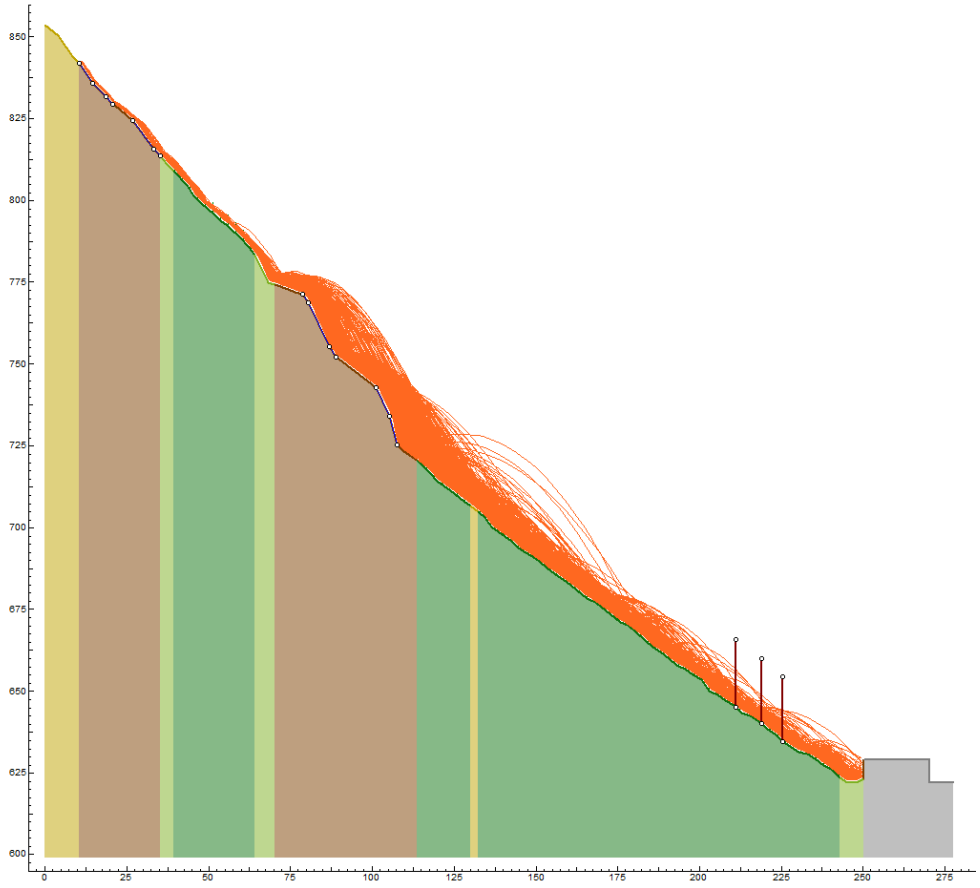

Figure 7.37 - Section S2, trajectories and collectors.

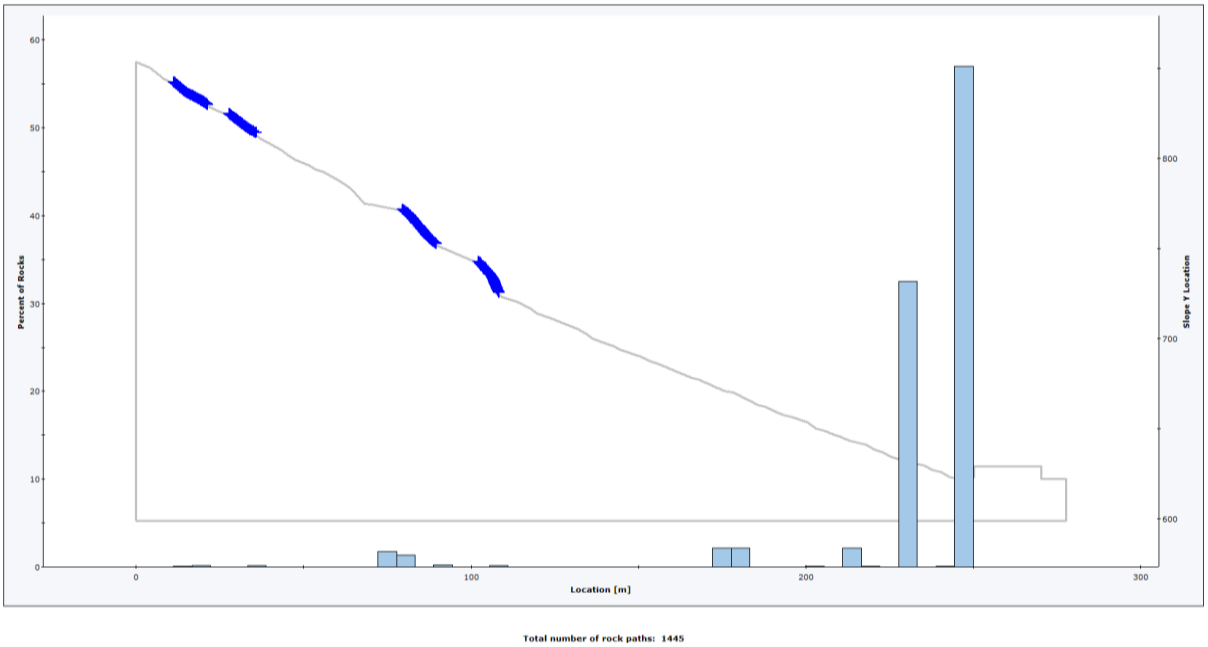

Figure 7.38 - Section S2, stop points along the slope.

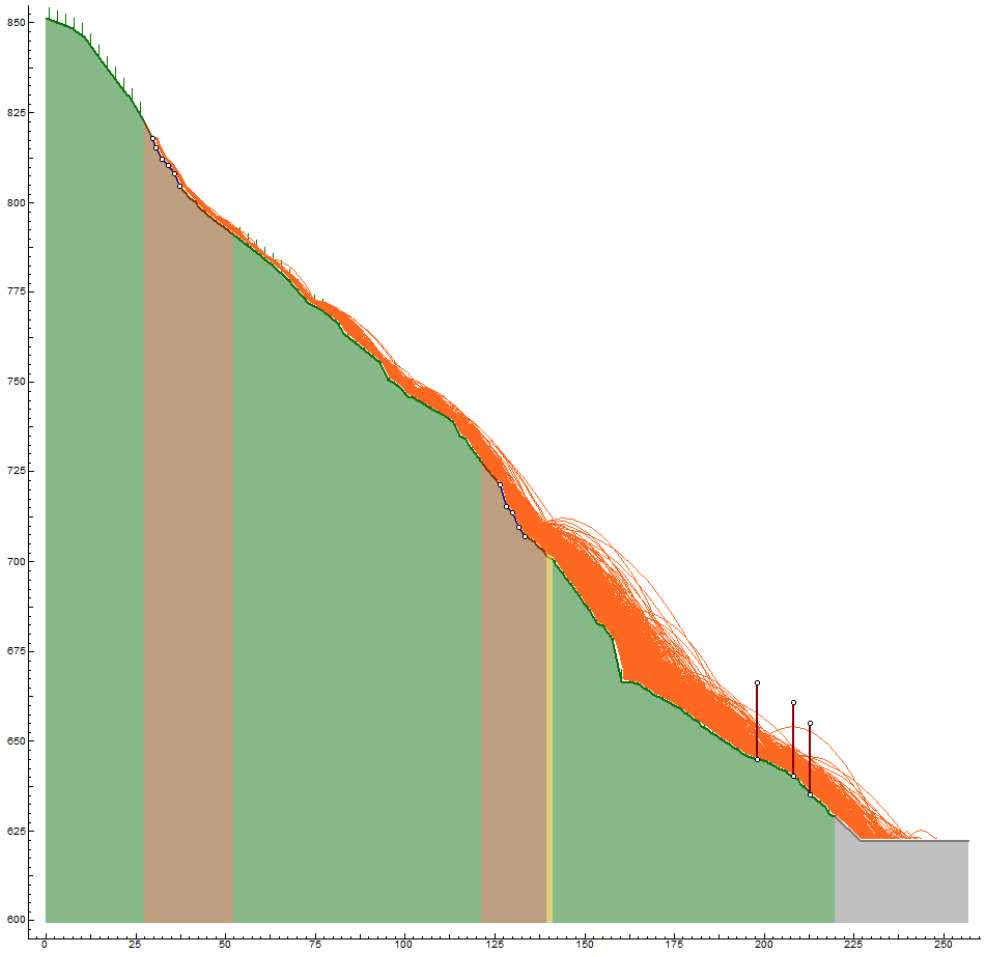

Figure 7.39 - Section S3, trajectories and collectors.

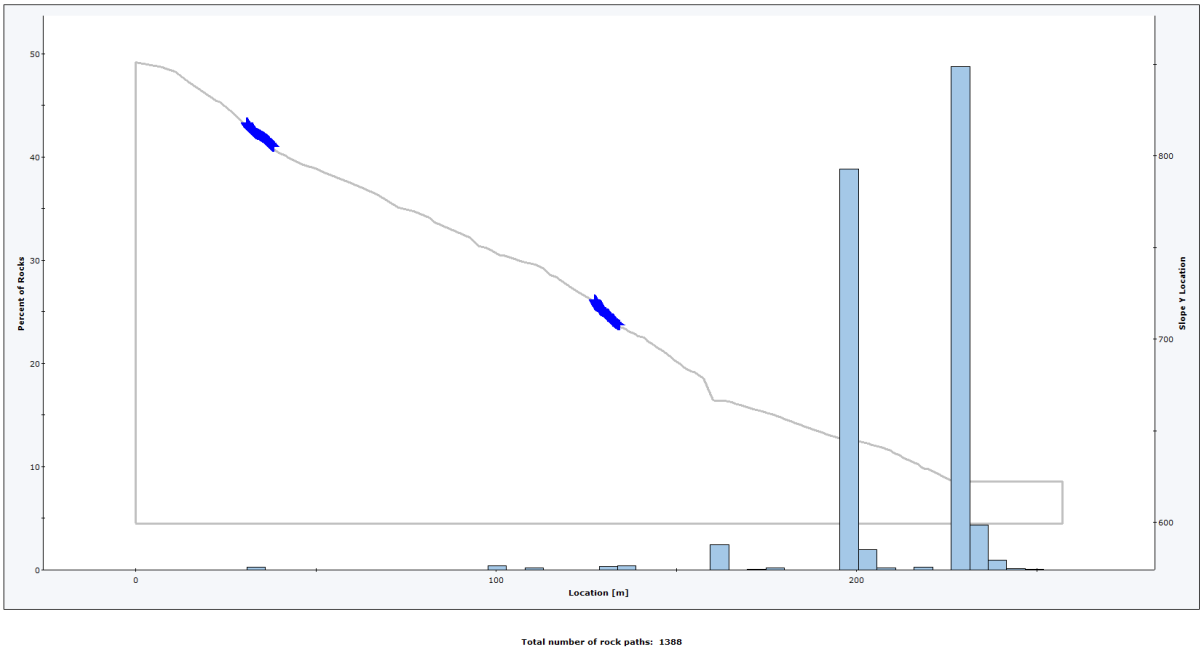

Figure 7.40 - Section S3, stop points along the slope

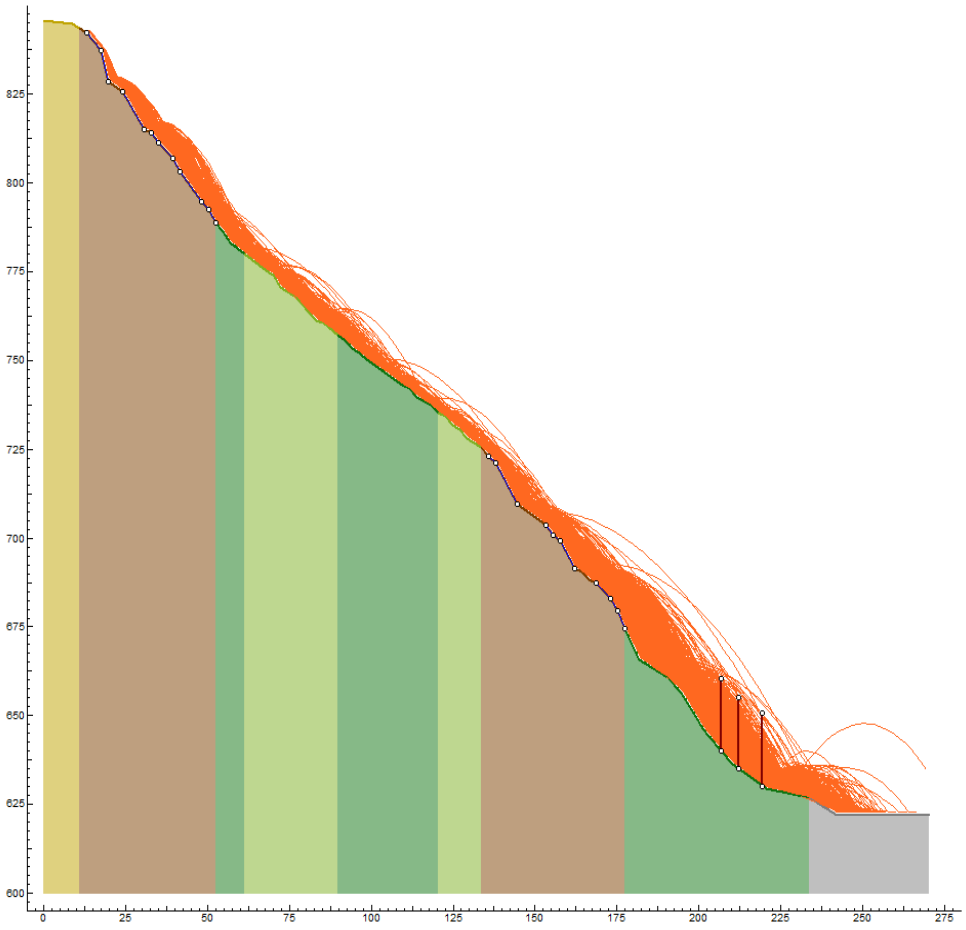

Figure 7.41 - Section S4, trajectories and collectors.

Analysing the trajectories on section S4, it can be depicted that vast majority of trajectories exhibit very high bouncing heights arriving to the base of the slope, where 20 m collector elements are placed as reference. Consequently, the design of a barrier high enough to intercept these blocks would be technically impracticable, as it would require an excessively large structure.

Higher on the slope, below the upper detachment zone, the bouncing height of the trajectories originating from the upper sector are considerable lower. To analyse this portion of the slope, an rigid barrier was placed at 735 m a.s.l. to intercept the blocks released from the upper detachment area and to evaluate weather this configuration leads to a reduction in bouncing heights downslope.

Figure 7.42 makes evident a considerable reduction in bouncing height downslope. Following these results, two levels of barriers will be considered in this sector to intercept the falling blocks.

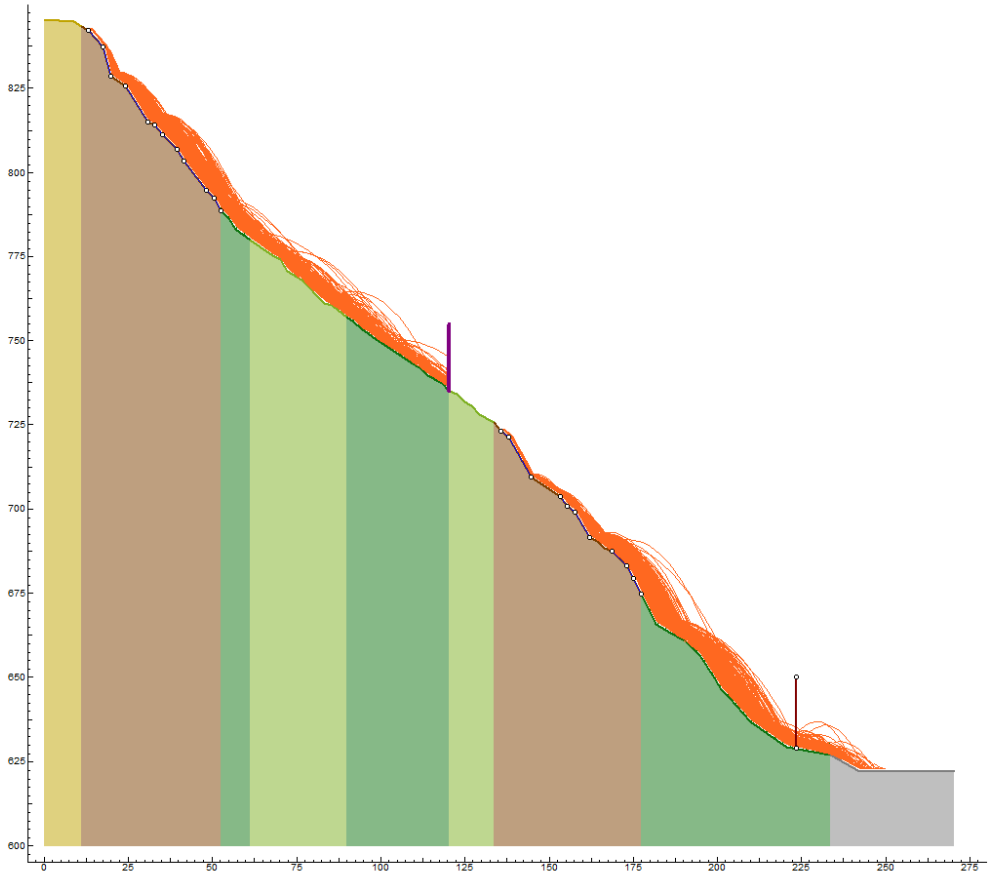

Figure 7.42 - Section S4 (b), trajectories and collectors.

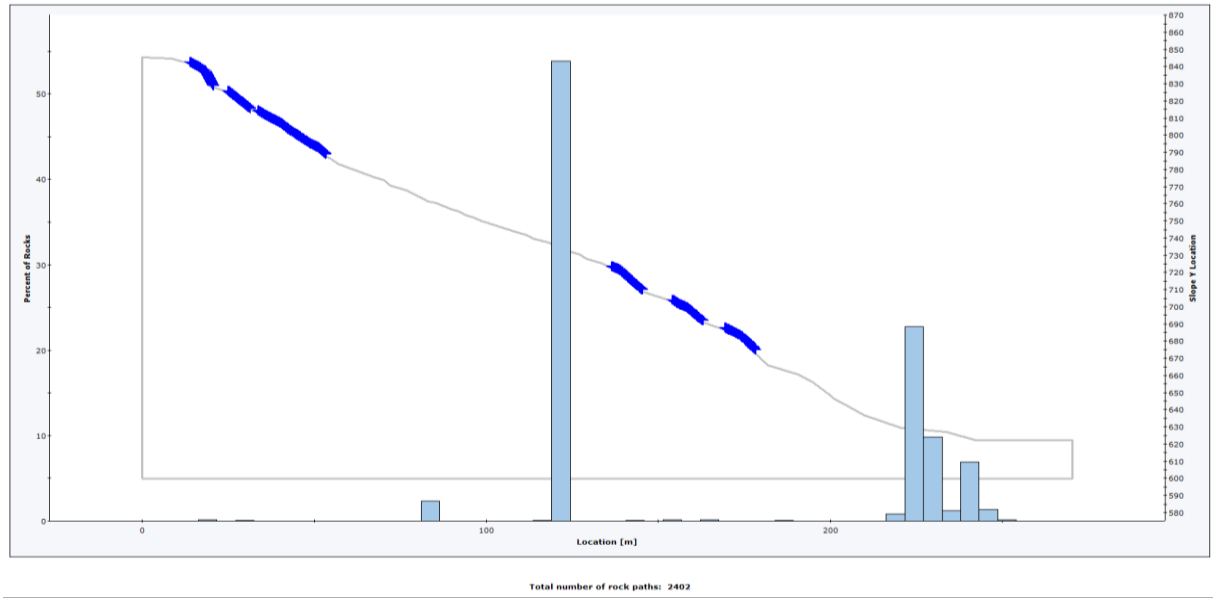

Figure 7.43 - Section S4 (b), stop points along the slope.

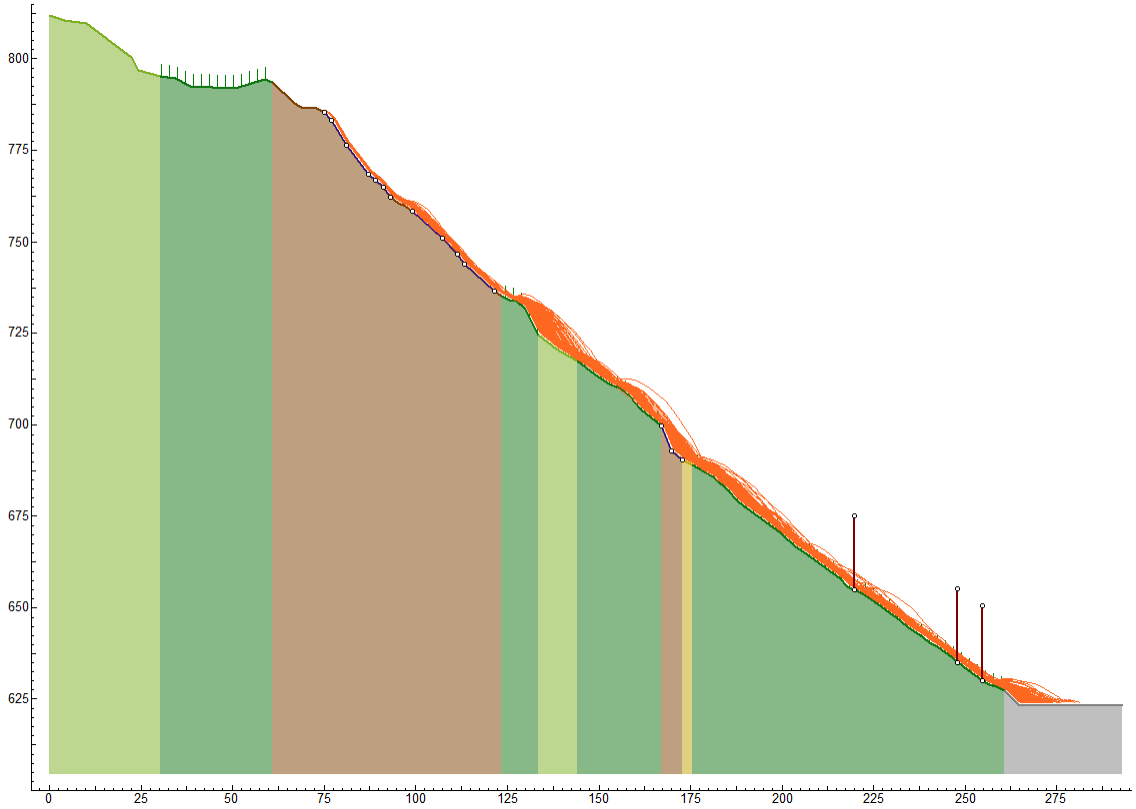

Figure 7.44 - Section S5, trajectories and collectors.

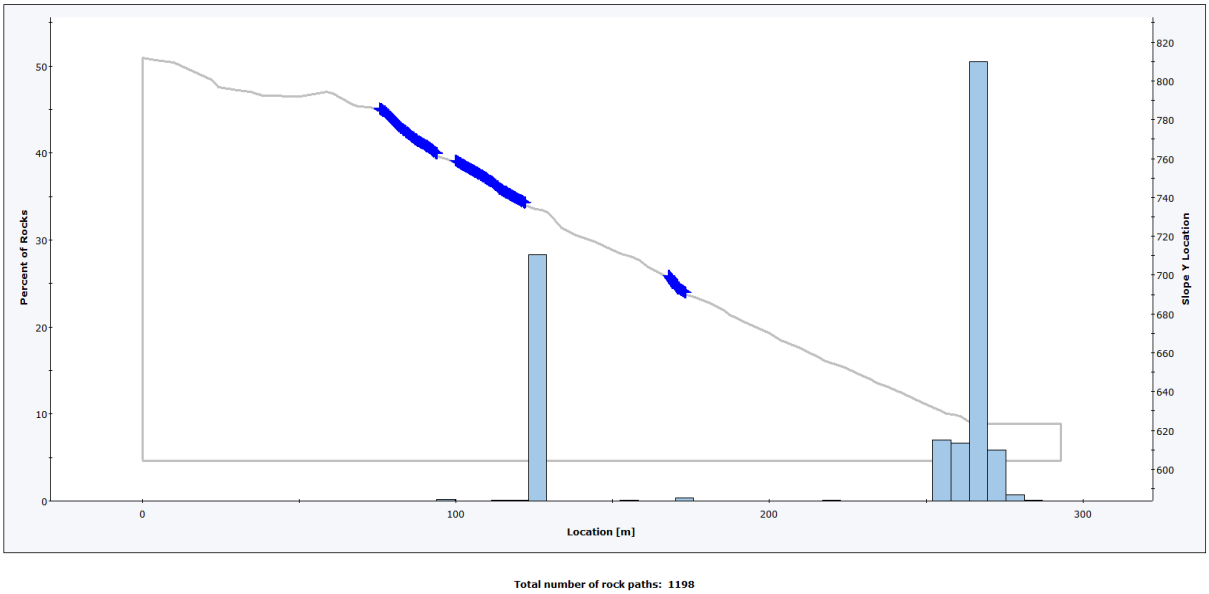

Figure 7.45 - Section S5, stop points along the slope.

Table 7.8 summarizes the collected data of the passing height and velocity at the 95th percentile for each section and elevation.

Table 7.8 - Collector data summary.

Section	Elevation (m a.s.l.)	Passing percentage of blocks (%)	Passing height at P95 (m)	Velocity at P95 (m/s)
S1	640	90,2	1,4	13,3
	645	90,9	1,3	12,6
	650	91,1	1,9	16,4
S2	635	81,4	3,4	16,6
	340	81,3	2,7	15,1
	345	83,4	2,6	16,9
S3	635	49,4	6,5	17,3
	640	49,8	4,3	16,5
	645	64,7	4,2	21,1
S4 (b)	628	32,3	2,5	14,9
	735 (b)	50,9	2,2	11,5
S5	1065	75,7	1,6	12,9
	1228	79,6	1,7	10,6
	1390	83,5	1,8	11,6

7.5 Protective Measures Project

For the project and design of the protection measures, the Italian Normative was considered, particularly UNI 11211-4-2018, Rockfall protective measures - Part 4: Definitive and executive design. This normative indicates that the actions of the falling blocks on the defence work must be determined by analyses of the dynamics of rockfall in order to determine its trajectory, both from a planimetric and altimetric point of view, as well as the fall frequency, velocity, and kinetic energy. It has to be verified that:

$$E_{Rd} \geq E_{Sd}$$

$$h_i \geq h_d + f_{min}$$

where; E_{Rd} is the resistance of the selected barrier of design; E_{Sd} acting kinetic energy of design; h_i is the barrier height declared by the manufacturer; h_d is the required height of design; f_{min} is the minimum clearance, equal to the block radius and in any case not less than 0,5 m.

The energy of design is calculated as:

$$E_{Sd} = \left(\frac{1}{2} \cdot m_d \cdot {v_d}^2\right) \cdot \gamma_R \qquad \textit{(Eq. 7.1)}$$

where m_d is the design mass of the blocks; v_d is the design velocity of the rock block; and γ_R is a safety coefficient depending on the phenomena consequences. The design mass of the block is defined as:

$$m_d = (Vol_b \cdot \gamma) \cdot \gamma_m \qquad \textit{(Eq. 7.2)}$$

$$\gamma_m = \gamma_{VolF1} \cdot \gamma_\psi \qquad \textit{(Eq. 7.3)}$$

where:

Vol_b is the volume of design

γ is the mass per unit volume of the involved material

γ_m is an amplification coefficient composed by:

γ_{VolF1}, a coefficient related to the precision of the volume of the block of design

γ_ψ, a coefficient related to the precision of the rock density (generally assumed equal to 1,00)

The velocity of design of the blocks is defined as the velocity at the point of impact with the structure affected by an amplification coefficient. It is calculated as:

$$v_d = v_t \cdot \gamma_F \quad \textit{(Eq. 7.4)}$$

$$\gamma_F = \gamma_{Tr} \cdot \gamma_{Dp} \quad \textit{(Eq. 7.5)}$$

where:

v_t corresponds to the 95th percentile of the velocities calculated in the trajectory analysis

γ_F is a amplification coefficient defined with:

γ_{Tr}, a reliability coefficient related to the trajectories calculations

γ_{Dp}, a coefficient related to the quality of the topographic discretization of the slope

The resistant energy of the barrier is obtained as the capacity declared by the manufacturer (E_i) affected by a safety factor related to the quality verification (γ_E):

$$E_{Rd} = E_i/\gamma_E \quad \textit{(Eq. 7.6)}$$

Finally, the intersection height of design is defined as the height of the impact point of the block's centre of gravity with the structure affected by an amplification coefficient:

$$h_d = h_t \cdot \gamma_F \quad \textit{(Eq. 7.7)}$$

where, h_t is defined as the impact point of the block centre of gravity with the structure corresponding to the 95th percentile of the heights obtained from the trajectory analysis; and γ_F is the same amplification coefficient used for the velocity of design calculation. Table 7.9 lists the values of the design coefficients for each case.

Table 7.9 - Design coefficients.

Coefficient	Value	Specification
γ_{VolF1}	1,02	accurate rock face surveys
	1,10	absence of surveys
γ_{Tr}	1,02	restitution coefficients obtained from back analysis
	1,10	restitution coefficients obtained only from bibliographic information
γ_{Dp}	1,02	slopes discretized with high-precision topographic survey
	1,10	slopes discretized with medium-low precision)
γ_R	1,00 – 1,20	high level of risk for human life depending on the risk value
	1,00	small economic consequences and damages easily serviceable
	1,05	relevant economic consequences, but damages easily serviceable
	1,10	relevant economic consequences and damages difficult to repair
	1,20	relevant economic consequences and extensive damages that cannot be repaired
γ_E	1,20	verification done on the basis of Maximum Energy Level (MEL)
	1,00	verification done on the basis of Service Energy Level (SEL)

It was decided to follow the energy verification in the Maximum Energy Level case, Table 7.10 shows the coefficients selected for calculations according to the employed methodology.

Table 7.10 - Selected design coefficients.

Coefficient	γ_{VolF1}	γ_{Tr}	γ_{Dp}	γ_R	γ_E
Case	surveyed	back analysis	high-precision	slight	MEL
Value	1,02	1,02	1,02	1,05	1,20

The protection system was design using standard nominal energy classes commercially available, specifically 1000, 2000, 3000, and 5000 kJ. Standard certified system heights often range between 4 and 7 m for the mentioned energy levels. Table 7.11 reports the resistant energy value for the selected energy classes for the design of the system and typical associated height ranges.

Table 7.11 - Resistant energy for standard energy classes and associated height ranges.

Nominal energy (E_i) (kJ)	Resistant energy (E_{Rd}) (kJ)	Typical height ranges (m)
1000	833,3	4 – 5
2000	1666,7	4 – 5
3000	2500,0	5 – 6
5000	4166,7	6 – 7

The barrier capacity was selected by verifying that its resistant energy value under the considered conditions exceeded the design impact energy, while its effective height was compatible with the design passing height obtained from the analysis. Selected classes and heights are presented in Table 7.12.

Table 7.12 - Selected barrier classes and heights.

Section	Barrier	Elevation (m a.s.l.)	h_d (m)	E_d (kJ)	Selected Energy Class (kJ)	Selected height (m)
S1	a	645	2,3	999,4	2000	4
	b	650	2,9	1683,7	3000	5
S2	c	645	3,7	1778,8	3000	5
S3	d	640	5,5	1704,3	3000	6
S4	e	628	3,6	1396,8	2000	4
	g	735	3,3	827,9	2000	4
S5	f	640	2,8	836,6	2000	4

The planimetric position of the barrier system was conditioned by the topographic constrains. In addition, supplier-related constrains generally limit the maximum number of modules to be installed in a single sequence to approximately 10, with each module typically measuring between 8 and 12 meters in length. Adjacent sequences are recommended to be overlapped by one full module to ensure continuity of interception and avoid unprotected gaps.

Figure 7.46 shows a proposed barrier system arrangement in accordance with the analysis carried out on each section and the layout constrictions. The rendering in Figure 7.47 illustrates the proposed rockfall protection layout, highlighting the location of the barriers to be installed along the slope. The model allows for a visual assessment of their spatial arrangement and interaction with the landscape.

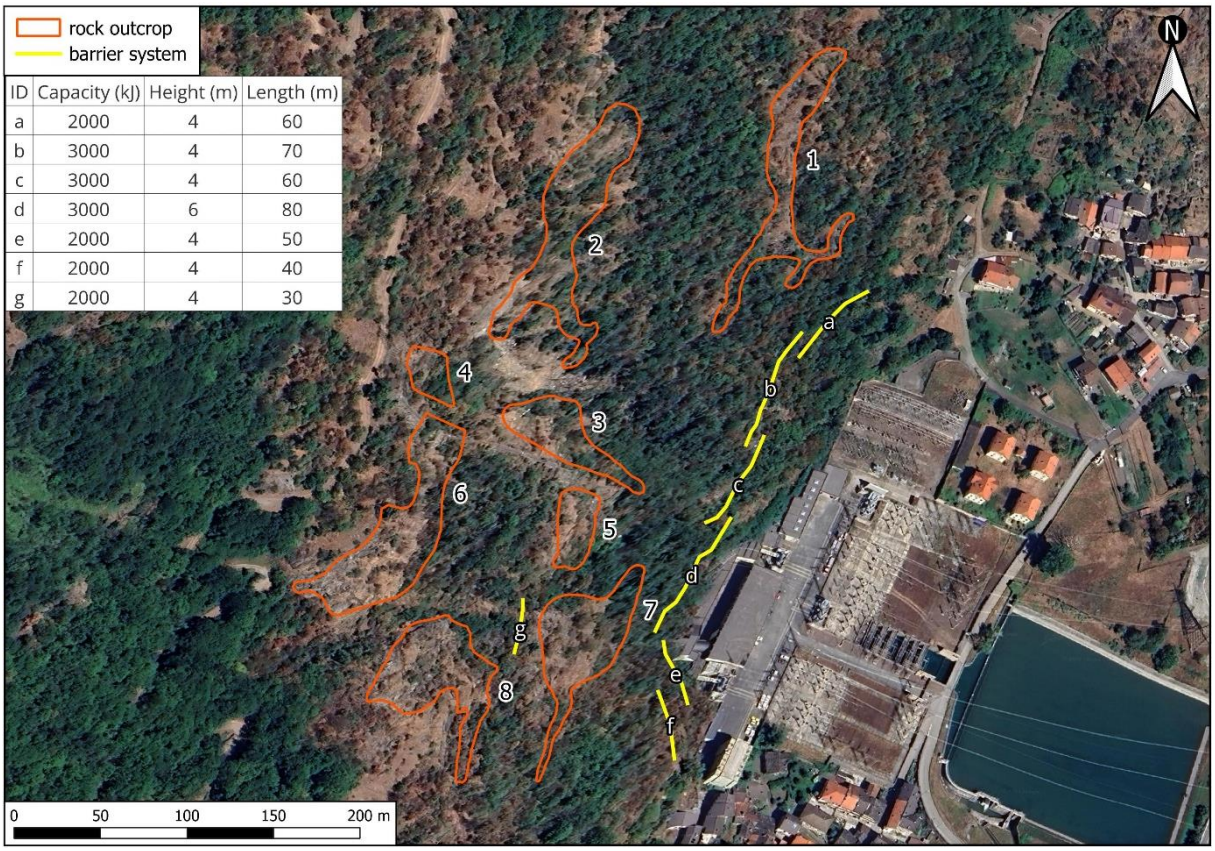

Figure 7.46 - Proposed barrier system arrangement.

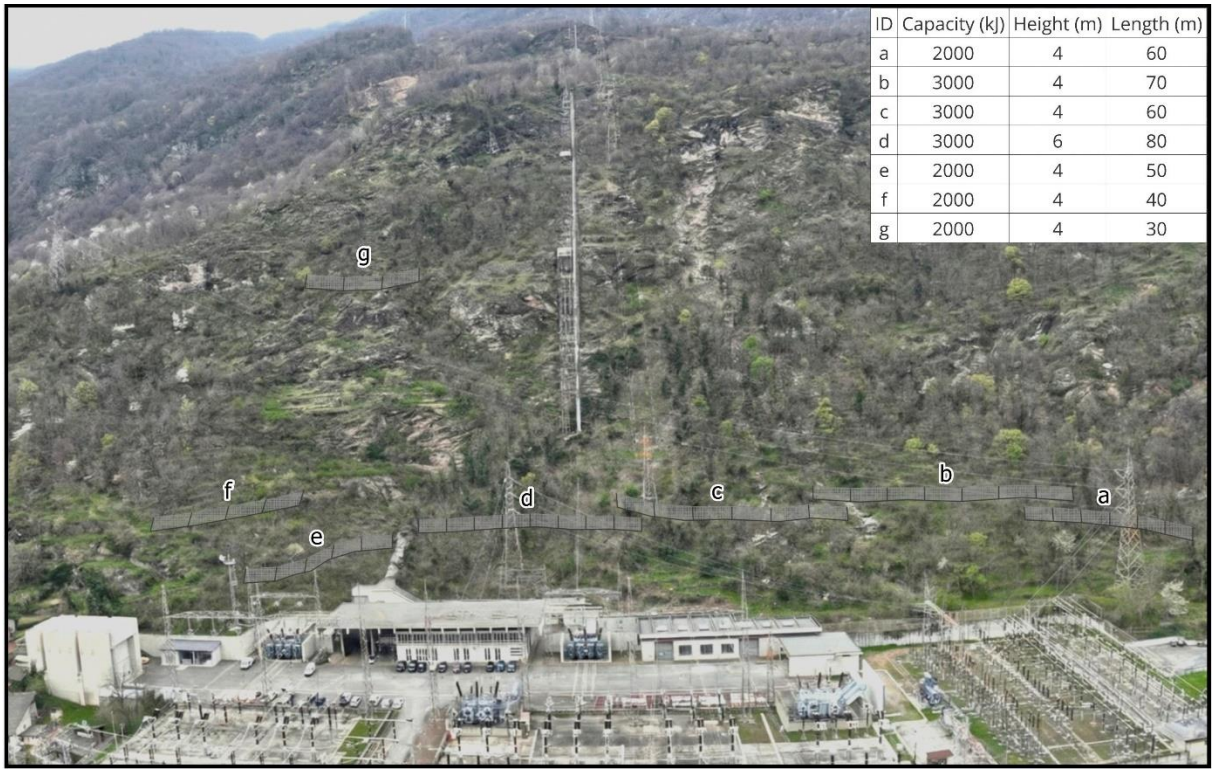

Figure 7.47 - Rendering of the proposed rockfall barriers on the slope.

Chapter 8

Final conclusions

The presented investigation has followed a comprehensive analysis of the rockfall phenomena, integrating traditional geological and geomechanical survey techniques with a novel approach for the characterization of release areas, and has scaled to multi dimension numerical modelling of the phenomena.

The work began with several surveys on the area of interest that allowed for the identification and systematic assessment of the parameters required for the Susceptibility Index to Failure (SIF) on eight rock walls, considered rockfall release areas. Subsequently, a progressive modelling sequence was applied, allowing for back analysis validation and comparison between different approaches. First, a three-dimensional preliminary analysis based on the Cone Method enhanced with the SIF enabled the identification of potentially affected areas and the computation of the Source Affecting Index (SAI), evidencing the most hazardous areas of detachment. Then, detailed 3D simulations incorporating terrain roughness and forest cover provided spatially distributed results in terms of propagation probability, kinetic energy, passing height, and deposition patterns. Finally, targeted 2D analyses along the preferred trajectories provided the kinematic parameters required for barrier design in accordance with technical standards.

Even tough in this case study the protection structures were ultimately installed all along the base of the slope, the analysis demonstrated how detailed release area characterization and analysis of source influence on elements at risk, through the Susceptibility Index to Failure (SIF) and the Source Affecting Index (SAI) respectively, can improve the reliability of susceptibility/hazard assessment and the effectiveness of mitigation and protective design.

It should be noted that a risk analysis was not carried out in this work. However, the propagation analysis performed is a necessary prerequisite for conducting a risk analysis, as it provides the fundamental information needed to understand how an event may spread and what areas may be affected.

A significant opportunity for the future development of rockfall simulation software lies in the transition of uniform release assumptions to a weighted detachment framework. Integrating geomechanical susceptibility indexes, such as the SIF methodology employed in this thesis, directly into simulation models would allow for spatially varied detachment probabilities across different sectors on the rock mass. This approach would lead to more advanced stochastic modelling by weighting the frequency and location of the release areas, such developments are crucial for generating more reliable time-independent hazard maps and for optimizing and prioritizing the technical and economic efficiency of mitigation structures design and placement.

Bibliography

Abramson, L., Lee, T., Sharma, S., & Boyce, G. (2002). *Slope Stability and Stabilization Methods.* New York, United States: Wiley-Interscience Publication, John Wiley & Sons Inc.

ARPA Piamonte; Cemagref; Politecnico di Torino; Consorzio Forestale Alta Valle di Susa; SIR s.r.l. (2008). *Rapport Final Projet n°165 PROVIALP – Protection de la viabilité alpine.*

Aydan, Ö. (2020). *Rock Mechanics and Rock Engineering* (Vol. I). Leiden, The Netherlands: CRC Press, Taylor & Francis Group.

Azzoni, A., Giani, G., Rosi, P., & Zaninetti, A. (1991). Stima dei Parametri Caratteristici del Moto di Caduta Blocchi.

Bromhead, E. (1992). *The Stability of Slopes.* London, United Kingdom: CRC Press, Taylor & Francis Group.

Bundesamt für Umwelt (BAFU). (2011). *Richtlinie Massenbewegungen (Guidelines for Mass Movements).* Berlin, Germany: Bundesamt für Umwelt.

Castelli, M., Torsello, G., & Vallero, G. (2021). Preliminary Modeling of Rockfall Runout: Definition of the Input Parameters for the QGIS Plugin QPROTO. *11*(2), 1-26.

Dearman, W. R. (1991). *Engineering Geological Mapping.* Oxford, United Kingdom: Butterworth-Heinemann, Elsevier Ltd.

Dorren, L. (2024). *Rockyfor3D (v6.0) revealed: Transparent description of the complete 3D rockfall model.* Bern, Switzerland: Int. ecorisQ Association.

Dorren, L., & Berger, F. (2005). Stem Breakage of Trees and Energy Dissipation During Rockfall. *26*, 63-71.

Dorren, L., Berger, F., & Patterus, U. (2006). Real-size Experiments and 3D Simulation of Rockfall on Forested and Non-forested Slopes. *6*, 145-153.

Elettri, F., & Pappalardo, G. (2025). *Interventi di Messa in Sicurezza della Centrale Idroelettrica di Venaus (TO).* GEODES S.r.l. for Campra Rocciatori S.r.l. and Enel Green Power.

Ente Nazionale Italiano di Unificazione (UNI). (2018). *UNI 11211-4:2018. Opere di difesa dalla caduta massi - Parte 4: Progetto definitivo ed esecutivo (Rockfall protective measures - Part 4: Definitive and executive design).* Milan, Italy: Ente Italiano di Unificazione.

Erismann, T., & Abele, G. (2001). *Dynamics of Rockslides and Rockfalls.* Berlin, Germany: Springer-Verlag Berlin Heidelberg.

Giani, G. (1992). Potenzialità dei Metodi di Analisi della Previsione del Moto di Caduta Massi lungo il Versante.

Giani, G. (1997). *Caduta di Massi, Analisi del Moto ed Opere di Protezione.* Benevento, Italy: Hevelius Edizioni srl.

González de Vallejo, L., Ferrer, M., Ortuño, L., & Oteo, C. (2002). *Ingeniería Geológica.* Madrid, España: Pearson Educación S.A.

Hoek, E. (1994). Strength of Rock and Rock Masses. *2* (2), 4-16.

Hoek, E., & Brown, E. (1997). *Practical Estimates of Rock Mass Strength.* International Journal of Rock Mechanics and Mining Sciences.

Hoek, E., & Brown, E. (1997). Practical Estimates of Rock Mass Strength. *38*(8), 1165-1186.

Hudson, J. A., & Harrison, J. P. (1997). *Engineering Rock Mechanics: An Introduction to the Principles.* Oxford, United Kingdom: Pergamon, Elsevier Ltd.

Jonsson, M. (2007). *Energy Absorption of Trees in a Rockfall Protection Forest.* Thesis, ETHZ.

Kim, B., & Cai, M. (2004, 2007). *Estimation of block sizes for rock masses with non-persistent joints.*

Kim, B., Cai, M., Kaiser, P., & Yang, H.-S. (2007). Estimation of Block Sizes for Rock Masses with Non-persistent Joints. *40*(2), 169-192.

Lambert, S., & Nicot, F. (2011). *Rockfall Engineering.* London, United Kingdom: ISTE Ltd. and John Wiley & Sons, Inc.

Milan, L., Napoli, M., Barbero, M., & Castelli, M. (2023). A Novel Approach to Assess the Influence of Rockfall Source Areas: The Case Study of Bardonecchia (Italy). *13*(12), 386.

Napoli, M., Barbero, M., Castelli, F., & Castelli, M. (2024). The Susceptibility Index to Failure (SIF) and the Source Affecting Index to Characterize Rockfall Release Areas. *50*(1), 3-10.

Nöel, F., Cloutier, C., Javoyredoff, M., & Locat, C. (2021). Impact-detection Algorithm that Uses Point Clouds as Topographic Inputs for 3D Rockfall Simulations. *11*(5), 188.

Nöel, F., Nordang, H., Javoyredoff, M., & Travelletti, J. (2023). Highly energetic rockfalls: back analysis of the 2015 event from the Mel de la Niva, Switzerland. *20*(8), 1561-1582.

Pfeiffer, T., & Bowen, T. (1989). Computer Simulation of Rockfalls. *26*(1), 135-146.

Picher, B., Hellmich, C., & Mang, H. (2005). Impact of rocks onto Gravel - Design and Evaluation of Experiments. *31*(5), 559-578.

Ribacchi, R. (2018). *Meccanica delle Rocce: Teoria e Applicazioni nell'Ingegneria.* Benevento, Italy: Edizioni Efesto and Hevelius Edizioni.

Schuster, R., & Krizek, R. (1978). *Landslides: Analysis and Control.* Washingthon D.C., United States: Transportation Research Board, National Academy of Sciences.

Simons, N., Menzies, B., & Mathews, M. (2001). *A Short Course in Soil and Rock Slope Engineering.* London, United Kingdom: Thomas Telford Publishing, Thomas Telford Ltd.

Sivakugan, N., Shukla, S. K., & Das, B. M. (2013). *Rock Mechanics: An Introduction.* Boca Raton, United States: CRC Press, Taylor & Francis Group.

Statham, I. (1979). A Simple Dynamic Model of Rockfall: Some Theoretical Principles and Model and Field Experiments.

Ulusay, R., & Hudson, J. (2007). *The Complete ISRM Suggested Methods for Rock Characterization, Testing and Monitoring: 1974-2006.* Ankara, Turkey: ISRM Turkish National Group.

Ulusay, R., & Hudson, J. A. (2007). *The Complete ISRM Suggested Methods for Rock Characterization, Testing and Monitoring: 1974-2006.* ISRM Turkish National Group and the ISRM.

Wyllie, D. (2015). *Rock Fall Engineering.* Boca Raton, United States: CRC Press, Taylor & Francis Group.

Wyllie, D., & Mah, C. (2005). *Rock Slope Engineering.* New York, United States: Spon Press, Taylor & Francis Group.

Zevenbergen, L., & Thorne, C. (n.d.). Quantitative Analysis of Land Surface Topography. *12*(1), 47-56.

Zhang, L. (2017). *Engineering Properties of Rocks.* Oxford, United Kingdom: Butterworth-Heinemann, Elsevier Ltd.

Sitography

Agenzia Regionale per la Protezione Ambientale. *Informazioni sulla stazione meteorologica: dati sulle precipitazioni giornaliere*. Retrieved from: https://www.arpa.piemonte.it/rischi_naturali/snippets_arpa_graphs/dati_giornalieri_meteo/

Istituto Nazionale di Geofisica e Vulcanologia. *Mappe interattive della pericolosità sismica (WebGis)*. Retrieved from: https://esse1-gis.mi.ingv.it/

Ministero dell'Ambiente e della Sicurezza Energetica. *Sistema Informartivo multimediale - Geoportale*. Retrieved from https://sim.mase.gov.it/portalediaccesso/mappe/#/viewer/new

Rocscience Inc. Hoek's Corner - *Published works & lectures from Dr. Evert Hoek*. Retrieved from: https://www.rocscience.com/learning/hoeks-corner

Rocscience Inc. *Rocfall2 User Guide*. Retrieved from: https://www.rocscience.com/help/rocfall/overview

Appendix

TABELLA A1.1
Rilievo geologico-strutturale su stazione

Commessa: 251401 | Località: Venaus | Data: 11/09/2025 | Operatore: FEL+GPA
Stazione: St1 | Litotipo: Micascisti con vene di quarzo | Dim. affioramento H x L: 10x20 | Orientamento (DD, Dip): 270/85

Progr (cm)	Set	Giacitura		Tipo	Spaziatura (m)			Persistenza (m)		Scabrezza		Apertura (mm)			Riempimento			Alterazione			Cond. Idr.	Note
		DD (°)	Dip (°)		min	max	medio	Lungh.	Termina-zione	P. Scala (JRC)	Grande scala	min	max	medio	Tipo	Spess. (mm)	Compo sizione	Tipo	Martello di Schmidt (discontinuità) Rimbalzi	Orientaz.		
	Sc	280	45	Sc			0.001	>20	X-X	12-14	O	0		<0.1	A			Deb	40 - 27 - 21 - 29 - 31 - 32 - 25 - 22 - 18 - 32		A	
		314	25																			
		320	24																			
		295	50																			
		275	34																			
		106	25																			
		270	35																			
		278	26																			
	J1	85	80	G	0.08	0.60	0.25	1-3	D-D	8-10	P	0.1-1	>5	1-5	A			Deb	43 - 36 - 52 - 52 - 48 - 49 - 48 - 40 - 45 - 46		A	
		90	82																			
		86	80																			
		85	81																			
		85	88																			
		85	80																			
		84	82																			
	J2	105	40	G	0.05	0.25	0.10	<1	D-X	10-12	P	<0.1	1-5	0.1-1	A			Deb - A	40 - 35 - 48 - 18 - 26 - 24 - 22 - 19 - 36 - 39		A	
		90	38																			
		95	40																			
		130	20																			
		115	20																			
		117	18																			
	J2a	113	75	G	0.05		0.25	1-3	X-D	10-12	P	0.1-1	>5	1-5	S	<5	S-L	Deb	42 - 37 - 36 - 28 - 41 - 43 - 30 - 42 - 40 - 43		A	
		115	64																			
		118	72																			
		120	60																			
		115	50																			
		116	70																			
		118	50																			
	J3	173	78	G	0.05	0.30	0.15	3-10	X-X	8-10	P	<0.1	>5	0.1-1	A			Deb - A	18 - 32 - 50 - 35 - 44 - 44 - 37 - 31 - 42 - 40		A	
		175	80																			
		170	82																			
		169	85																			
		166	88																			
		174	80																			
		169	86																			
		173	85																			
		175	85																			

LEGENDA

Giacitura	Tipo	Persistenza	Scabrezza		Apertura	Riempimento		Alterazione	Condizioni idrauliche		ALTRI PARAMETRI
DD=Dip Dir. Immersione	**St**ratificazione	*Lunghezza*	*Piccola Scala (JRC)*	*Grande Scala*		*Tipo* *Spessore*		*Tipo*	*Acqua su 10 m lineari*		**Vb (block size l*h*t [cm]):**
Dip Inclinazione	**Sc**istosità	< 1 m **Molto bassa**	0 - 2 Levigata	**P**iana	0 mm	**A**ssente		**A**ssente		l/min	60x25x15
	Clivaggio	1 - 3 m **Bassa**	2 - 4 Levigata	**O**ndulata	< 0.1 mm	**Du**ro < 5 mm		**Deb**olmente alterata	**A**sciutto	0	150x150x85
	Giunto	3 - 10 m **Media**	4 - 6 Liscia	**S**egmentata	0.1 - 1.0 mm	**Du**ro > 5 mm		**Mod**eratamente alterata	**U**mido	< 10	15x5x3
	Vena	10 - 20 m **Alta**	6 - 8 Liscia		1 5 mm	**So**ffice < 5 mm		**Mol**to alterata	**B**agnato	10 -25	**Jn (n. giunti al m):**
	Faglia	> 20 m **Molto alta**	8 - 10 Poco Scabra		> 5 mm	**So**ffice > 5 mm		**Dec**omposta	**S**tillicidi	25 - 125	
		Terminazione	10 - 12 Poco Scabra			*Composizione*		*Martello di Schmidt*	**F**luente	> 125	**GSI:** 55-60
	Spaziatura	**R** - roccia	12 - 14 Scabra			**A**rgilla **Cal**cite		**Rimbalzi**			
	Distanza perpendicolare tra due discontinuità della stessa famiglia	**D** - contro altra discontinuità	14 - 16 Scabra			**L**imo **Q**uarzo		valore rimbalzi			
		X - fuori affioramento	16 - 18 Molto Scabra			**Sa**bbia **Cl**orite		**Orientazione**			
			18 - 20 Molto Scabra			**G**hiaia **Os**sidi		direzione applicazione martello (perpendicolare alla discontinuità)			
						Altro					

GE●DES

TABELLA A1.2
Rilievo geologico-strutturale su stazione

Commessa:	251401		Località:	Venaus							Data:	11/09/2025				Operatore:	FEL+GPA						
Stazione:	St1		Litotipo:	Micascisti con vene di quarzo							Dim. affioramento H x L:				10x20	Orientamento (DD, Dip):	270/85						

Progr (cm)	Set	Giacitura		Tipo	Spaziatura (m)			Persistenza (m)		Scabrezza		Apertura (mm)			Riempimento			Alterazione			Cond. Idr.	Note			
		DD (°)	Dip (°)		min	max	medio	Lungh.	Termina-zione	P. Scala (JRC)	Grande scala	min	max	medio	Tipo	Spess. (mm)	Compo sizione	Tipo	Martello di Schmidt (discontinuità) Rimbalzi	Orientaz.					
	J4	206	50	G	0.10	0.60	0.25	3-10	X-X	14-16	P	0.1-1	>5	1-5	S	<5	S-L	Deb	26 - 30 - 31 - 44 - 34 - 15 - 26 - 42 - 39 - 19	↘	A				
		198	70																						
		195	62																						
		208	70																						
		196	52																						
		195	64																						
		202	60																						
		200	72																						
		208	59																						
	J5	276	70	G	0.10	0.60	0.30	3-10	D-D	12-14	P	0.1-1	>5	1-5	S	<5	S	Deb - A	35 - 43 - 38 - 30 - 22 - 18 - 38 - 43 - 33 - 22	↖	A				
		270	68																						
		272	70																						
		260	52																						
		268	60																						
		270	65																						
		266	50																						
		268	63																						
	F1	265	70	F				3-10	X-X	16-18	P							Deb	26 - 32 - 28 - 44 - 29 - 28 - 31 - 34 - 29 - 24	↖	A	Faglia diretta, si individuano degli indicatori cinematici, costituiti da strie di movimento e gradini di calcite			

LEGENDA

Giacitura	Tipo
DD=Dip Dir.	**S**tratificazione
Immersione	**Sc**istosità
Dip	**Cl**ivaggio
Inclinazione	**G**iunto
	Vena
	Faglia

Spaziatura
Distanza perpendicolare tra due discontinuità della stessa famiglia

Persistenza

Lunghezza

< 1 m	**M**olto **b**assa
1 - 3 m	**B**assa
3 - 10 m	**M**edia
10 - 20 m	**A**lta
> 20 m	**M**olto **a**lta

Terminazione
R - roccia
D - contro altra discontinuità
X - fuori affioramento

Scabrezza

Piccola Scala (JRC)		*Grande Scala*
0 - 2	Levigata	**P**iana
2 - 4		**O**ndulata
4 - 6	Liscia	**S**egmentata
6 - 8		
8 - 10	Poco Scabra	
10 - 12		
12 - 14	Scabra	
14 - 16		
16 - 18	Molto Scabra	
18 - 20		

Apertura

0 mm
< 0.1 mm
0.1 - 1.0 mm
1 5 mm
> 5 mm

Riempimento

Tipo	*Spessore*
Assente	
Duro	< 5 mm
Duro	> 5 mm
Soffice	< 5 mm
Soffice	> 5 mm

Composizione
Argilla **Cal**cite
Limo **Q**uarzo
Sabbia **Cl**orite
Ghiaia **Os**sidi
Altro

Alterazione

Tipo
Assente
Debolmente alterata
Moderatamente alterata
Molto alterata
Decomposta

Martello di Schmidt
Rimbalzi
valore rimbalzi
Orientazione
direzione applicazione martello (perpendicolare alla discontinuità)

Condizioni idrauliche

Acqua su 10 m lineari

	l/min
Asciutto	0
Umido	< 10
Bagnato	10 -25
Stillicidi	25 - 125
Fluente	> 125

ALTRI PARAMETRI

Vb (block size l*h*t [cm]):
60x25x15
150x150x85
15x5x3
Jn (n. giunti al m):
GSI: 55-60

TABELLA A1.3

Rilievo geologico-strutturale su stazione

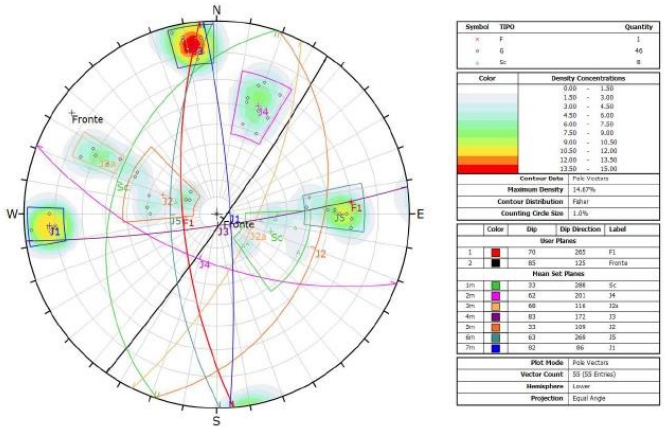

Symbol	TIPO	Quantity
×	F	1
◇	G	46
○	Sc	6

Color	Density Concentrations
	0.00 - 1.50
	1.50 - 3.00
	3.00 - 4.50
	4.50 - 6.00
	6.00 - 7.50
	7.50 - 9.00
	9.00 - 10.50
	10.50 - 12.00
	12.00 - 13.50
	13.50 - 15.00

Contour Data	Pole Vectors
Maximum Density	14.67%
Contour Distribution	Fisher
Counting Circle Size	1.0%

	Color	Dip	Dip Direction	Label
User Planes				
1		70	265	F1
2		85	125	Fronte
Hoan Set Planes				
1m		32	288	Sc
2m		62	201	J4
3m		68	114	J2a
4m		83	171	J3
5m		33	169	J2
6m		63	269	J5
7m		82	86	J1

Plot Mode	Pole Vectors
Vector Count	55 (55 Entries)
Hemisphere	Lower
Projection	Equal Angle

Note/descrizione:

Micascisti di colore grigio quarzitici con vene di quarzo di dimensioni da centimetriche a pluricentimetriche. Sulle superfici fresche si evidenzia l'abbondante presenza di mica chiara, seguita da minerali di colorazione verde, verosimilmente clorite. Le vene di quarzo hanno forma lenticolare ed estensioni importanti, subparallele alla scistosità (Sc).

TABELLA A2.1
Rilievo geologico-strutturale su stazione

Commessa: 251401 | Località: Venaus | Data: 11/09/2025 | Operatore: FEL+GPA
Stazione: St2 | Litotipo: Micascisti con vene di quarzo | Dim. affioramento H x L: 8x20 | Orientamento (DD, Dip): 115/70

Progr (cm)	Set	Giacitura		Tipo	Spaziatura (m)			Persistenza (m)		Scabrezza		Apertura (mm)			Riempimento			Alterazione			Cond. Idr.	Note
		DD (°)	Dip (°)		min	max	medio	Lungh.	Terminazione	P. Scala (JRC)	Grande scala	min	max	medio	Tipo	Spess. (mm)	Composizione	Tipo	Martello di Schmidt (discontinuità) Rimbalzi	Martello di Schmidt (discontinuità) Orientaz.		
	Sc	310	40	Sc			0.001	>20	X-X	10-12	O	0			A			Deb - A	32 - 30 - 18 - 30 - 40 - 24 - 30 - 16 - 23 - 23	↖	A	
		320	30																			
		310	45																			
		305	38																			
		306	45																			
		290	35																			
		316	40																			
		310	38																			
		318	45																			
		316	37																			
		315	40																			
	J1	78	80	G	0.02	0.30	0.15	1-3	X-D	8-10	P	0			A			Deb - A	43 - 41 - 37 - 22 - 42 - 40 - 22 - 32 - 40 - 32	↙	A	
		75	88																			
		75	83																			
		76	88																			
		77	86																			
		77	83																			
		83	84																			
		75	89																			
		88	73																			
		66	70																			
		82	80																			
		80	72																			
	J2	135	30	G	0.05	0.30	0.10	3-10	X-D	10-12	P	<0.1	1-5	0.1-1	S	<5	S-L	Deb - A	28 - 29 - 32 - 24 - 22 - 24 - 29 - 16 - 17 - 15	↘	A	
		141	27																			
		150	25																			
		163	25																			
		128	32																			
		135	38																			
		151	30																			
		197	20																			
		173	35																			
	J2a	170	78	G	0.10	0.60		1-3	D-D	14-16	P	0	0.1-1	<0.1	A - S	<5	S-L	A			A	
		142	68																			
		182	77																			
		224	72																			
		140	72																			
		167	64																			

LEGENDA

Giacitura	Tipo	Persistenza		Scabrezza		Apertura	Riempimento		Alterazione	Condizioni idrauliche		ALTRI PARAMETRI
DD=Dip Dir.	**St**ratificazione	*Lunghezza*		*Piccola Scala (JRC)*	*Grande Scala*		*Tipo*	*Spessore*	*Tipo*	*Acqua su 10 m lineari*		**Vb (block size l*h*t [cm]):**
Immersione	**Sc**istosità	< 1 m	Molto **b**assa	0 - 2 Levigata	**P**iana	0 mm	**A**ssente		**A**ssente		l/min	55x30x15
Dip	**Cl**ivaggio	1 - 3 m	**B**assa	2 - 4	**O**ndulata	< 0.1 mm	**Du**ro	< 5 mm	**Deb**olmente alterata	**A**sciutto	0	20x15x3
Inclinazione	**G**iunto	3 - 10 m	**M**edia	4 - 6 Liscia	**S**egmentata	0.1 - 1.0 mm	**Du**ro	> 5 mm	**Mod**eratamente alterata	**U**mido	< 10	100x75x40
	Vena	10 - 20 m	**A**lta	6 - 8		1 5 mm	**So**ffice	< 5 mm	**Mol**to alterata	**B**agnato	10 -25	**Jn (n. giunti al m):**
	Faglia	> 20 m	Molto **a**lta	8 - 10 Poco Scabra		> 5 mm	**So**ffice	> 5 mm	**Dec**omposta	**S**tillicidi	25 - 125	
				10 - 12			*Composizione*		*Martello di Schmidt*	**F**luente	> 125	**GSI:** 55-60
		Terminazione		12 - 14 Scabra			**Ar**gilla	**Cal**cite	**Rimbalzi**			
		R - roccia		14 - 16			**Li**mo	**Q**uarzo	valore rimbalzi			
		D - contro altra discontinuità		16 - 18 Molto Scabra			**Sa**bbia	**Cl**orite	**Orientazione**			
		X - fuori affioramento		18 - 20			**Gh**iaia	**Os**sidi	direzione applicazione martello (perpendicolare alla discontinuità)			
							Altro					

Spaziatura
Distanza perpendicolare tra due discontinuità della stessa famiglia

TABELLA A2.2
Rilievo geologico-strutturale su stazione

Commessa: 251401 | Località: Venaus | Data: 11/09/2025 | Operatore: FEL+GPA
Stazione: St2 | Litotipo: Micascisti con vene di quarzo | Dim. affioramento H x L: 8x20 | Orientamento (DD, Dip): 115/70

Progr (cm)	Set	Giacitura		Tipo	Spaziatura (m)			Persistenza (m)		Scabrezza		Apertura (mm)			Riempimento			Alterazione			Cond. Idr.	Note
		DD (°)	Dip (°)		min	max	medio	Lungh.	Terminazione	P. Scala (JRC)	Grande scala	min	max	medio	Tipo	Spess. (mm)	Composizione	Tipo	Martello di Schmidt (discontinuità) Rimbalzi	Martello di Schmidt (discontinuità) Orientaz.		
	J5	267	72	G	0.02	0.30	0.15	1-3	X-D	8-10	P	0			A			Deb - A	28 - 18 - 26 - 30 - 28 - 34 - 27 - 22 - 40 - 35	↖	A	
		250	78																			
		253	80																			
		272	60																			
		270	60																			
		260	68																			
		265	68																			
	J6	10	80	G	0.10	0.60		1-3	D-D	14-16	P	0	0.1-1	<0.1	A - S	<5	S-L	A	30 - 39 - 25 - 24 - 18 - 29 - 30 - 19 - 26 - 35	↖	A	
		338	80																			
		350	70																			
		320	89																			
		316	70																			
		2	85																			
		330	60																			
		345	70																			
		325	70																			

LEGENDA

Giacitura	Tipo
DD=Dip Dir.	**St**ratificazione
Immersione	**Sc**istosità
Dip	**Cl**ivaggio
Inclinazione	**G**iunto
	Vena
	Faglia

Spaziatura
Distanza perpendicolare tra due discontinuità della stessa famiglia

Persistenza

Lunghezza

< 1 m	**M**olto **b**assa
1 - 3 m	**B**assa
3 - 10 m	**M**edia
10 - 20 m	**A**lta
> 20 m	**M**olto **a**lta

Terminazione

R - roccia
D - contro altra discontinuità
X - fuori affioramento

Scabrezza

Piccola Scala (JRC)		*Grande Scala*
0 - 2	Levigata	**P**iana
2 - 4		**O**ndulata
4 - 6	Liscia	**S**egmentata
6 - 8		
8 - 10	Poco Scabra	
10 - 12		
12 - 14	Scabra	
14 - 16		
16 - 18	Molto Scabra	
18 - 20		

Apertura

0 mm	
< 0.1 mm	
0.1 - 1.0 mm	
1 5 mm	
> 5 mm	

Riempimento

Tipo	*Spessore*
Assente	
Duro	< 5 mm
Duro	> 5 mm
Soffice	< 5 mm
Soffice	> 5 mm

Composizione

Argilla	**Ca**lcite
Limo	**Q**uarzo
Sabbia	**Cl**orite
Ghiaia	**Os**sidi
Altro	

Alterazione

Tipo
Assente
Debolmente alterata
Moderatamente alterata
Molto alterata
Decomposta

Martello di Schmidt
Rimbalzi
valore rimbalzi
Orientazione
direzione applicazione martello (perpendicolare alla discontinuità)

Condizioni idrauliche

Acqua su 10 m lineari

	l/min
Asciutto	0
Umido	< 10
Bagnato	10 -25
Stillicidi	25 - 125
Fluente	> 125

ALTRI PARAMETRI

Vb (block size l*h*t [cm]):
55x30x15
20x15x3
100x75x40
Jn (n. giunti al m):
GSI: 55-60

TABELLA A2.3

Rilievo geologico-strutturale su stazione

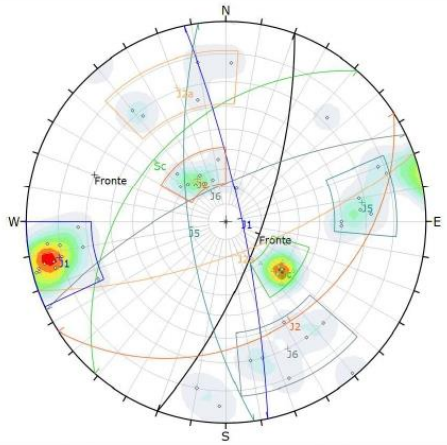

Symbol	TIPO	Quantity
◦	G	43
◦	Sc	11

Color	Density Concentrations
	0.00 - 1.60
	1.60 - 3.20
	3.20 - 4.80
	4.80 - 6.40
	6.40 - 8.00
	8.00 - 9.60
	9.60 - 11.20
	11.20 - 12.80
	12.80 - 14.40
	14.40 - 16.00
Contour Data	Pole Vectors
Maximum Density	15.39%
Contour Distribution	Fisher
Counting Circle Size	1.0%

	Color	Dip	Dip Direction	Label
User Planes				
1		70	110	Fronte
Mean Set Planes				
1m		39	311	Sc
2m		81	78	J1
3m		70	334	J6
4m		29	147	J2
5m		69	262	J5
6m		71	160	J2a

Plot Mode	Pole Vectors
Vector Count	54 (54 Entries)
Hemisphere	Lower
Projection	Equal Angle

Note/descrizione:

Micascisti di colore grigio quarzitici con vene di quarzo di dimensioni da centimetriche a pluricentimetriche. Sulle superfici fresche si evidenzia l'abbondante presenza di mica chiara, seguita da minerali di colorazione verde, verosimilmente clorite. Le vene di quarzo hanno forma lenticolare ed estensioni importanti, subparallele alla scistosità (Sc).

TABELLA A3.1

Rilievo geologico-strutturale su stazione

Commessa: 251401 | Località: Venaus | Data: 11/09/2025 | Operatore: FEL+GPA

Stazione: St3 | Litotipo: Micascisti con vene di quarzo | Dim. affioramento H x L: 30x20 | Orientamento (DD, Dip): 085/80

Progr (cm)	Set	Giacitura		Tipo	Spaziatura (m)			Persistenza (m)		Scabrezza		Apertura (mm)			Riempimento			Alterazione			Cond. Idr.	Note
		DD (°)	Dip (°)		min	max	medio	Lungh.	Termina-zione	P. Scala (JRC)	Grande scala	min	max	medio	Tipo	Spess. (mm)	Compo sizione	Tipo	Martello di Schmidt (discontinuità) Rimbalzi	Orientaz.		
	Sc	300	30	Sc			0.001	>20	X-X	12-14	O	0	1-5		A - S	<5	S-L	Deb	20 - 27 - 22 - 20 - 21 - 16 - 15 - 23 - 29 - 22	↗	A	
		275	42																			
		287	40																			
		293	30																			
		280	40																			
		255	30																			
		280	30																			
		278	40																			
		275	36																			
		293	40																			
		286	50																			
	J1	75	80	G			0.05	1-3	D-D	12-14	O							Deb	32 - 30 - 32 - 28 - 21 - 27 - 21 - 25 - 32 - 30	→	A	
		75	85																			
		75	50																			
		75	70																			
		70	80																			
		83	80																			
	J2	132	33	G	0.05	0.40		<1	X-D	14-16	P	<0.1	1-5	0.1-1	S	<5	S	Deb	11 - 22 - 13 - 14 - 15 - 18 - 23 - 36 - 24 - 15	→	A	
		125	45																			
		118	44																			
		110	40																			
		136	50																			
		152	40																			
		145	44																			
	J2a	132	78	G	0.03	0.30	0.13	1-3	D-D	14-16	P	0.1-1	>5	1-5	A - S	>5	S	Deb	12 - 11 - 18 - 26 - 22 - 20 - 16 - 20 - 22 - 24	→	A	
		135	64																			
		133	87																			
		135	70																			
		150	70																			
		125	80																			
		125	78																			
		123	70																			
	J4	225	73	G	0.05	0.50	0.15	1-3	D-D	10-12	P	0	>5	0.1-1	A - S	<5	S	Deb - A	13 - 23 - 12 - 21 - 16 - 18 - 30 - 14 - 26 - 20	↗	A	
		230	65																			
		212	63																			
		232	80																			
		208	80																			
		195	85																			

LEGENDA

Giacitura	Tipo	Persistenza		Scabrezza			Apertura	Riempimento		Alterazione	Condizioni idrauliche		ALTRI PARAMETRI
DD=Dip Dir. Immersione	**St**ratificazione	*Lunghezza*		*Piccola Scala (JRC)*		*Grande Scala*		*Tipo*	*Spessore*	*Tipo*	*Acqua su 10 m lineari*		**Vb (block size l*h*t [cm]):**
Dip Inclinazione	**Sc**istosità	< 1 m	**M**olto **b**assa	0 - 2	Levigata	**P**iana	0 mm	**A**ssente		**A**ssente		l/min	50x15x20
	Clivaggio	1 - 3 m	**B**assa	2 - 4		**O**ndulata	< 0.1 mm	**Du**ro	< 5 mm	**Deb**olmente alterata	**A**sciutto	0	20x10x5
	Giunto	3 - 10 m	**M**edia	4 - 6	Liscia	**S**egmentata	0.1 - 1.0 mm	**Du**ro	> 5 mm	**Mod**eratamente alterata	**U**mido	< 10	65x50x40
	Vena	10 - 20 m	**A**lta	6 - 8			1 5 mm	**So**ffice	< 5 mm	**Mol**to alterata	**B**agnato	10 -25	**Jn (n. giunti al m):**
	Faglia	> 20 m	**Molto a**lta	8 - 10	Poco Scabra		> 5 mm	**So**ffice	> 5 mm	**Dec**omposta	**St**illicidi	25 - 125	
				10 - 12				*Composizione*		*Martello di Schmidt*	**Fl**uente	> 125	**GSI:** 50-55
		Terminazione		12 - 14	Scabra			**Ar**gilla	**Cal**cite	**Rimbalzi**			
Spaziatura		**R** - roccia		14 - 16				**Li**mo	**Qu**arzo	valore rimbalzi			
Distanza perpendicolare tra due discontinuità della stessa famiglia		**D** - contro altra discontinuità		16 - 18	Molto Scabra			**Sa**bbia	**Cl**orite	**Orientazione**			
		X - fuori affioramento		18 - 20				**Gh**iaia	**Os**sidi	direzione applicazione martello (perpendicolare alla discontinuità)			
								Altro					

TABELLA A3.2
Rilievo geologico-strutturale su stazione

Commessa: 251401 Località: Venaus Data: 11/09/2025 Operatore: FEL+GPA
Stazione: St3 Litotipo: Micascisti con vene di quarzo Dim. affioramento H x L: 30x20 Orientamento (DD, Dip): 085/80

Progr (cm)	Set	Giacitura		Tipo	Spaziatura (m)			Persistenza (m)		Scabrezza		Apertura (mm)			Riempimento			Alterazione			Cond. Idr.	Note
		DD (°)	Dip (°)		min	max	medio	Lungh.	Terminazione	P. Scala (JRC)	Grande scala	min	max	medio	Tipo	Spess. (mm)	Composizione	Tipo	Martello di Schmidt (discontinuità) Rimbalzi	Orientaz.		
	J4a	45	60	G	0.05	0.50	0.15	1-3	D-D	10-12	P	0	>5	0.1-1	A - S	<5	S	Deb - A	18 - 20 - 24 - 14 - 24 - 40 - 35 - 32 - 14 - 54	↘	A	
		34	72																			
		20	80																			
		15	80																			
		45	72																			
		40	68																			
		30	89																			
		20	70																			
	J6	310	80	G	0.03	0.30	0.13	1-3	D-D	14-16	P	0.1-1	>5	1-5	A - S	>5	S	Deb	23 - 21 - 20 - 19 - 16 - 16 - 19 - 21 - 28 - 26	↗	A	
		304	88																			
		300	75																			

LEGENDA

Giacitura	Tipo	Persistenza		Scabrezza		Apertura	Riempimento		Alterazione	Condizioni idrauliche	ALTRI PARAMETRI
DD=Dip Dir. Immersione	**St**ratificazione	*Lunghezza*		*Piccola Scala (JRC)*	*Grande Scala*		*Tipo* *Spessore*		*Tipo*	*Acqua su 10 m lineari*	**Vb (block size l*h*t [cm]):**
Dip Inclinazione	**Sc**istosità	< 1 m	**M**olto **b**assa	0 - 2 Levigata	**P**iana	0 mm	**A**ssente		**A**ssente	l/min	50x15x20
	Clivaggio	1 - 3 m	**B**assa	2 - 4	**O**ndulata	< 0.1 mm	**Du**ro < 5 mm		**Deb**olmente alterata	**A**sciutto 0	20x10x5
	Giunto	3 - 10 m	**M**edia	4 - 6 Liscia	**S**egmentata	0.1 - 1.0 mm	**Du**ro > 5 mm		**Mod**eratamente alterata	**U**mido < 10	65x50x40
	Vena	10 - 20 m	**A**lta	6 - 8		1 5 mm	**So**ffice < 5 mm		**Mo**lto alterata	**B**agnato 10 -25	**Jn (n. giunti al m):**
	Faglia	> 20 m	**Mo**lto **a**lta	8 - 10 Poco Scabra		> 5 mm	**So**ffice > 5 mm		**Dec**omposta	**St**illicidi 25 - 125	
		Terminazione		10 - 12			*Composizione*		*Martello di Schmidt*	**Fl**uente > 125	**GSI:** 50-55
	Spaziatura	**R** - roccia		12 - 14 Scabra			**Ar**gilla **Ca**lcite		**Rimbalzi**		
	Distanza perpendicolare tra due discontinuità della stessa famiglia	**D** - contro altra discontinuità		14 - 16			**Li**mo **Q**uarzo		valore rimbalzi		
		X - fuori affioramento		16 - 18 Molto Scabra			**Sa**bbia **Cl**orite		**Orientazione**		
				18 - 20			**Gh**iaia **Os**sidi **Al**tro		direzione applicazione martello (perpendicolare alla discontinuità)		

GE●DES

TABELLA A3.3

Rilievo geologico-strutturale su stazione

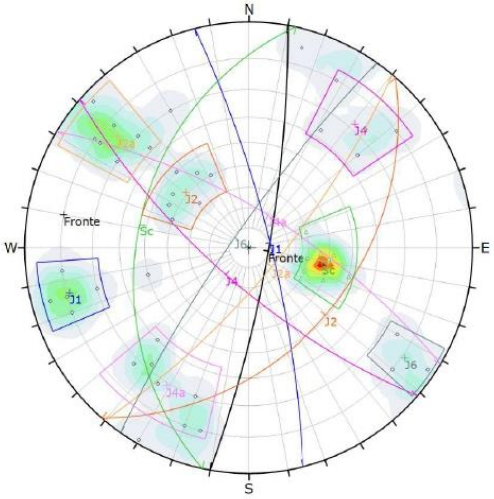

Symbol	TIPO	Quantity
◆	G	38
▲	Sc	11

Color	Density Concentrations
	0.00 - 1.30
	1.30 - 2.60
	2.60 - 3.90
	3.90 - 5.20
	5.20 - 6.50
	6.50 - 7.80
	7.80 - 9.10
	9.10 - 10.40
	10.40 - 11.70
	11.70 - 13.00

Contour Data	Pole Vectors
Maximum Density	12.46%
Contour Distribution	Fisher
Counting Circle Size	1.0%

	Color	Dip	Dip Direction	Label
User Planes				
1		80	100	Fronte
Mean Set Planes				
1m		37	282	Sc
2m		71	31	J4a
3m		72	221	J4
4m		79	76	J1
5m		41	121	J2
6m		75	136	J2a
7m		81	305	J6

Plot Mode	Pole Vectors
Vector Count	49 (49 Entries)
Hemisphere	Lower
Projection	Equal Angle

Note/descrizione:

Micascisti di colore grigio quarzitici con vene di quarzo di dimensioni da centimetriche a pluricentimetriche. Sulle superfici fresche si evidenzia l'abbondante presenza di mica chiara, seguita da minerali di colorazione verde, verosimilmente clorite. Le vene di quarzo hanno forma lenticolare ed estensioni importanti, subparallele alla scistosità (Sc).

Appendix II. Forest Survey

Scheda di Rilevamento Forestale

Generale	Data	5/12/2025	Tipologia di Zona
	Località	Venaus	☐ Sorgente
	Nr. Poligono	1	☒ Transito
	Pendenza		☐ Deposito

Foresta	Area di indagine	_____m x _____ m	m^2

ID	Specie*	CBH** (cm)
1a	NC	90 a
2a		76 a
3a		72 a
a		30 a
		69
		94
		40
b		50
b		51
a		75
a		90
a		69
c		65
c		38
c		47
c		41
c		46
c		43
c		26
c		30
c		28
c		29
c		50
		29
d		41
Tot	C	NC	Media

ID	Specie	CBH (cm)
d		58
e		63
e		51
e		69
f		69
f		65
f		60
g		35
g		55
g		97
g		90
g		75
g		95
g		80
g		90
g		62
g		
Tot	C	NC	Media

ID	Specie	CBH (cm)
Tot	C	NC	Media

* conifera (C) o non conifera (NC)

** circonferenza misurata all'altezza del petto

ronchi / ettaro	
DBH media (cm)	
DBH dev.std (cm)	
% conifere	

g ⌀ 8,20 (circ)

(g - a) 6 (c - e) 6

(g - c) 8 (c - b) 8

a ⌀ 2,5 (b - g) 10

Scheda di Rilevamento Forestale

Generale			
	Data	5/12/25	Tipologia di Zona
	Località	Venetis	☐ Sorgente
	Nr. Poligono	2	☒ Transito
	Pendenza		☐ Deposito

Foresta	Area di indagine	_____m x _____ m	m^2

ID	Specie*	CBH** (cm)
a		42
a		70
a		37
●		205 -
b		45
b		70
b		31
c		35
c		46
		33
		27
		38
d		55
d		60
d		64
		26
e		32
e		57
e		30
e		32
		41
		54
		46
f		52
f		35
Tot	C / NC	Media

ID	Specie	CBH (cm)
f		53
g		36
g		55
g		25
g		42
Tot	C / NC	Media

ID	Specie	CBH (cm)
Tot	C / NC	Media

* conifera (C) o non conifera (NC)

** circonferenza misurata all'altezza del petto

ronchi / ettaro	
DBH media (cm)	
DBH dev.std (cm)	
% conifere	

(b - c) 4 m
(a - 205) 5 m
(205 - d) 4 m
(a - d) 6 m
(e - f) 3 m
(f - d) 9 m

d ● ▭ 1,30 m
b ▭ 1,70 m
e ▭ ∅ 1,25 m
f ∅ 4,30 m

Scheda di Rilevamento Forestale

Generale			
	Data	05 / 12 / 2025	Tipologia di Zona
	Località	VENAUS	☐ Sorgente
	Nr. Poligono	3	☒ Transito
	Pendenza		☐ Deposito

Foresta	Area di indagine	_____m x _____ m	m^2

ID	Specie*	CBH** (cm)
		68
a		53
a		35
a		59
b		19
b		22
b		27
b		15
b		15
b		16
b		25
b		41
b		40
b		20
b		42
b		25
b		18
b		19
b		17
c		21
c		18
c		24
d		25
d		25
d		27

Tot	C	NC	Media

ID	Specie	CBH (cm)
d		26
d		17
d		16
d		15
e		28
e		26
e		25
e		28
e		28
e		20
e		24
e		23
		30
f		27
f		39

Tot	C	NC	Media

ID	Specie	CBH (cm)

Tot	C	NC	Media

* conifera (C) o non conifera (NC)

** circonferenza misurata all'altezza del petto

ronchi / ettaro	
DBH media (cm)	
DBH dev.std (cm)	
% conifere	

a ▭ 2,60 m

b ⌀ 2 m

d ⌀ 1,5 m

e ⌀ 1,7 m

f ⌀ 50 cm

(a - b) 4 m

(b - c) 5 m

(c - d) 2 m

(c - e) 6 m

(f - e) 4 m

Scheda di Rilevamento Forestale

Generale			
	Data	05/12/25	Tipologia di Zona
	Località	VENAUS	☐ Sorgente
	Nr. Poligono	4	☒ Transito
	Pendenza		☐ Deposito

Foresta	Area di indagine	_____m x _____ m	m^2

ID	Specie*		CBH** (cm)
			46
			38
			130
			32
			31
			33
			48
			33
			64
			55
a			52
a			39
a			60
			27
b			35
b			40
b			61
b			21
b			36
b			37
b			88
b			39
c			63
c			35
c			38
Tot	C	NC	Media

ID	Specie	CBH (cm)
c		36
c		60
c		63
c		55
c		50
c		30
c		70
cl		72
d		30
d		124
d		60
e		74
e		39
e		45
e		46
Tot	C	NC	Media

ID	Specie	CBH (cm)
Tot	C	NC	Media

* conifera (C) o non conifera (NC)

** circonferenza misurata all'altezza del petto

ronchi / ettaro	
DBH media (cm)	
DBH dev.std (cm)	
% conifere	

a ϕ 90 cm
b ϕ 2 m
c ϕ 2,5 m
d ϕ 1,3 m
e ϕ 1,5 m

(b - c) 6 m
(c - d) 2 m
(d - e) 1,5 m

Scheda di Rilevamento Forestale

Generale			Tipologia di Zona
	Data	05/12/25	☐ Sorgente
	Località	Venaus	☒ Transito
	Nr. Poligono	5	☐ Deposito
	Pendenza		

Foresta	Area di indagine	_____m x _____ m	m^2

ID	Specie*	CBH** (cm)
		46
a		60
a		51
a		49
a		41
a		50
a		62
		75
		48
b		36
b		46
b		27
b		29
b		54
b		41
C		22
C		46
C		31
C		48
C		55
C		91
		47
		40
		34
		24
Tot	C	NC	Media

ID	Specie	CBH (cm)
		28
		29
		28
		27
		22
		22
		28
		23
		1
		2
		3
		4
		5
		6
		7
		8
		9
		10
		40
d		60
d		38
d		35
d		30
d		32
d		36
Tot	C	NC	Media

ID	Specie	CBH (cm)
d		20
e		30
e		40
e		38
e		42
e		25
e		15
e		15
f		75
f		33
f		30
f		32
f		43
f		49
f		38
f		42
f		56
f		42
f		57
f		40
f		38
f		40
f		56
f		28
f		36
Tot	C	NC	Media

* conifera (C) o non conifera (NC)

** circonferenza misurata all'altezza del petto

ronchi / ettaro	
DBH media (cm)	
DBH dev.std (cm)	
% conifere	

Nota = gruppi di 6 alberi sparsi in raimpe di 1 - 6 m.

a ϕ 1,5 m
b ϕ 1,3 m
c ϕ 2,5 m
d ϕ 1,30 m
e ϕ 1,5 m
f ϕ 2 m

(a - b) 4 m
(b - c) 7 m
(d - c) 11 m
(d - e) 5 m
(e - f) 5 m
(f - g) 6 m

Scheda di Rilevamento Forestale

Generale			Tipologia di Zona
	Data	05/12/25	☐ Sorgente
	Località	Venaus	☒ Transito
	Nr. Poligono	6	☐ Deposito
	Pendenza		

Foresta	Area di indagine	_____m x _____ m	m^2

ID	Specie*	CBH** (cm)
[illegible]		[illegible]
a		87
a		38
a		79
a		115
b		75
b		80
b		77
		22
		131
		22
		42
c		65
c		65
d		ϕ 28
d		ϕ 24
d		ϕ 34
d		ϕ 13
d		ϕ 24
e		27
e		62
e		36
e		40
f		35
f		83
Tot	C / NC	Media

ID	Specie	CBH (cm)
f		40
f		76
f		35
		ϕ 80
g		120
g		54
g		67
g		112
h		29
h		62
h		49
h		67
		67
i		52
i		33
i		62
i		54
i		64
i		62
		37
		92
		34
Tot	C / NC	Media

ID	Specie	CBH (cm)
Tot	C / NC	Media

* conifera (C) o non conifera (NC)

** circonferenza misurata all'altezza del petto

a ϕ 1,5 m
b ϕ 1,3 m
e ϕ 1,2 m
f ϕ 2,2 m
g ϕ 2 m
h ϕ 1,3 m
i ϕ 2 m

(a - b) 2,5 m
(a - d) 7 m
(c - e) 4 m
(e - f) 6 m
(g - h) 4 m
(g - f) 6 m
(h - i) 8 m

ronchi / ettaro	
DBH media (cm)	
DBH dev.std (cm)	
% conifere	

Appendix III. SIF Calculation Codes

Factor F1 (slope angle)

```
CASE WHEN "slope" < 15 THEN 0
CASE WHEN "slope" >= 15 AND "slope" < 30 THEN 0.5
CASE WHEN "slope" >= 30 AND "slope" < 45 THEN 1
CASE WHEN "slope" >= 45 AND "slope" <= 70 THEN 2
CASE WHEN "slope" > 70 THEN 3
```

Σ(Pfi)

```
coalesce("F1",0) +
coalesce("F2",0) +
coalesce("F3",0) +
coalesce("F4",0) +
coalesce("F5",0) +
coalesce("F6",0) +
coalesce("F7",0) +
coalesce("F8",0) +
coalesce("F9",0) +
coalesce("F10",0) +
coalesce("F11",0) +
coalesce("F12",0) +
coalesce("F13",0) +
coalesce("F14",0)
```

Σmin(Pfi)

```
CASE WHEN "F13" IS NOT NULL THEN -1 ELSE 0 END
```

Σmax(Pfi)

```
CASE WHEN "F1" IS NOT NULL THEN 3 ELSE 0 END +
CASE WHEN "F2" IS NOT NULL THEN 3 ELSE 0 END +
CASE WHEN "F3" IS NOT NULL THEN 3 ELSE 0 END +
CASE WHEN "F4" IS NOT NULL THEN 2 ELSE 0 END +
CASE WHEN "F5" IS NOT NULL THEN 3 ELSE 0 END +
CASE WHEN "F6" IS NOT NULL THEN 2 ELSE 0 END +
CASE WHEN "F7" IS NOT NULL THEN 3 ELSE 0 END +
CASE WHEN "F8" IS NOT NULL THEN 2 ELSE 0 END +
CASE WHEN "F9" IS NOT NULL THEN 2 ELSE 0 END +
CASE WHEN "F10" IS NOT NULL THEN 2 ELSE 0 END +
CASE WHEN "F11" IS NOT NULL THEN 2 ELSE 0 END +
CASE WHEN "F12" IS NOT NULL THEN 1 ELSE 0 END +
CASE WHEN "F13" IS NOT NULL THEN 0 ELSE 0 END +
CASE WHEN "F14" IS NOT NULL THEN 1 ELSE 0 END
```

SIF

```
("S(Pfi)"-"Smin(Pfi)")/("Smax(Pfi)"-"Smin(Pfi)")
```

Appendix IV. Sections Examined for the Estimation of the Lateral Dispersion angle

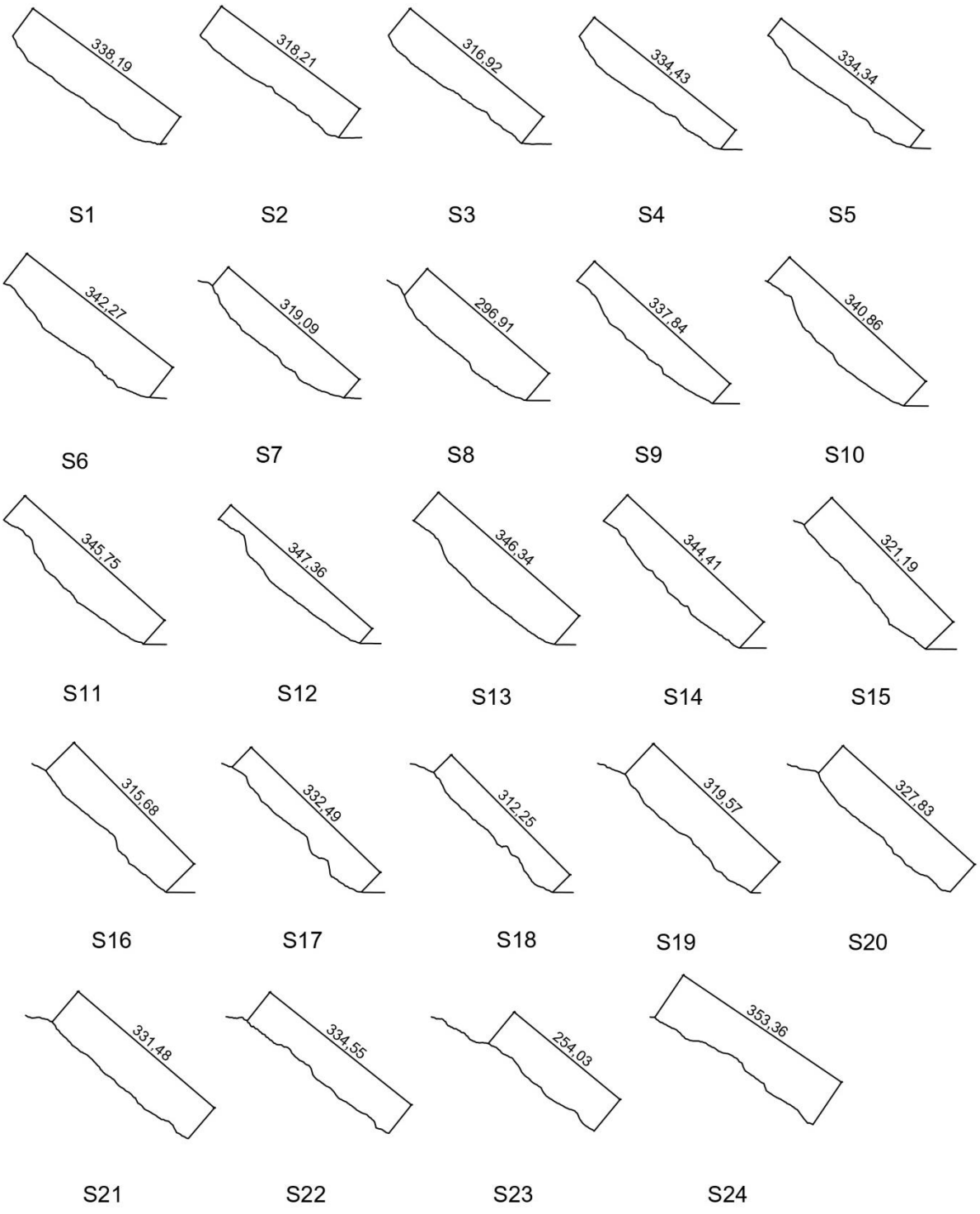

Appendix V. Examples of Roughness and Soiltype Values

Photo	rg70	rg20	rg10	soiltype
	0	0	0.05	6
	0	0.05	0.1	5
	0.25	0.5	0.9	4
	0.03	0.05	0.05	3
	0.05	0.05	0.1	4
	0.05	0.1	0.2	4
	0.03	0.03	0.03	3
	0	0	0.05	3

	0	0	0	7
	0.15	0.15	0.25	4
	0.1	0.35	0.15	4
	0	0	0	1
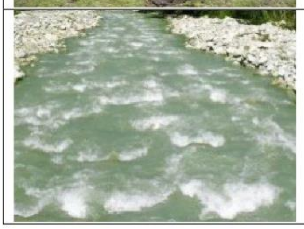	100	100	100	0